Multi-BK-Net: Multi-Branch Multi-Kernel Convolutional Neural Networks for Clinical EEG Analysis

Anonymous authors
Paper under double-blind review

Abstract

Classifying an electroencephalography (EEG) recording as pathological or non-pathological is an important first step in diagnosing and managing neurological diseases and disorders. As manual EEG classification is costly, time-consuming and requires highly trained experts, deep learning methods for automated classification of general EEG pathology offer a promising option to assist clinicians in screening EEGs. Convolutional neural networks (CNNs) are well-suited for classifying pathological EEG signals due to their ability to perform end-to-end learning. In practice, however, current CNN solutions suffer from limited generalisation due to I) a single-scale network design that cannot fully capture the high intra- and inter-subject variability of the EEG signal, the diversity of the data, and the heterogeneity of pathological EEG patterns; and II) the small size and limited diversity of the dataset commonly used to train and evaluate the networks. These challenges result in a low sensitivity score and a performance drop on other datasets, further hindering their reliability for real-world applications. Here, we propose a novel multi-branch, multi-scale CNN called Multi-BK-Net (Multi-Branch Multi-Kernel Network), comprising five parallel branches that incorporate temporal convolution, spatial convolution, and pooling layers, with temporal kernel sizes defined based on five clinically relevant frequency bands within its first block. Evaluation is based on two public datasets with predefined test sets: the Temple University Hospital (TUH) Abnormal EEG Corpus and the TUH Abnormal Expansion Balanced EEG Corpus. Our Multi-BK-Net outperforms five baseline architectures and state-of-the-art end-to-end approaches in terms of accuracy and sensitivity on these datasets, setting a new benchmark. Furthermore, ablation experiments highlight the effectiveness of the multi-branch, multi-scale input block of the Multi-BK-Net. Overall, our approach demonstrates the effectiveness of multi-branch, multi-scale CNNs in accurately and reliably classifying general EEG pathology, while being more effective at handling data heterogeneity, and constitutes a next step towards deep end-to-end classification of general EEG pathology.

1 Introduction

Electroencephalography (EEG) is a non-invasive method of measuring and recording electrical activity in the brain. EEG has high temporal resolution, low equipment cost and is highly sensitive to dynamic changes in neural signals. Due to its high efficiency and usability, EEG is most commonly used in clinical practice for the diagnosis and management of various neurological conditions (Lopez et al., 2015; Zhang et al., 2023b). For this purpose, a preliminary important step in clinical practice is to classify an EEG recording as non-pathological or pathological (Brogger et al., 2018; Lopez et al., 2015). To this end, human EEG experts visually analyse recordings from long-term monitoring or multiple short sessions, which is a tedious and time-consuming process (Brogger et al., 2018). They also consider various additional patient-related factors, such as medical history, age, or medication (Beuchat et al., 2021; Nayak & Anilkumar, 2020). Furthermore, it requires years of training to achieve a thorough understanding of pathological EEG patterns and to distinguish them from normal EEG, normal benign variants, and artefacts (Amin et al., 2023; Emmady & Anilkumar, 2023; Hoppe, 2018). Thus, these challenges result in inter-rater variability and diagnostic errors. For the task of classifying EEG recordings as pathological or non-pathological, previous research has reported

an inter-rater agreement of 86–88% between two neurologists (Houfek & Ellingson, 1959; Rose et al., 1973). At the same time, Beuchat et al. (2021) has found even lower inter-rater agreements of 82-86% between multiple EEG technologists and neurologists.

In this sense, introducing automated EEG classification, or at least some level of automation such as clinical decision support systems, has the potential to improve or accelerate the EEG classification process, thereby enhancing the quality of patient care. To this end, the use of deep learning approaches for EEG classification has received increasing attention in recent years (for a detailed review, see Amrani et al., 2021; Craik et al., 2019; Faust et al., 2018; Rahman et al., 2024; Roy et al., 2019b; Praveena et al., 2022). It has also spurred their application to the task of classifying general EEG pathology (Schirrmeister et al., 2017b). In this regard, research has shown that convolutional neural networks (CNNs) have been quite effective for general EEG pathology classification due to their ability to extract relevant feature representations directly from raw or minimally preprocessed EEG data (Darvishi-Bayazi et al., 2023; Gemein et al., 2020; Khan et al., 2022; Kiessner et al., 2023; 2024; Van Leeuwen et al., 2019; Western et al., 2021, Appendix A.1 provides more details on the related works.). In practice, however, the generalisation performance of current state-of-the-art CNN methods is mainly limited due to three reasons. First, the EEG presents inherent challenges which make the application of deep learning methods to real-world EEG datasets more difficult. For example, the recorded EEG signals are high-dimensional, non-linear, nonstationary (Cole & Voytek, 2019; Gramfort et al., 2013; Jia et al., 2021), have a low signal-to-noise ratio (Bigdely-Shamlo et al., 2015; Jas et al., 2017), are strongly influenced by artefacts caused by external environmental factors (e.g. electrical interference from external sources) (Islam et al., 2016; Kane et al., 2017) or physiological sources (e.g. cardiac, muscle activity, eye movements, or fatigue) (Britton et al., 2016), and variations in recording protocols and labelling standards within clinical data can occur (Poziomska et al., 2024). In addition, pathological EEG patterns exhibit a wide range of physiological variability across both patients (Nahmias et al., 2019) and neurological conditions (Emmady & Anilkumar, 2023; Nayak & Anilkumar, 2020; Smith, 2005). Due to these challenges, the classification performance can vary between patients (Altuwaijri et al., 2022; Lashgari et al., 2020; Roy et al., 2019b; Schirrmeister et al., 2017b). Second, due to the scarcity of publicly available datasets, current approaches are mainly trained and evaluated on a single dataset, the TUH Abnormal EEG Corpus (TUAB) (López de Diego, 2017). While it is therefore well established that these methods perform well on this small, homogeneous dataset, this limitation restricts the generalisability of these approaches. For example, recent studies have observed significant differences in the performance of several previously established models after training or validating them on other datasets (Darvishi-Bayazi et al., 2023; Khan et al., 2022; Kiessner et al., 2023; 2024; Nahmias & Kontson, 2020; Poziomska et al., 2024; Van Leeuwen et al., 2019; Western et al., 2021). Lastly, single-scale convolutions, with manually and arbitrarily defined kernel sizes (Emsawas et al., 2022), are mainly used for designing CNNs; however, they are less capable of handling individual differences in the EEG signal. For example, several studies have found that, due to variability in the EEG signal, the optimal kernel size differs from subject to subject and from time to time for the same subject (Altaheri et al., 2023b; Altuwaijri et al., 2022; Jia et al., 2021). While multi-branch, multi-scale¹, or parallel architectures (Altuwaijri et al., 2022; Belwafi et al., 2017; Ingolfsson et al., 2020; Jia et al., 2021; Riyad et al., 2020; Szegedy et al., 2015; Zhang et al., 2023a) have shown promising results in addressing the challenge of heterogeneity in various EEG classification tasks (Cai et al., 2024; Jia et al., 2021; Siddiqa et al., 2024; Yan et al., 2025; Zhu et al., 2023), only a few attempts have been made to address the challenges of general EEG pathology classification by using CNNs with a set of three convolution scales (Brenner et al., 2024; Roy et al., 2019a; Wu et al., 2021). However, these CNN approaches have achieved classification performance similar to that of other CNNs, with accuracies ranging from 85.10% to 87.10%; they also inherit the disadvantages found in their single-scale counterparts. For example, these results were based on the TUAB, and no attempts have been made to evaluate the performance of these CNNs on a larger, more heterogeneous dataset. In addition, smaller kernel sizes are preferred due to lower computational costs (Emsawas et al., 2022), which, however, tend to learn shorter temporal patterns from faster frequency bands (Cohen, 2014; Jia et al., 2021). This also limits these CNNs' ability to capture the heterogeneity of the EEG signal (Altaheri et al., 2023b; Emsawas et al., 2022). Therefore, developing an accurate and reliable CNN solution for general EEG pathology classification requires a network design that addresses the high intra- and inter-subject variability in the EEG signal, data diversity, and the heterogeneity of pathological EEG patterns.

¹In this work, we will use "multi-scale" and "multi-kernel" interchangeably.

In this work, we propose a novel, multi-branch, multi-scale CNN, called Multi-Branch Multi-Kernel Network (Multi-BK-Net) for general EEG pathology classification that extracts long-term and short-term spatiotemporal EEG features by incorporating five parallel branches within the first convolution-pooling block (see Section 2.1). Each branch employs a temporal convolution layer with a different kernel size that was defined considering five clinically relevant frequency bands, namely delta (1–3 Hz), theta (4–7 Hz), alpha (8–13 Hz), beta (14–30 Hz) and low gamma (30-80 Hz) (Brenner et al., 2024). Aiming at the problem of a small amount of training data and to increase data diversity, we combined the predefined training sets of two publicly available datasets for general EEG pathology classification, the TUH Abnormal EEG Corpus (TUAB) (López de Diego, 2017) and TUH Abnormal Expansion Balanced EEG Corpus (TUABEXB) (Kiessner et al., 2023), to optimise and train our Multi-BK-Net. The hyperparameters of the Multi-BK-Net were optimised using multivariate tree-structured Parzen estimators (TPE) (Bergstra et al., 2011; 2013) from the Optuna library (Akiba et al., 2019) with respect to the mean validation accuracy and mean validation sensitivity values from a 5-fold cross-validation. Our study presents the following contributions to research on deep end-to-end CNNs for general EEG pathology classification:

- We propose the Multi-BK-Net, a multi-branch, multi-scale CNN designed for general EEG pathology
 classification. We combine the concepts of multi-scale and multi-branch CNNs with the idea of
 adapting the temporal kernel size based on five clinically relevant frequency bands to accommodate
 the challenge of heterogeneity inherent in the EEG signal.
- We evaluate our proposed Multi-BK-Net on the predefined test sets of two publicly available datasets, the TUAB and the TUABEXB datasets. Our Multi-BK-Net achieves mean accuracies of 87.75% and 87.01% and mean sensitivities of 83.10% and 84.25%, respectively, and thus outperforms five architectures used as a baseline (Section 3.4), as well as previously reported state-of-the-art deep learning approaches (Section 3.5) on these datasets, setting a new benchmark. In addition, with mean accuracies in the narrow range of 87–88%, the Multi-BK-Net approaches the upper limit of inter-rater agreement among human experts, thus bringing deep learning-based general EEG pathology classification closer to human-level performance. An improvement in evaluation sensitivity demonstrates further practical gains of our method. In comparison to the baseline architectures, Multi-BK-Net achieved the highest mean sensitivities at a fixed specificity of 95% on both test sets (82.78% and 84.25%). The significance of this result lies in applications such as deep learning-based EEG classification and clinical decision support systems in clinical practice, for which a high, robust sensitivity is crucial for accurately identifying EEG pathology. In deep learning-based clinical EEG analysis, high accuracy and sensitivity are crucial for improved patient outcomes, reduced diagnostic errors, and enhanced clinical efficiency. Thus, even minor gains significantly improve the reliability and trustworthiness of such systems.
- Our ablation experiments show that using both multiple temporal kernel lengths and multiple parallel branches in the first block significantly improves the performance of the model, particularly in terms of mean accuracy and mean sensitivity (Section 3.6).
- To interpret the trained Multi-BK-Net, we visualise the learned features using Uniform Manifold Approximation and Projection (UMAP) (McInnes et al., 2018) method (Section 3.7) and observe that the Multi-BK-Net forms distinct and compact clusters of samples from the pathological and non-pathological classes, which partly explains the good performance of this architecture. Additionally, we perform an amplitude gradient analysis (Section 3.8) showing that the model's pathological prediction is sensitive to localised patterns of amplitude changes in different frequency bands. These patterns align with the current neurophysiological knowledge for pathological EEG patterns (Amin et al., 2023; Emmady & Anilkumar, 2023; Hoppe, 2018; Kane et al., 2017; Medithe & Nelakuditi, 2016; Tatum & William, 2021) and with the pathological patterns that have been identified by human experts in the corresponding clinical EEG reports.
- A qualitative review of clinical EEG reports corresponding to false negative and false positive classified EEG recordings by the Multi-BK-Net suggests that the CNN struggles to identify context-dependent abnormalities. While clinicians include additional information about the patient's age,

vigilance, medication, and clinical history to interpret EEG patterns, our CNN, which was trained only on the EEG signal, does not have access to this contextual information. This results in the model being at a disadvantage in comparison to clinicians and highlights the potential for further performance improvement by incorporating contextual information into the training and classification approach.

Overall, our results demonstrate the effectiveness of our multi-branch, multi-scale CNN solution in
accurately and reliably classifying general EEG pathology. Our findings contribute to the broader
discussion on the challenges of deep learning-based general EEG pathology classification, providing
new insights for the design of future end-to-end CNNs. This will ultimately advance the development
of more reliable and robust methods for automated classification of general EEG pathology.

2 Methods

2.1 Multi-Branch Multi-Kernel Network (Multi-BK-Net)

We propose a novel deep, multi-scale, and multi-branch CNN, called Multi-BK-Net, for general EEG pathology classification. This model extracts long-term and short-term spatiotemporal EEG features by incorporating a dedicated multi-branch, multi-scale first block that processes EEG inputs for different temporal patterns. The block is followed by three standard convolution-mean-pooling blocks and a softmax classification layer. Figure 1 shows the overall structure of the proposed Multi-BK-Net architecture. The first convolutional block is divided into five branches (multi-branches). Each convolutional branch contains two convolutional layers and a mean-pooling layer. The first convolutional layer performs temporal filtering with a set of seven convolutional filters. Each branch uses a different kernel size for temporal filtering (multiscale). This allows the model to extract and combine features from different time scales. The choice of kernel size was based on five frequency bands, namely, delta (0.5 to 4 Hz), theta (4 to 7 Hz), alpha (8 to 12 Hz), beta (13 to 30 Hz), and low gamma (30 to 80 Hz) (Brenner et al., 2024; Navak & Anilkumar, 2020), by also considering the sampling rate. In this study, the EEG signal is represented as a 2D input, with the dimension (E×T) and with a window size of 60 seconds and a sampling frequency of 100 Hz, corresponding to 6000 time points, an input shape of 21×6000 (for more details, see Section 3.1). Accordingly, we used five different temporal kernel sizes: 1×200 , 1×25 , 1×13 , 1×7 and 1×3 . In the second layer, a spatial convolution is applied. Each filter performs a spatial convolution with weights for all possible electrode pairs, using the filters from the preceding temporal convolution. Note that there is no activation function between the two layers; therefore, in principle, they could be combined into a single layer. However, we chose a split convolution because it has been shown to outperform a combined temporal-spatial convolutional layer (Schirrmeister et al., 2017a;b). After the spatial convolution, mean pooling is applied. As successfully done by (Schirrmeister et al., 2017a), the pooling strides were moved directly to the convolutional layers preceding each pooling. Finally, the outputs of each branch are concatenated along the feature axis, resulting in a feature vector of shape (1, 35, 397, 1). The concatenated tensors are then passed through three convolutionmean-pooling blocks. Each convolution-mean-pooling block consists of a convolutional layer and a mean pooling layer. The output of the fourth block is then passed through a softmax classification layer to receive the final prediction. In total, the Multi-BK-Net contains 1,038,683 trainable parameters. We implemented our model in Braindecode (BD), an open-source Python toolbox for decoding raw electrophysiological brain data with deep learning models (Schirrmeister et al., 2017b). The Xavier initialisation method (Glorot & Bengio, 2010) was used to initialise the weights. The biases have been initialised to 0. We applied group normalisation (Wu & He, 2018) to the output of the convolutional layers before the nonlinearity. We used Gaussian Error Linear Units, or GELUs $(GELU(x) = xP(X \le x) = x\Phi(x))$ (Hendrycks & Gimpel, 2023) as activation functions. Additionally, we used dropout as a regularisation strategy (Srivastava et al., 2014). Appendix A.3 provides a more detailed description of the design choices and hyperparameter optimisation procedure.

2.2 Network Training

For optimisation, we used the adaptive moment estimation with decoupled weight decay (AdamW) optimiser (Loshchilov & Hutter, 2019) with an optimised learning rate and beta1 parameter and the negative log

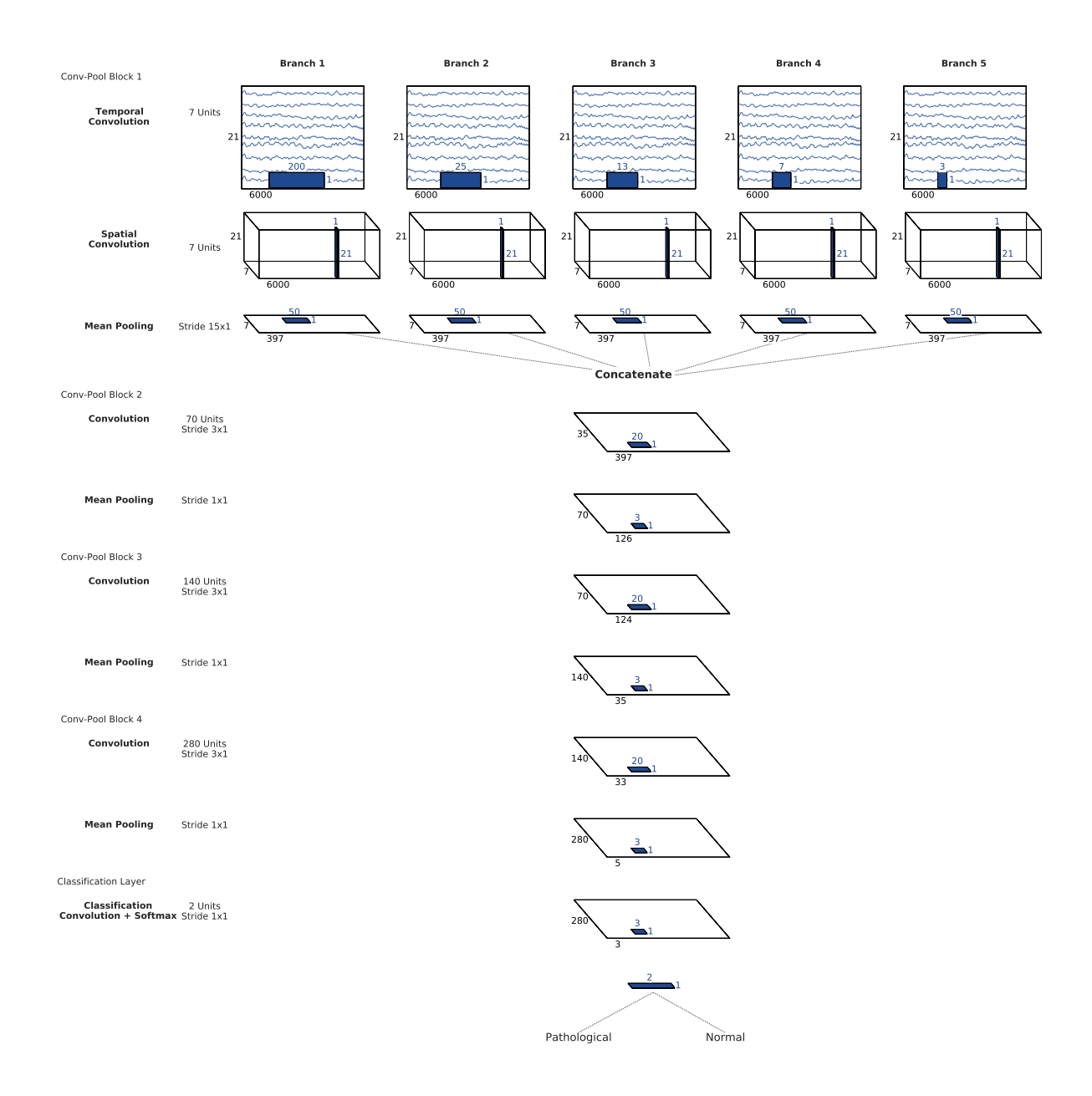


Figure 1: Multi-BK-Net architecture. The first block is divided into five branches, each applying a temporal convolution with a different kernel size, followed by a spatial convolution. There is no activation function between the two convolutional layers; after that, a mean-pooling layer is added. The EEG input (at the top) is passed through each branch. The outputs of all branches are concatenated and then used as input for the subsequent convolution-mean-pooling blocks. Black cuboids: input/feature maps; coloured cuboids: convolution/pooling kernels. The corresponding sizes are shown in black or in colour. Note that the proportions of maps and kernels in this schematic are only approximate.

likelihood loss (Terven et al., 2024). We used cosine annealing (Loshchilov & Hutter, 2016) to schedule the learning rates for both the gradient and weight decay updates, and refrained from restarting the learning rate. We trained the model on non-overlapping, equally sized time windows of size 60 seconds using the

Table 1: Hyperparameters of the Multi-BK-Net architecture. Hyperparameters have been optimised in preliminary experiments; more details on the hyperparameter optimisation and design choices are provided in Appendix A.3.

Hyperparameter	Selected value
Total number of temporal convolution filters	35 (7 filters per branch)
Normalisation	$\operatorname{GroupNorm}$
Activation functions	GELU
Pooling mode first block	Mean
Pooling mode remaining blocks	Mean
Forth conv-pooling-block	True
Forth conv-pooling-block broader	True
Pool length	3
Pool stride	3
Stride before pool	True
Dropout	0.502959339666169
Filter length convolution blocks	20
Input window size	6000
Weighted loss factor pathological	1
Optimizer	AdamW
Optimizer beta1	0.5
Learning rate	0.0031414364096615
Weight decay	$1.8397405899531204 \mathrm{e}\text{-}05$
Batch size	64
Number of epochs	42
Number of channels	21

trial-wise training strategy² as described by Schirrmeister et al. (2017b). We repeated the training ten times, using a fixed set of different random seeds to account for model variance, due to random weight initialisation. The final predictions are obtained by first averaging the predictions of each window for each recording, and then calculating the overall performance across recordings (see Section 3.3 for more details). The list of hyperparameters for training is provided in Table 1. The code of this study is available at anonymous.4open.science/r/Multi-BK-Net-general-EEG-pathology-classification-4FE5.

3 Experiments and Results

To demonstrate the effectiveness of our method, we evaluated the Multi-BK-Net on two public datasets for general EEG pathology classification: I) the small, homogeneous, public dataset TUH Abnormal EEG Corpus (TUAB) (López de Diego, 2017) for comparison with previously published accuracies and II) the larger, recently introduced TUH Abnormal Expansion Balanced EEG Corpus (TUABEXB) (Kiessner et al., 2023) to evaluate the classification methods with a larger heterogeneous number of EEG recordings. First, we compared the performance of the Multi-BK-Net to five baseline architectures. Following this, we conducted a performance comparison with previously reported state-of-the-art deep learning approaches. We then performed ablation experiments to demonstrate the superiority of the proposed Multi-BK-Net, further highlighting the importance of using multiple temporal kernel sizes and multiple branches in the first block. In addition, we visualised the learned features of the Multi-BK-Net to highlight its robustness and provide a comprehensive understanding of model performance. Lastly, we performed an amplitude gradient study to determine how sensitive the Multi-BK-Net's prediction is to amplitude changes in different frequency bands.

²During trial-wise training, a complete window is pushed through the network. The network then produces a prediction, which is compared to the target (label) for that window (trial) to compute the loss.

3.1 Datasets and Preprocessing Steps

The TUAB consists of 2,993 recordings (49.18% pathological) from 2,329 patients (52.09% female, mean age: 48.55 ± 17.86 years) that are divided into a predefined training set (2,717 recordings) and an evaluation set (276 recordings). In contrast, the TUABEXB contains 8,879 recordings (49.75% pathological) obtained from 7,006 patients (mean age: 47.7 ± 21.2 years; 51.7% female) and is divided into a predefined training set (7990 recordings) and an evaluation set (889 recordings). For training, we used the concatenation of the TUAB and TUABEXB training sets, which we refer to as the TUH Abnormal Combined EEG Corpus (TUABCOMB). The TUABCOMB contains 10,707 recordings from 8,549 patients (mean age: 47.91 ± 20.53 years; 52.5% female), of which 5,321 recordings (49.70%) are classified as pathological. We evaluated our models on the predefined test set of both datasets, TUAB and TUABEXB, respectively (for more details on the datasets, see Section 3.3). There is no overlap of patients between the TUAB and the TUABEXB datasets. In both datasets, there is also no overlap of patients between the predefined training set and the final evaluation set.

We applied the following minimal preprocessing steps to the raw EEG data: a) selected a set of 21 electrode positions 3 present in all recordings; b) discarded the first 60 seconds of each recording as they contain stronger artefacts; c) used up to 20 minutes of the remaining recording to speed up the computations; d) clipped the EEG recordings at \pm 800 μ V to reduce the effect of strong artefacts; e) re-referenced all recordings to the Common Average Reference (CAR) f) resampled the data to 100 Hz to account for the different sampling rates and to further speed up the computation. To apply CNNs to EEG classification, the raw EEG signals measured in microvolts (μ V) can be represented as input as a 2D array with the number of time steps (T, temporal dimension) as the width and the number of electrode channels (E, spatial dimension) as the height, resulting in an input shape of E×T. To create the inputs for the networks, we process sliding windows over the EEG data, $D \in \mathbb{R}^{T \cdot E}$, where T represents the recording duration and E denotes the number of electrodes. Windows are created as input features $x_t \in R^I$ with input dimensionality $I = E \cdot \lfloor T/S \rfloor \cdot f_s$ at time point t, where S is the stride and f_s is the sampling frequency. We use non-overlapping windows of 60 seconds, which corresponds to a stride of S = 60 seconds. The corresponding labels are $y \in \{0,1\}^{\lfloor T/S \rfloor}$, where $y_i = 0$ indicates a non-pathological window and $y_i = 1$ indicates a pathological window. A tensor of the shape (batch size, E, T) is given as input to the architectures.

3.2 Baselines

To illustrate the superiority of the proposed Multi-BK-Net, we compare it to several approaches reported in previous work. For general EEG pathology classification, comparing approaches is challenging without evaluating them within the same framework, due to factors such as different evaluation methods, preprocessing steps, training strategies, and various datasets or dataset versions. Therefore, to evaluate the performance of our architecture, we compared our method with the following five baseline architectures:

- Deep4Net (Schirrmeister et al., 2017b;a), a CNN consisting of four convolution-max-pooling blocks.
- ShallowNet (Schirrmeister et al., 2017b;a), a CNN with a convolution-pooling block that was inspired by the Filter Bank Common Spatial Patterns pipeline (Ang et al., 2008; Chin et al., 2009).
- TCN (Bai et al., 2018; Chrabąszcz, 2018; Gemein et al., 2020), a temporal CNN consisting of five residual blocks.
- EEGNet (Lawhern et al., 2018), a compact CNN with depthwise and separable convolutions.
- ChronoNet (Roy et al., 2019a), a deep recurrent neural network combining multiple Conv1D layers with multiple filters of varying sizes and stacked Gated Recurrent Unit (GRU) layers.

These architectures have been implemented in Braindecode and have also shown high performance on the TUAB and/or TUABEXB in various studies using different preprocessing steps. Additional details on the

³This set of EEG channels included the channels A1, A2, C3, C4, Cz, F3, F4, F7, F8, Fp1, Fp2, Fz, O1, O2, P3, P4, Pz, T3, T4, T5 and T6.

baseline architectures, the list of hyperparameters for training and details on the training procedure are provided in the Appendix A.4.

3.3 Evaluation of Classification Performance

We trained each architecture on the full TUABCOMB training set and then evaluated the model on the withheld final evaluation sets, as predefined in the TUAB and TUABEXB, respectively. To manage the statistical variance caused by initialisation and to improve the comparison between training and model configurations, we repeated the training and evaluation ten times for each model and reported the average of evaluation metrics across ten independent runs (Bouthillier et al., 2021; Picard, 2023; Wightman et al., 2021). To ensure comparability with previous work, we evaluated the overall performance of a model using the prediction for each recording. The model's prediction for a recording was calculated by averaging the outputs from all windows of that recording. Each recording was then classified as non-pathological or pathological based on its mean window probability. The performance of the different architectures was evaluated using the following general classification metrics: accuracy, balanced accuracy, sensitivity, specificity and F2-score. We computed the evaluation metrics for each run and then averaged the results across ten independent runs. In addition, we used the Mann-Whitney U test (Mann & Whitney, 1947) to test for the statistical significance of the difference in performance metrics between the proposed Multi-BK-Net and each of the baseline architectures (H1). The null hypothesis (H0: No significant differences in the performance of Multi-BK-Net compared to a baseline architecture) was rejected with a p-value of p < 0.05. To correct for multiple testing, we additionally performed a Bonferroni correction (Bonferroni, 1936) with $\alpha = 0.05$ for all performance comparisons involving our Multi-BK-Net and each baseline architecture on the corresponding evaluation set. Statistical evaluation is based on 10 independent runs. In addition, we calculate the mean Receiver Operating Characteristic (ROC) curve and Precision-Recall (PR) curves. To this end, ROC and PR curves were computed for each run, respectively. The curves from all 10 independent runs were then averaged pointwise to obtain the mean ROC and PR curves. We also calculated the area under the curve (ROC-AUC and PR-AUC) for each run and reported the mean and standard deviation across runs.

3.4 Performance Comparision to Baseline Architectures

In this section, we examine the performance of the proposed Multi-BK-Net in comparison to five baseline architectures on two predefined test datasets, the TUAB and the TUABEXB. The classification performance of the Multi-BK-Net and all baseline architectures on the TUAB is shown in Figure 2. With a mean accuracy of 87.75%, the Multi-BK-Net shows the best classification performance. This was also statistically significantly better than the baseline models (p < 0.001, Mann-Whitney U test). However, in medical diagnosis, such as EEG pathology classification, it is more important to identify all potential pathological cases (high recall/sensitivity) even at the expense of some false positives (lower precision). In this context, the F2-score is a suitable additional metric to compare the different architectures. With a mean sensitivity of 83.10% and a mean F2-score of 84.05%, Multi-BK-Net statistically significantly outperformed all other architectures (p < 0.001, Mann-Whitney U test), indicating better performance in terms of recall. Figure 3 compares the classification performance of the Multi-BK-Net and five baseline architectures on the TUABEXB evaluation set. Again, the Multi-BK-Net outperformed the baseline models. In particular, Multi-BK-Net achieved a higher mean accuracy of 87.01% on the dedicated test set, which was also statistically significantly different from the baseline CNNs (p < 0.001, Mann-Whitney U test). We can also see that the Multi-BK-Net achieved statistically significantly better mean sensitivity (84.25%) and mean F2-score (85.17%) than each of the baseline CNNs (p < 0.001, Mann-Whitney U test). Additional classification results are presented in Appendix A.6.1. For a more in-depth analysis of model performances, we report the classification performances on subsets created based on age and sex information in Section A.6.5, Table 18 and Table 19. With minor exceptions, e.g. on patients younger than 25 years of the TUAB, Multi-BK-Net achieved higher mean accuracies and sensitivities than the baseline models across all subsets. In addition, we report mean ROC curves of the Multi-BK-Net and all five baseline models on the TUAB and TUABEXB test set in Figure 4. The Multi-BK-Net achieved the highest AUC of 0.874 and 0.870 on the TUAB and TUABEXB, respectively, indicating superior sensitivity and overall robustness. ShallowNet and TCN follow closely, whereas Deep4Net achieved the lowest AUC. Figure 5 shows the mean PR curves of the Multi-BK-Net and all five baseline models on the TUAB and TUABEXB test set, respectively. On both test sets, the Multi-BK-Net achieved the highest AUC scores of 0.821 on the TUAB and 0.828 on the TUABEXB. This indicates that Multi-BK-Net achieves superior discriminative performance and reliability compared to the baseline architectures. To evaluate model performance in a clinically meaningful manner, we report sensitivity at a fixed specificity of 95% in Table 2. This metric reflects the true positive rate achieved when the false positive rate is constrained to 5%, corresponding to an acceptable level of false alarms in clinical practice. Unlike the overall AUC, which summarises performance across all thresholds, sensitivity at high specificity provides a threshold-specific measure that aligns with real-world diagnostic requirements and allows for a more relevant comparison between models. In comparison to the baseline architectures, Multi-BK-Net achieved the highest mean sensitivities at a fixed specificity of 95% on both test sets (82.78% and 84.25%). The smaller standard deviations further suggest less variability between runs and thus more consistency, improved robustness and generalisation compared to baseline models. In general, our method achieved higher classification performance than five baseline architectures and was more effective in identifying pathological recordings.

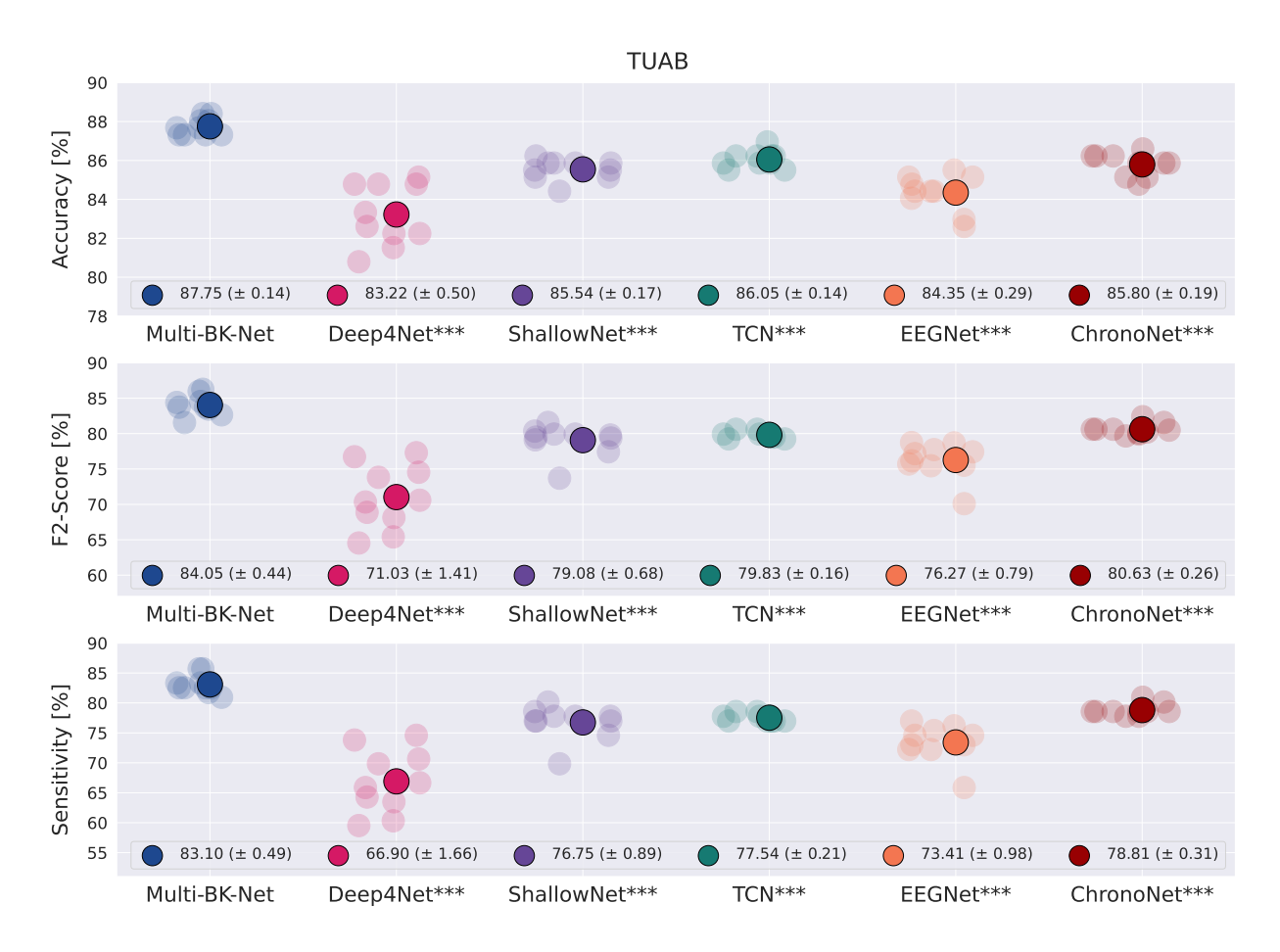


Figure 2: Performance comparison between our proposed Multi-BK-Net and five baseline architectures on the predefined TUAB evaluation set. Each transparent marker represents the performance of a single run, and each larger, bold symbol represents the mean performance score averaged across ten independent runs (n=10). The mean standard error is given in parentheses. Stars indicate statistically significant differences in performance score between the corresponding baseline architecture and the Multi-BK-Net (Bonferronicorrected two-sided Mann-Whitney U test, p < 0.05: *, p < 0.01: ***, p < 0.001: ***; n=10). For additional results, see Figure 8, Appendix A.6.1.

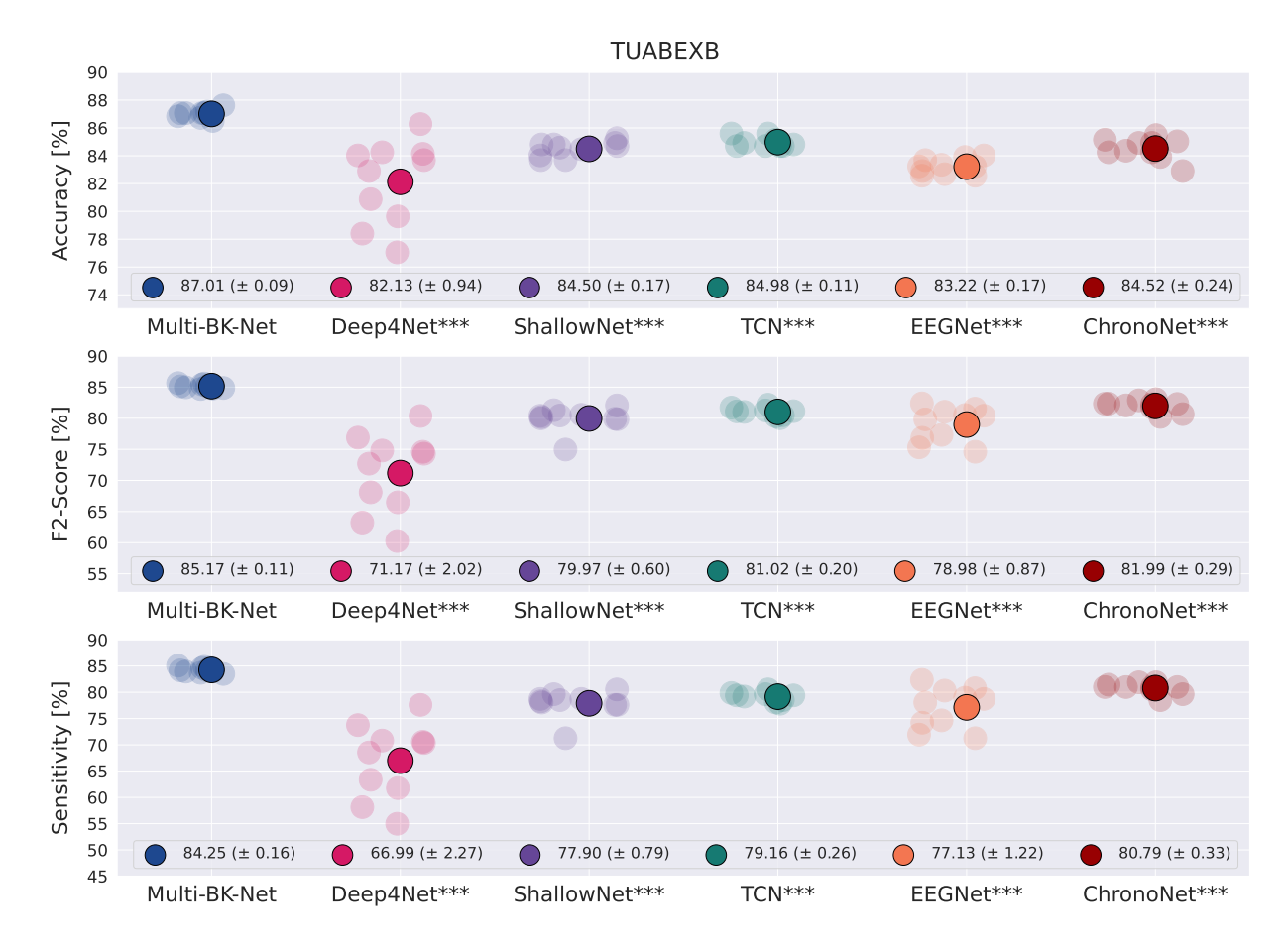


Figure 3: Performance comparison between our proposed Multi-BK-Net and five baseline architectures on the predefined TUABEXB evaluation set. Conventions as in Figure 2. For additional results, see Figure 9, Appendix A.6.1.

Table 2: Mean sensitivity [%] at 95% specificity. Standard deviation is given in parentheses. For each architecture and test set, sensitivity at a fixed specificity of 95% was calculated for each run and then averaged across all ten runs (n=10).

Architecture	TUAB	TUABEXB
Deep4Net	$48.97 (\pm 32.52)$	$66.99 (\pm 6.80)$
ShallowNet	$55.87 (\pm 36.60)$	$77.90 (\pm 2.37)$
TCN	$77.94 (\pm 0.59)$	$79.16 (\pm 0.79)$
EEGNet	$70.48 \ (\pm \ 2.90)$	$52.78 (\pm 34.64)$
ChronoNet	$78.89~(\pm~0.95)$	$40.34 \ (\pm \ 40.35)$
Multi-BK-Net	$82.78 \ (\pm \ 1.85)$	$84.25 (\pm 0.49)$

3.5 Performance Comparision to Previously Reported State-of-the-art Approaches

To further evaluate the Multi-BK-Net, we compared its classification performance with that of other state-of-the-art end-to-end approaches reported in previous studies. More details on the previously published studies are provided in Appendix A.6.2. Table 3 and Table 4 summarise the comparison between our Multi-BK-Net and other methods on the TUAB and TUABEXB datasets, respectively. Overall, the Multi-BK-Net achieved a similar or higher level of performance than other deep learning approaches in all three evaluation metrics, with small advantages for the Multi-BK-Net in some settings. In particular, for the TUAB evaluation set,

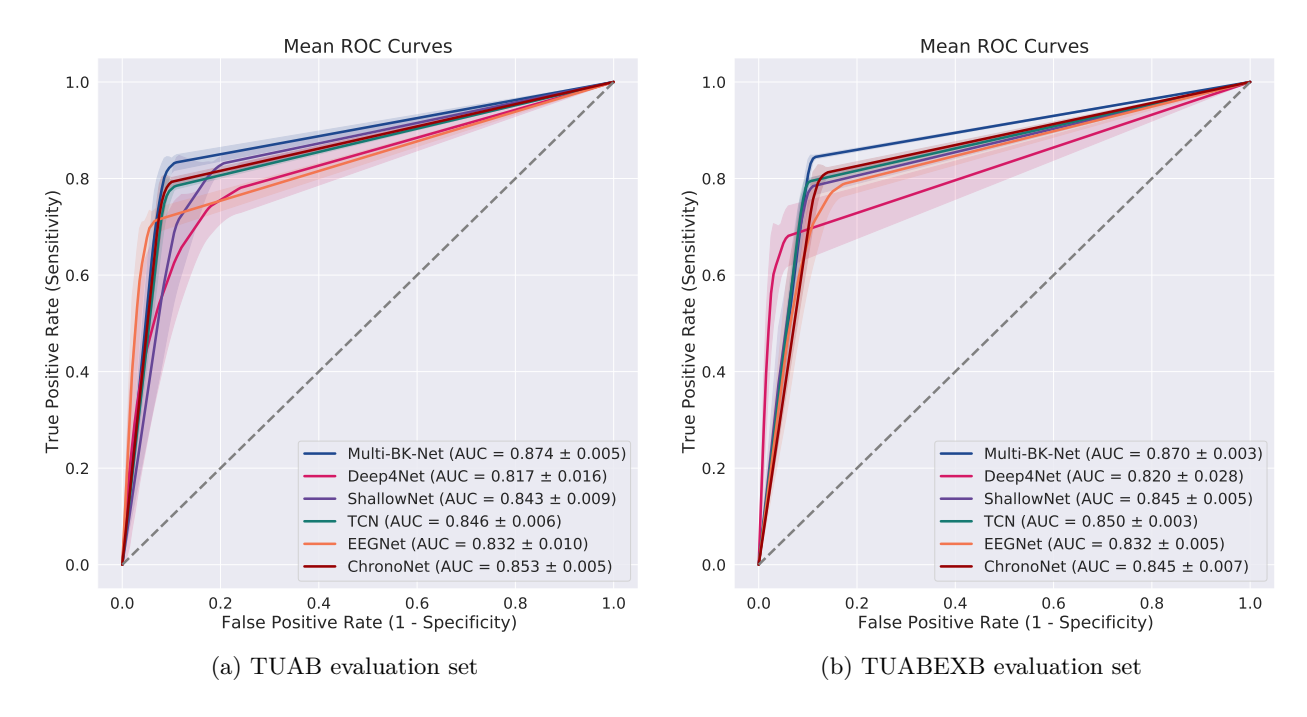


Figure 4: Mean Receiver Operating Characteristic (ROC) curves of our proposed Multi-BK-Net and five baseline architectures on the predefined test sets of the TUAB (left) and of the TUABEXB (right) averaged across 10 independent runs. Each curve represents the mean interpolated ROC performance across runs (n=10), with shaded areas indicating ± 1 standard deviation. The identity line is shown in a grey dotted line. Mean \pm SD values of the area under the curve (AUC) are shown in the legend for each model.

the following observations can be made by further analysis of the Table 3: First, compared to the four singlescale CNNs, namely Deep4Net, ShallowNet, TCN and EEGNet (Darvishi-Bayazi et al., 2023; Gemein et al., 2020; Khan et al., 2022; Kiessner et al., 2023; 2024; Schirrmeister et al., 2017a; Western et al., 2021), Multi-BK-Net improves the mean classification accuracy by 1.85%, 2.24%, 1.26% and 3.08%, respectively. Second, compared to the three architectures using a set of three convolutional scales, i.e. ChronoNet (Roy et al., 2019a), XceptionTime model (Brenner et al., 2024) and IRCNN (Wu et al., 2021), Multi-BK-Net improves the classification accuracy by 1.18%, 1.65% and 0.65%, respectively. In other words, the Multi-BK-Net achieved a classification accuracy of 87.75%, thus outperforming the best previously reported state-of-theart performance of the IRCNN (Wu et al., 2021). Third, Multi-BK-Net also demonstrates higher classification accuracy than two pre-trained transformer-based foundation models, BIOT (3.2M parameters) and LaBraM (396M parameters), both of which require a substantial amount of additional EEG data for pre-training and substantial computational resources due to their large number of parameters. Finally, perhaps the most clinically important finding is that, with a mean sensitivity of 83.10%, Multi-BK-Net outperforms all other approaches, reporting mean sensitivity averaged over multiple runs, by at least 3.26% (see Table 3). Furthermore, for the TUABEXB evaluation set, we have the following observations from further analysis of Table 4: Compared to previous results (Kiessner et al., 2023; 2024), the Multi-BK-Net achieved a better mean accuracy of 87.01% and a mean sensitivity of 84.25%, representing improvements of at least 1.66% and 2.76%, respectively. Thus, Multi-BK-Net achieved new state-of-the-art results on the predefined TUABEXB evaluation set, setting a new benchmark. Additional results and a more detailed discussion are provided in Appendix A.6.2. Overall, we can see that the Multi-BK-Net outperforms previously reported results on both datasets, in terms of mean accuracy. In addition, Multi-BK-Net achieved a higher mean sensitivity of 83–84%, indicating improved performance for real-world medical applications, particularly for medical screening methods where high sensitivity is crucial for accurately identifying the presence of EEG pathology.

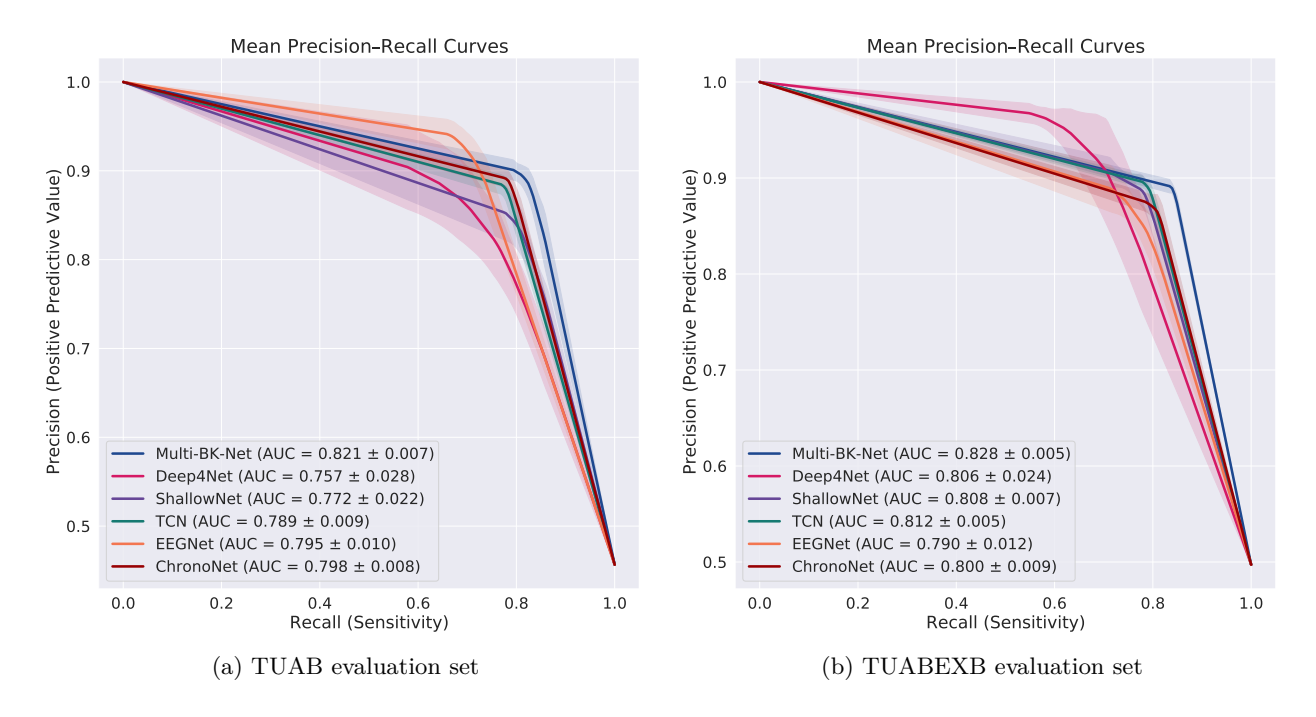


Figure 5: Mean Precision–Recall (PR) curves of our proposed Multi-BK-Net and five baseline architectures on the predefined test sets of the TUAB (left) and of the TUABEXB (right) averaged across 10 independent runs. Each curve represents the mean interpolated PR performance across runs (n=10), with shaded areas indicating ± 1 standard deviation. Mean \pm SD values of the area under the PR curve (PR-AUC) are shown in the legend for each model.

3.6 Ablation Experiments

To further validate the effectiveness of the proposed Multi-BK-Net and to highlight the importance of the multi-scale and multi-branch components in the Multi-BK-Net, we performed several ablation experiments, where we a) compared the performance of the Multi-BK-Net to larger variants of the Deep4Net having the same width or approximately the same size as the Multi-BK-Net ("larger Deep4Net variants"); b) removed four of the five branches of the Multi-BK-Net (Single-Temporal-Kernel Single-Branch Net, STKSBNet, "single temporal kernel + single branch") while changing the number of filters from 7 to 35; and c) used five different temporal kernel lengths but one branch, i.e. concatenating the output of the five temporal convolution layers before the spatial convolution layer (Multi-Temporal-Kernel Single-Branch Net, MTKSBNet, "multiple temporal kernels + single branch"). The results of these experiments can be seen in Table 5 and Table 6, while Appendix A.6.4 provides more details on the ablation experiments, the size of the models (see Table 17) and a more detailed discussion of the results. In comparison to the Multi-BK-Net, "larger Deep4Net variants" achieved statistically significantly lower mean accuracies and mean sensitivities (Table 5), indicating that the superiority of the Multi-BK-Net over the baseline models was not due to the increased model size alone. When compared against our Multi-BK-Net (Table 6), the networks with "single temporal kernel + single branch" and "multiple temporal kernel + single branch" suffered from a statistically significant drop in classification performance, especially in terms of mean accuracies and mean sensitivities, thereby highlighting the importance of these components towards classification.

3.7 Network Interpretation using a UMAP Visualisation

To interpret the proposed network, we extracted the learned features of the last convolution-pooling block of the Multi-BK-Net and visualised them using the Uniform Manifold Approximation and Projection (UMAP) (McInnes et al., 2018) method, which is a dimensionality reduction technique well-suited for visualising high-dimensional data, such as feature representation vectors. Figure 6 shows the UMAP visualisation of

Table 3: Performance comparisons of the Multi-BK-Net with previously reported state-of-the-art deep learning methods on the TUAB dataset. Accuracy (ACC), sensitivity (SENS) and specificity (SPEC) scores are given in %, n.a.: not available. Results marked with \bowtie are reported as balanced accuracy. R: Publicly available reimplementation. Studies marked with \bowtie used data augmentation. Studies marked with \triangleleft used only the first minute of each recording for performance evaluation. Studies marked with \bowtie reported mean results averaged across several independent runs. Results marked with \bowtie are the performance on TUAB using the TUABEXB training (Kiessner et al., 2023) instead of the TUAB training set for training. Results marked with \diamondsuit are averaged across ten runs (n=10).

Study	Architecture	ACC [%]	SENS[%]	SPEC [%]
Schirrmeister et al. (2017a) $\natural \varnothing$	Deep4Net	85.40	75.12	94.13
	ShallowNet	84.50	77.32	90.53
Roy et al. $(2018) \triangleleft \varnothing$	1D-CNN-RNN	82.27	n.a.	n.a.
Roy et al. (2019a) Ø	ChronoNet	86.57	n.a.	n.a.
Gemein et al. (2020) $\not \varnothing$	TCN	86.10	79.70	91.60
	Deep4Net	84.60	75.90	91.90
	ShallowNet	84.10	79.70	87.90
	EEGNet	83.40	72.10	92.90
Western et al. (2021) \varnothing	Deep4Net	85.90	77.00	93.30
Wu et al. $(2021) \triangleleft \varnothing$	IRCNN	87.10	n.a.	n.a.
Khan et al. (2022)	ChronoNet R	81.00	n.a.	n.a.
	ShallowNet	85.00	n.a.	n.a.
	Deep4Net	84.00	n.a.	n.a.
	Hybrid CNN+LSTM	85.00	n.a.	n.a.
Darvishi-Bayazi et al. (2023) ר	Deep4Net	81.64 ⋈	n.a.	n.a.
	ShallowNet	$82.40 \bowtie$	n.a.	n.a.
	TCN	$81.69 \bowtie$	n.a.	n.a.
	EEGNet	$81.40 \bowtie$	n.a.	n.a.
Kiessner et al. (2023) $\natural \varnothing$	Deep4Net	85.51	75.95	93.53
	ShallowNet	84.13	79.84	87.73
	TCN	85.72	78.81	91.53
	EEGNet	84.67	72.94	94.53
	Deep4Net †	84.89	70.95	96.60
	ShallowNet †	85.51	77.30	92.40
	TCN †	86.49	77.06	94.40
	EEGNet †	83.51	77.22	88.80
Yang et al. (2023) ⋈	BIOT	$79.59 \bowtie$	n.a.	n.a.
Kiessner et al. (2024) $\natural \varnothing$	Deep4Net‡	85.29	73.73	95.00
	ShallowNet‡	85.22	76.83	92.27
	TCN‡	86.09	77.70	93.13
	EEGNet‡	83.80	78.41	88.33
Brenner et al. $(2024) \triangleleft$	XceptionTime model	85.10	85.70	84.70
Jiang et al. $(2024) \bowtie$	LaBraM-Huge	82.58 ⋈	n.a.	n.a.
Proposed method $\emptyset\lozenge$	Multi-BK-Net	87.75	83.10	91.93

the learned features. As can be seen in the plot, the representations for the pathological and non-pathological samples form distinct and compact clusters with minimal overlap, indicating that our proposed Multi-BK-Net is very robust in classifying pathological samples and extracts well-classifiable features, which partly explains the good performance of this architecture. Further analysis in Appendix A.6.3 reveals that compared to Multi-BK-Net, the three baseline models (Deep4Net, TCN and ChronoNet) tend to form smaller and more

Table 4: Performance comparisons of the Multi-BK-Net with previously reported state-of-the-art deep learning methods on the TUABEXB dataset. Accuracy (ACC), sensitivity (SENS) and specificity (SPEC) scores are given in %, n.a.: not available. Conventions as in Table 3.

Study	Architecture	ACC [%]	SENS[%]	SPEC [%]
Kiessner et al. (2023) $\natural \varnothing$	Deep4Net	83.94	71.99	95.75
	ShallowNet	84.47	79.32	89.55
	TCN	83.73	77.49	89.91
	EEGNet	82.38	80.79	83.96
Kiessner et al. (2024) $\natural \varnothing$	Deep4Net ‡	85.35	75.27	95.32
	ShallowNet‡	84.58	79.79	89.31
	TCN‡	85.08	79.12	90.98
	EEGNet‡	82.65	81.49	83.80
Proposed method $\emptyset\lozenge$	Multi-BK-Net	87.01	$\bf 84.25$	89.73

Table 5: Ablation experiment "larger Deep4Net variants". Comparison of the classification performance of Multi-BK-Net with larger Deep4Net variants on the predefined TUAB and TUABEXB evaluation sets. Deep4Net as defined in Schirrmeister et al. (2017a;b). Deep4Net35 (No. start filters: 35); Deep4Net47 (No. start filters: 47); Deep4Net48 (No. start filters: 48). Performance metrics are averaged across ten independent runs (n=10). The mean standard error is given in parentheses. ACC: Accuracy, BACC: Balanced accuracy, F2: F2-score, SENS: Sensitivity, SPEC: Specificity. Stars indicate statistically significant differences in performance between the corresponding model variant and the Multi-BK-Net (Bonferronicorrected, one-sided Mann-Whitney U test, p < 0.05: *, p < 0.01: ***, p < 0.001: ***; n=10).

Dataset	Architecture	ACC [%]	BACC [%]	F2 [%]	SENS [%]	SPEC [%]
TUAB	Deep4Net	83.22***	81.92***	71.03***	66.90***	96.93
	Deep4Net35	84.78***	83.63***	74.21***	70.40***	96.87
	Deep4Net47	84.89***	83.90***	75.72***	72.46***	95.33
	Deep4Net48	84.96***	83.94***	75.52***	72.14***	95.73
	Multi-BK-Net	87.75	87.36	84.05	83.10	91.93
TUABEXB	Deep4Net	82.13***	82.04***	71.17***	66.99***	97.09
	Deep4Net35	83.52***	83.45***	74.59***	70.88***	96.02
	Deep4Net47	84.50***	84.44***	76.73***	73.42***	95.46
	Deep4Net48	83.87**	83.80**	75.14***	71.52***	96.09
	Multi-BK-Net	87.01	86.99	85.17	84.25	89.73

dispersed clusters, possibly indicating greater within-class variability or a less precise representation of the pathological class. These results further align with the quantitative performance metrics, such as accuracy and sensitivity, shown in Section 3.4. Overall, the results of the UMAP visualisation of the learned features further support the effectiveness of our method in extracting features and identifying pathological samples.

3.8 Network Interpretation using an Amplitude Gradient Analysis

In this section, we investigate how sensitive the Multi-BK-Net's pathological prediction is to amplitude changes in the input. Previous neurophysiological studies and glossaries have described the most common abnormal EEG patterns, for example, amplitude changes within multiple frequency bands (Amin et al., 2023; Emmady & Anilkumar, 2023; Hoppe, 2018; Kane et al., 2017; Medithe & Nelakuditi, 2016; Tatum & William, 2021). Hence, amplitude changes are useful for EEG classification. To determine how sensitive the Multi-BK-Net prediction is to amplitude changes in different frequency bands, we calculated the gradients of the output with respect to the amplitudes of the input, i.e. the recordings of both the TUAB and TUABEXB evaluation sets (Ancona et al., 2018; 2019; Gemein et al., 2020; Schirrmeister et al., 2017a). The gradients were then grouped by pathological status and averaged over all ten runs. The gradients of the model prediction with

Table 6: Ablation experiments "single temporal kernel + single branch" and "multiple temporal kernels + single branch". Comparison of the classification performance of STKSBNet variants, MTKSBNet variant and Multi-BK-Net on the predefined TUAB and TUABEXB evaluation set. STKSBNet uses a single kernel size (e.g., STKSBNet7: kernel size of 7) and a single branch in the first block. MTKSBNet uses five different kernel sizes, but one branch in the first block. Performance metrics are averaged across ten independent runs (n=10). The mean standard error is given in parentheses. Conventions as in Table 5.

Dataset	Architecture	ACC [%]	BACC [%]	F2 [%]	SENS [%]	SPEC [%]
TUAB	STKSBNet3	84.71***	84.33***	81.00***	79.92***	88.73**
	STKSBNet7	84.13***	83.76***	80.46**	79.44**	88.07***
	STKSBNet10	84.96***	84.57***	81.20**	80.08*	89.07**
	STKSBNet13	86.45**	85.99**	82.17*	80.71**	91.27
	STKSBNet25	86.27**	85.81**	82.00**	80.56**	91.07
	STKSBNet200	86.38***	85.92***	82.09**	80.63**	91.20
	MTKSBNet	86.59**	86.16**	82.55*	81.19*	91.13
	Multi-BK-Net	87.75	87.36	84.05	83.10	91.93
TUABEXB	STKSBNet3	82.73***	82.72***	81.48***	80.93***	84.52***
	STKSBNet7	84.85***	84.83***	82.60***	81.54***	88.12**
	STKSBNet10	86.09**	86.07**	83.76***	82.62***	89.51
	STKSBNet13	85.94**	85.82**	83.58**	82.44**	89.40
	STKSBNet25	85.95***	85.93***	83.65***	82.53***	89.33
	STKSBNet200	86.16**	86.14**	83.62***	82.38***	89.91
	MTKSBNet	86.46	86.44	84.26*	83.19*	89.69
	Multi-BK-Net	87.01	86.99	85.17	84.25	89.73

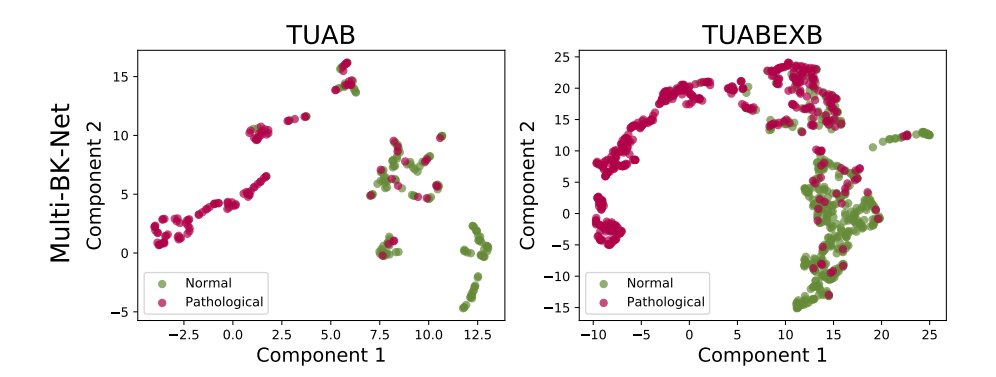


Figure 6: UMAP visualisation of feature representations learned with Multi-BK-Net for pathological and non-pathological recordings on the predefined TUAB (left column) and the TUABEXB (right column) evaluation sets. Pink dots represent the pathological class, while green dots represent the non-pathological class.

respect to the input amplitudes linearly approximate how the prediction of a class behaves in response to changes in the inputs. For example, if the amplitude at a certain channel is changed by a value x, the model output for the class pathological will change approximately by gradient*x. The resulting patterns linearly approximate how changes in input amplitude affect the model's prediction of pathology, indicating which changes in input amplitudes are most informative or interesting with respect to the task of classifying general EEG pathology. In addition, we analysed the clinical EEG reports, which are included in the TUAB and TUABEXB datasets. Figure 7 shows scalp maps of the amplitude gradients across different frequency bands

for the pathological class. The largest absolute values are observed in the delta (0-4 Hz), theta (4-7 Hz) and alpha (8-12 Hz) frequency bands, indicating that the model's pathological prediction is most sensitive to amplitude changes in these specific frequency bands. In particular, in the delta and theta frequency bands, peaks for positive gradients can be seen at temporal (T3, T4) electrode locations. Specifically, an increase in amplitude in the temporal areas led to an increase in the prediction of the pathological class. This localised pattern is also consistent with the clinical EEG reports, which often mention that recordings are classified as pathological because of the presence of non-epileptiform abnormalities, such as diffuse or focal slowing in the theta or delta bands (Emmady & Anilkumar, 2023; Nayak & Anilkumar, 2020). Moreover, the clinical EEG reports often cite the "absence of posterior dominant rhythm" as a reason for pathological labelling. Similarly, a negative gradient peak in the alpha band was observed in the occipital brain region, indicating that the predicted probability of the pathological class decreases as the amplitude of the alpha frequency at the occipital electrode locations increases, which, in turn, suggests the presence of the PDR. Overall, the results align with current neurophysiological knowledge on pathological EEG patterns, pathological patterns identified by human experts in clinical EEG reports, as well as recent studies that implicate the role of low-frequency oscillations in CNNs' classification of general EEG pathology (Gemein et al., 2020: Nahmias & Kontson, 2020; Schirrmeister et al., 2017a).

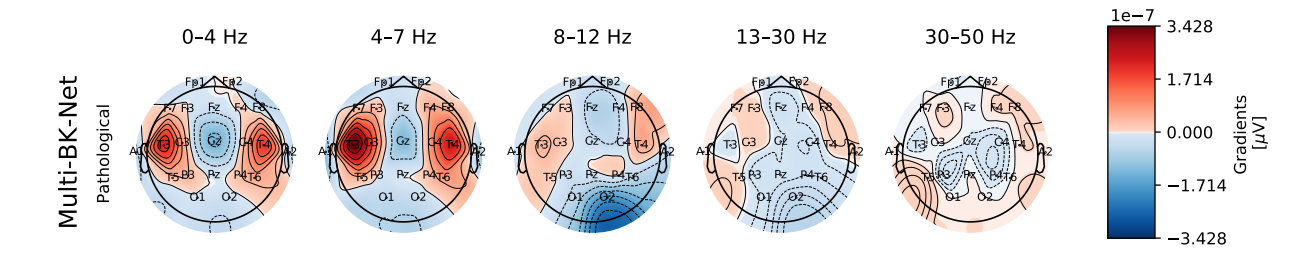


Figure 7: Gradients with respect to the input amplitudes for the pathological class with respect to different frequency bands for the Multi-BK-Net on the combined TUAB and TUABEXB evaluation sets. Delta (0-4 Hz), theta (4-7 Hz), alpha (8-12 Hz), beta (13-30 Hz) and low gamma (30-50 Hz) frequency bands. The red colour indicates positive gradients, while the blue colour indicates negative gradients for the pathological class. Scalp maps are scaled to the absolute maximum value. However, the amplitude gradient results reflect the behaviour of the trained model, and any interpretation of the data itself must be made carefully (Schirrmeister et al., 2017b).

3.9 Insights from the Textual EEG Reports

To better understand what kind of EEG recordings are challenging for our Multi-BK-Net to classify, we qualitatively analysed the textual EEG reports of each recording that was falsely classified. In particular, for each run of our Multi-BK-Net, we identified all false-positive and false-negative recordings and extracted the corresponding EEG reports. In total, 147 pathological recordings (TUABEXB: 116 recordings; TUAB: 31 recordings) were falsely classified as non-pathological (false negatives, FN), while 139 non-pathological recordings (TUABEXB: 113 recordings; TUAB: 26 recordings) were falsely classified as pathological (false positives, FP). We performed a qualitative analysis of the clinical EEG reports independently for both FN and FP, focusing on the impression and clinical correlation sections.

The qualitative analysis of the FN clinical EEG reports reveals several commonalities due to which the Multi-BK-Net might incorrectly classify them as non-pathological: i) Failure to detect subtle, small, mild abnormalities: Most notably, terms such as "small amount", "very mildly" or "subtle" were used to describe EEG abnormalities that, while not overtly prominent, were still significant enough to be noted clinically. It is possible that this subtlety of change caused the classification errors ("a small degree of background organisation", "this is a very subtle abnormal EEG", "some subtle focal slowing", "this is a mildly abnormal EEG"). ii) Missing single, infrequent or intermittent events: In some cases, single or infrequent events were the reasons why an EEG recording was rated abnormal by the human expert ("A single generalized discharge noted in stage II sleep.", "infrequent, shifting focal slowing is present.", "rare bursts of shifting

slowing"). Abnormalities described as "infrequent" or "single" could be missed by the CNNs, as the model might average them out or consider them statistical outliers. It is also possible that these events are not included in the data, as we only used the first 21 minutes of the recordings for training and evaluation (see Section 3.1). iii) Misinterpretation of "nonspecific" abnormalities: Within the FN EEG reports, many abnormalities listed in the impression section are described as "etiologically nonspecific". This implies that even while an abnormality is present, it does not clearly indicate a specific disease. It is therefore possible that the CNN might struggle to classify these less specific but still abnormal findings as being within the range of normal variability, resulting in a false negative prediction. iv) Lack of clinical context: In EEG reports for FN recordings, clinicians include additional information to help interpret EEG patterns as pathological, such as patients' age, current medications, or clinical history. For example, experts often correlate observed EEG patterns with the patient's clinical history. Thus, some nonspecific abnormalities are rated as indicating pathology based on the clinical history of the patient ("The overall record is relatively unremarkable. The 7.8 Hz activity is of unclear significance and may represent a normal variant. Given the past history of neurologic pathology, however, it may also represent evidence of an underlying diffuse disturbance of cerebral function."). In contrast, without a clinical context, the CNN classifies these recordings as normal. Also, the term "age" is consistently used as a factor in determining EEG patterns as pathological, illustrating an age-dependent interpretation ("very mildly abnormal EEG for an adult of this age." "This EEG is just outside of the range of normal for a subject of this age"). This suggests that certain physiological variations are rated as pathological within specific age groups. In addition, clinicians often list EEG patterns that could be due to medication ("The minimal excess theta identified above is nonspecific, but could be associated with this patient's medications.", "The findings described above could be due to this patient's medications.", "The slowing of the alpha rhythm may be due to the patient's medications."). It is possible that CNN can recognise medication-induced patterns (Nahmias et al., 2020) and thus classify recordings as non-pathological. Moreover, reports often mentioned terms such as "sleep" or "drowsiness", indicating that the experts used the patient's (partial) sleep during the recording to interpret the EEG. During drowsiness, eye movement artefacts, such as blinks and slow or roving eye movements, are commonly observed and can complicate EEG analysis (Mohammedi et al., 2023).

Qualitative analysis of FP clinical EEG reports reveals several commonalities that may cause Multi-BK-Net to misclassify normal recordings as pathological: i) Limitations of routine EEG: The primary reasons listed for "normal" classification are often "the absence of definite epileptiform activity or significant focal abnormalities during routine recording". Frequently, clinical suspicion remains high despite a normal routine EEG, and further comprehensive evaluation is recommended in the clinical EEG reports. The FP reports frequently emphasised the nuances and limitations of EEG interpretations, particularly when dealing with conditions such as epilepsy or seizures. While reports often conclude the findings described as "essential normal" or "within normal limits", they consistently include reservations and recommendations for further clinical correlation ("Midly diffuse cerebral dysfunction cannot be ruled out", " A normal routine EEG does not exclude the diagnosis of epilepsy.", "This is an essentially normal awake and drowsy 1-hour EEG, though a mild diffuse cerebral dysfunction cannot be ruled out."). ii) Misinterpretation of nonspecific findings: Terms like "etiologically nonspecific" mentioned in the EEG reports indicate abnormal findings ("There were no specifically pathological sharp waves observed.","The amplitude is mildly high for the patient's age, but this is nonspecific."). The CNN might detect these abnormal patterns but cannot recognise their nonspecific nature, leading to a false-positive classification. iii) Lack of clinical context: As noted above in our FN analysis, the EEG reports of the FP also frequently include contextual information about the patient's age, state (awake, drowsy, sleep), medication and clinical history to classify the recording as non-pathological. For example, using information from the patient's clinical history, experts correlate EEG patterns with known skull defects and rate the breach rhythm as a benign variant secondary to structural changes. In contrast, without the contextual information of a pre-existing skull defect, the CNN might classify these patterns as abnormal rather than a benign variant. Also, EEG patterns are rated as benign variants based on the patient's age ("EEG within normal limits for age", "within in normal limits", "EEG at the limits of normal for a subject of this age"). While these are not explicitly listed as reasons for an abnormal EEG, reports often mention "mild diffuse cerebral dysfunction" or "minor shifting slowing in drowsiness", indicating that even subtle non-epileptiform findings have been noted and are frequently correlated with the patient's history ("Occasional mild independent bitemporal slowing is not considered abnormal in the patients above 65 years of age."). While human experts rate abnormalities as clinically insignificant based on additional context, the CNN might identify them as abnormal patterns in the absence of such context. This further supports the assumption that the lack of clinical context is a crucial factor in the CNN's misclassification of EEG recordings. Information about sleep and drowsiness indicates that experts used the fact that the patients were (partially) asleep during the recording to interpret the EEG ("EEG at the limits of normal primarily in drowsiness." "The EEG is remarkable for excess drowsiness. However, when the patient can be awakened, her pattern is within normal limits", "This EEG is compatible with a sedated, sleep pattern."). During drowsiness, physiologically normal but diagnostically challenging changes occur that can closely resemble pathological findings, such as slowed background frequencies and increased slow eye movements, complicating automated or visual EEG analysis (Amin et al., 2023; Strijbis et al., 2022). In contrast, the CNN lacks access to patient information, including the patient's state, age, medications, and clinical history. As a result, the model may misclassify age-appropriate or medication-related variations as pathological abnormalities. iv) Presence of large artefacts: In some FP reports, the presence of large artefacts in the EEG obscuring significant portions of the EEG channels is given as the reason why features are under-recognised or cannot be reliably identified and thus additional studies are recommended ("This EEG include electrode artifact on the right as well as an inability to adequately stimulate the patient. Consequently focal features may be under recognised."). It is possible that the Multi-BK-Net can recognise abnormal EEG patterns despite the presence of large artefacts (Kalita et al., 2024; Tjepkema-Cloostermans et al., 2025).

Overall, this qualitative review suggests that the Multi-BK-Net struggles to identify context-dependent abnormalities. Clearly, our Multi-BK-Net, which was only trained on the EEG signal, does not have access to this contextual information. This results in the model being at a disadvantage in comparison to clinicians, emphasising the potential benefit of incorporating contextual information, such as age and vigilance, into the training and classification approach. Moreover, integrating ratings from multiple experts to train and evaluate the model using averaged ratings, so-called "fuzzy labels", which represent a probability of pathology, might further enhance performance and better reflect diagnostic uncertainty in EEG interpretation (Stephansen et al., 2018). For example, converting classification tasks to probabilistic predictions using fuzzy labels for ambiguous samples (Xu et al., 2024) can help to identify when a model is less specific, guiding clinicians on which samples might require additional manual review (Kang et al., 2021). For a more detailed discussion, see Section 4.

3.10 Cross-Institutional Generalisation Performance

Although TUABEXB is larger and more diverse than the TUAB, both datasets originate from the same institution, the Temple University Hospital (TUH), raising concerns about cross-institutional generalisation. At the same time, the possibilities to empirically investigate generalisation performance across multiple datasets are still limited to date due to the lack of publicly available datasets labelled for general EEG pathology classification. One open-source dataset for general EEG pathology classification that is not derived from the TUH and that contains the same subset of 21 EEG channels as the TUAB and TUABEXB dataset is the NUST-MH-TUKL (NMT) EEG dataset (Khan et al., 2022). The NMT contains 2,417 recordings collected from a South Asian demographic, comprising 2,417 unique patients at the Pak-Emirates Military Hospital. The NMT training set is imbalanced, with 325 pathological and 1907 non-pathological recordings. The NMT evaluation set contains 90 pathological and 95 non-pathological recordings (for more information about the dataset, please refer to Khan et al. (2022)).

To evaluate the cross-institutional generalisation performance, we assessed the generalisation performance of the Multi-BK-Net and all baseline models trained on the TUABCOMB on the predefined evaluation set of the NMT. For more details on performance evaluation, see Section 3.3. We preprocessed the NMT evaluation set data as described in Section 3.1. We observed significant performance degradation across all architectures when applied to the NMT dataset, as shown in Table 7, but less so for our proposed Multi-BK-Net compared to the baseline CNNs. Compared to the five baseline architectures, Multi-BK-Net achieved the highest accuracy, balanced accuracy, and F2-score. Although Deep4Net and ShallowNet demonstrated slightly higher sensitivity, their specificity was considerably lower. Both models achieved an accuracy of around 50%, suggesting they perform at chance level. Overall, all models performed significantly worse on the NMT than on the TUAB and TUABEXB evaluation sets. This also accords with previous studies, which

Table 7: Cross-institutional generalisation performance comparison between our proposed Multi-BK-Net and five baseline architectures, which were trained on TUH data and applied to the predefined NMT evaluation set. Mean scores are averaged across ten independent runs (n=10). ACC: Accuracy, BACC: Balanced accuracy, F2: F2-score, SENS: Sensitivity, SPEC: Specificity. The standard deviation is given in parentheses. Stars indicate statistically significant differences in performance between the corresponding baseline model and the Multi-BK-Net (Bonferroni-corrected, two-sided Mann-Whitney U test, p < 0.05: *, p < 0.01: **, p < 0.01: **, p < 0.00: ***, p < 0.00: **, p < 0.00: **, p < 0.00: ***, p < 0.00: ***

Architecture	ACC [%]	BACC [%]	F2 [%]	SENS [%]	SPEC [%]
Deep4Net	$49.73(\pm 2.25)***$	50.26(±1.86)***	$69.6(\pm 28.23)$	$82.78(\pm 35.51)$	$17.74(\pm 37.54)$
ShallowNet	$52.02(\pm 6.19)**$	$52.62(\pm 5.76)**$	$75.85(\pm 16.16)$	$89.0(\pm 24.24)$	$16.24 \ (\pm 34.44)$
TCN	$54.75(\pm 2.84)***$	$54.03(\pm 2.94)***$	$11.86(\pm 10.32)***$	$10.0(\pm 9.04)***$	$98.06(\pm 3.39)***$
EEGNet	$50.82(\pm0.0)***$	$50.0(\pm0.0)***$	$0.0(\pm0.0)***$	$0.0(\pm0.0)***$	$100.0(\pm 0.0)***$
ChronoNet	$58.20(\pm 4.41)**$	$57.76(\pm 4.61)***$	$33.62(\pm 19.94)***$	$33.62(\pm 19.94)***$	$84.19(\pm 14.35)**$
Multi-BK-Net	$67.32\ (\pm 2.3)$	$67.46\ (\pm2.17)$	$73.12\ (\pm 3.65)$	$75.89\ (\pm6.18)$	$59.03\ (\pm 10.28)$

showed that the performance of deep learning approaches trained on the TUAB degrades significantly when they are evaluated on the NMT without any prior exposure to the target dataset and vice versa (Darvishi-Bayazi et al., 2023; Khan et al., 2022). Khan et al. (2022) have evaluated the generalisation performance of Deep4Net and ShallowNet on the NMT after training the models on the TUAB dataset and observed a degradation in performance (48-50% accuracy), indicating a distribution shift. In addition, the authors discussed several factors that may have contributed to this cross-institutional variability, including differences in demographics and the use of other hardware for data collection (for a more detailed discussion of these factors, please refer to Khan et al. (2022)). Similarly, Darvishi-Bayazi et al. (2023) observed performance degradation in four CNNs trained on the TUAB when applied to the NMT evaluation set, and vice versa. On the other hand, for training and testing models on the NMT, the accuracies are in the range of 70-80% (Darvishi-Bayazi et al., 2023; Khan et al., 2022). Table 8 summarises the comparison of cross-dataset generalisation performance between our Multi-BK-Net and other methods reported in previous studies. When compared with previously reported results shown in Table 8, the Multi-BK-Net demonstrated superior accuracy of 67.32%, compared with the cross-institutional generalisation performance reported by other studies, which ranged from 45.00% to 63.04%. Together, these results suggest that current deep learningbased approaches are at risk of institutional bias, which limits their generalisability and could potentially lead to differences in performance based on demographics, technical and environmental factors (Bomatter & Gouk, 2025; Saab et al., 2020; Tjepkema-Cloostermans et al., 2025). Furthermore, Khan et al. (2022) demonstrated that fine-tuning can mitigate the impact of cross-institutional variability. Darvishi-Bayazi et al. (2023) also observed that pretraining models on the TUAB and fine-tuning them on NMT enhances the performance on the NMT evaluation set, but at the same time significantly reduces the performance on the TUAB evaluation set, indicating a negative transfer. This shows that there is still room for improvement in transferring knowledge from TUH to NMT. Overall, these results emphasise the need for strategies to mitigate these challenges, as well as for more publicly available datasets from multiple institutions. We discuss this topic further in Section 4.

4 Discussion and Conclusion

In this work, we demonstrated that through the incorporation of a) multiple temporal kernel lengths based on five clinically relevant frequency bands and b) multiple parallel branches within the first convolution-pooling block, our proposed CNN can outperform five baseline methods in classifying general EEG pathology, while being more effective at capturing the heterogeneity of pathological EEG recordings than their single-scale counterparts. To that end, our Multi-BK-Net extracted task-discriminative long-term and short-term spatiotemporal EEG features for general EEG pathology classification, achieving higher performance than comparable deep end-to-end state-of-the-art methods on two public datasets. The ablation experiments further highlight the effectiveness of the multi-branch, multi-scale components in our proposed CNN archi-

Table 8: Cross-institutional generalisation performance comparisons of the Multi-BK-Net with state-of-the-art deep learning methods previously reported, which were trained on TUH data and applied to the NMT dataset. Accuracy (ACC), sensitivity (SENS) and specificity (SPEC) scores are given in %, n.a.: not available. Conventions as in Table 3.

Study	Architecture	Trained on	ACC [%]	SENS[%]	SPEC [%]
Khan et al. (2022)	TUAB	Deep4Net	48.00	n.a.	n.a.
	TUAB	ShallowNet	45.00	n.a.	n.a.
Darvishi-Bayazi et al. (2023) ר	TUAB	Deep4Net	62.77⋈	n.a.	n.a.
	TUAB	ShallowNet	$62.02\bowtie$	n.a.	n.a.
	TUAB	TCN	63.04	n.a.	n.a.
	TUAB	EEGNet	61.45 \bowtie	n.a.	n.a.
Proposed method $\emptyset \Diamond$	TUABCOMB	Multi-BK-Net	67.32	75.89	59.03

tecture. Additionally, the UMAP visualisation of the learned features shows that the Multi-BK-Net forms more compact and distinct features than the baseline CNNs, which partly explains the good performance of this architecture. Moreover, the correspondence between the model's sensitivity to localised patterns of amplitude changes in different frequency bands and both current neurophysiological knowledge of pathological EEG patterns and the pathological patterns identified by human experts in the clinical EEG report increased the reliability of the method.

This work addresses a significant gap in CNN approaches, which has hindered their development into a robust and generalisable approach for deep learning-based general EEG pathology classification. While CNN-based methods have shown state-of-the-art performance on the task of general EEG pathology classification (Darvishi-Bayazi et al., 2023; Gemein et al., 2020; Khan et al., 2022; Kiessner et al., 2023; 2024; Van Leeuwen et al., 2019; Western et al., 2021; Wu et al., 2021), their generalisation performance is limited mainly due to the high intra- and inter-subject variability of the EEG signal (Lashgari et al., 2020; Nahmias et al., 2019; Schirrmeister et al., 2017b), the heterogeneity of general EEG pathology patterns (Emmady & Anilkumar, 2023; Nayak & Anilkumar, 2020) and the use of one limited evaluation set (Kiessner et al., 2023; Poziomska et al., 2024). We demonstrated here that an appropriately constructed CNN, incorporating a multi-scale and multi-branch network design, can achieve more accurate and reliable classification performance than state-of-the-art CNN methods. This is evident through the high mean evaluation accuracies and sensitivities achieved by our method on two public datasets, as well as shown in our ablation experiments, thus highlighting its practical effectiveness in classifying general EEG pathology. Our model addresses the challenges inherent to EEG, including its heterogeneity.

An improvement in evaluation sensitivity demonstrates further practical gains of our method. Our method achieved mean sensitivities of 83.10% and 84.25% on the TUAB and TUABEXB, respectively, outperforming all other approaches by 3.26% and 2.76%, while attaining high classification accuracies. In comparison to the baseline architectures, Multi-BK-Net achieved the highest mean sensitivities at a fixed specificity of 95% on both test sets (82.78% and 84.25%). The significance of this result lies in applications such as deep learning-based EEG classification or clinical decision support systems in clinical practice, for which a high and robust sensitivity is crucial to ensure the accurate identification of EEG pathology. In deep learningbased clinical EEG analysis, high accuracy and sensitivity are of most significant importance because they directly translate to improved patient outcomes, reduced diagnostic errors, and enhanced clinical efficiency. High sensitivity ensures that critical events, such as seizures, are not missed, preventing potential patient harm and delays in treatment (Iešmantas & Alzbutas, 2020; Wang et al., 2023). High accuracy is crucial for reliable diagnosis and proper patient management. Thus, even minor improvements in these metrics are valuable because they can significantly reduce false detections, achieve expert-level agreement, and expedite physician analysis, making the systems more trustworthy and practical for everyday clinical use (Hogan et al., 2025; King-Stephens, 2024; Saab et al., 2020). Such advancements can also lead to better trade-offs between sensitivity and false-positive rates, allowing clinicians to tune the system for optimal performance in specific scenarios (Wang et al., 2023). To be applied in real-world clinical practice, the proposed method must be reliable and utilise robust, well-classifiable features to achieve high performance across patients. That is why the evaluation on a larger, more heterogeneous dataset was central in this work. Moreover, we interpreted the model using an amplitude gradient study, which shows that the model's pathological prediction is sensitive to localised patterns of amplitude changes, aligning well with current neurophysiological knowledge of abnormal EEG patterns (Emmady & Anilkumar, 2023; Kane et al., 2017; Nayak & Anilkumar, 2020) and pathological patterns mentioned in clinical EEG reports. In addition, the UMAP visualisation of the learned features further supports the effectiveness of our method in extracting features and identifying pathological samples.

While our findings show promise, the generalisability of these results is subject to certain limitations. For instance, the current study is based on data obtained from a single institution, i.e. Temple University Hospital (TUH). Although using public datasets such as the TUH EEG Corpus (TUEG), which was collected directly in a clinical setting over 14 years and exhibits wide variation in essential parameters such as patient age and diagnosis, is a vital first step in developing deep learning methods that represent the variability of EEG data in real-world applications, it is important to acknowledge the potential for institutional bias and demographic performance disparities. Indeed, these challenges have already been demonstrated in evaluating the cross-institutional generalisation performance between the datasets from the Temple University Hospital and the NMT dataset from the Pak-Emirates Military Hospital (Darvishi-Bayazi et al., 2023; Khan et al., 2022, see also Section 3.10). Darvishi-Bayazi et al. (2023) highlighted the challenges associated with negative transfer, while also emphasising some key components to overcome distribution shifts and potential spurious correlations. Building on the insights into cross-dataset transfer learning provided by Darvishi-Bayazi et al. (2023), further studies should explore additional transfer learning strategies. To this end, diverse datasets from multiple institutions and countries are needed to better understand institutional bias and the risks of demographic disparities. Also, while our proposed method demonstrates strong performance on large, public datasets, the absence of validation in a real-world clinical setting (e.g., clinician feedback or pilot deployment) represents another limitation, thereby limiting conclusions about the model's practical adoption or usability. The issues of cross-institutional generalisability and validation in real-world clinical settings are intriguing and therefore an essential next step to establish the practical adoption and usability of multi-branch, multikernel CNNs for general EEG pathology classification.

Despite its limitations, this study certainly contributes to the advancement of deep learning-based general EEG pathology classification. This paper describes our efforts to improve the generalisation performance and robustness of CNN methods for general EEG pathology classification. To this end, we proposed the Multi-BK-Net, a novel network architecture with multiple temporal kernels and multiple branches in the first block to suit the challenges of variability and heterogeneity inherent in EEG signals. Overall, our results demonstrate the effectiveness of multi-branch, multi-scale CNN solutions in classifying general EEG pathology by discovering task-relevant features in the recorded brain activity, which can better capture the heterogeneity in pathological samples (Altaheri et al., 2023b; Altuwaijri et al., 2022; Cai et al., 2024; Jia et al., 2021; Liu & Yang, 2021; Liu et al., 2023; Riyad et al., 2020; Siddiqa et al., 2024; Yang et al., 2021; Zhu et al., 2023). Our method is a better fit for deep learning-based general EEG pathology classification than traditional single-scale CNN methods. It thus has significant potential to improve the practicality of deep learning-based general EEG pathology classification.

Further performance improvements could be achieved by exploiting advances in the training of CNNs. Some of these include the incorporation of (self-)attention methods (Altaheri et al., 2023; Liu et al., 2024; Petit et al., 2021) or increasing the size and diversity of the data by using data from multiple sources (Aerts et al., 2017; Poziomska et al., 2024; Schinkel et al., 2023). In addition, the use of medications by most patients poses an additional challenge for deep learning-based EEG classification and should be addressed in further studies (Kamrud et al., 2021). Future research could use Large Language Models to extract more information from clinical EEG reports, providing more valuable insights, clearer explanations of diagnoses, and additional information about the clinical context. Additionally, inspection of the textual reports emphasised the importance of integrating contextual information, such as medication use or clinical history. As human experts also consider patient-specific information (e.g. age, medication, clinical history) during EEG analysis (Beuchat et al., 2021; Kane et al., 2017; Limotai et al., 2020), future research could extend our methods to incorporate contextual information about the patients' age, medication and clinical history, leveraging approaches similar to those explored by Joo et al. (2023), Samak et al. (2023) and Thapa et al. (2024).

Moreover, there is abundant room for further progress in determining whether the use of multi-rater annotations or fuzzy labels can enhance model performance and more accurately reflect diagnostic uncertainty in general EEG pathology classification. Multi-rater annotations can enhance performance for several key reasons. First, consensus annotations from multiple experts can serve as a "gold standard" to train and evaluate the performance of deep learning approaches in clinical EEG classification (Hogan et al., 2025) and to provide a more reliable ground truth than single-expert labelling (Stephansen et al., 2018). Second, high-quality, labelled data is essential for developing accurate and reliable deep learning models. The use of labels from multiple expert raters enables the creation of high-quality datasets, which, in turn, allow models to achieve human-expert-level performance across various clinical tasks (Ge et al., 2021). Multiple raters can be used to empirically estimate human-level performance. It can also improve label quality by reducing data noise. A systematic optimisation of labelling quality might even help to overcome the current asymptotic limits of predictive accuracy observed in general EEG pathology classification (Darvishi-Bayazi et al., 2023; Kiessner et al., 2024; Poziomska et al., 2024), and hence represent promising avenues for exploration. Moreover, imperfect or ambiguous annotations from a diverse group of experts can be effectively used to train deep learning models. For example, Saab et al. (2020) have shown that combining various ratings, even if individually imperfect, can improve seizure detection performance. Furthermore, multi-rater annotations reflect diagnostic uncertainty. Annotations from multiple raters can be used to quantify inter-rater agreement (Beuchat et al., 2021), thereby implicitly quantifying the degree of diagnostic uncertainty among human experts, against which deep learning models can be compared. Reflecting diagnostic uncertainty is also essential for clinical adoption. Understanding inter-rater variability provides a benchmark for evaluating the performance of deep learning approaches relative to the range of human expert opinions (Hogan et al., 2025). For example, model performance can be compared with human inter-rater agreement to measure the impact of replacing an expert with deep learning models on overall agreement (Hogan et al., 2025). The potential of deep learning-based approaches for clinical support is evident when the models align with expert ratings (Tjepkema-Cloostermans et al., 2025).

Lastly, with multi-rater annotations, fuzzy labels and fuzzy logic systems can be used for model training and evaluation. These systems provide probabilistic rather than binary classifications of pathology, introducing ambiguity and uncertainty into EEG interpretations. The use of fuzzy labels can improve model robustness and performance, particularly in challenging scenarios. Fuzzy logic systems are well-suited for handling the noise, nonlinearity, and high variability inherent in EEG signals (Ahmadieh et al., 2025; Sorkhi et al., 2022). Also, fuzzy labels can lead to enhanced feature extraction and classification, resulting in superior accuracy, precision, recall, and F-scores compared to single-rater label models (Gu & Cao, 2020; Shoeibi et al., 2022). For example, fuzzy-logic-based classification algorithms have achieved improved performance and specificity in classifying Alzheimer's disease, Mild Cognitive Impairment, and healthy subjects (Amezquita-Sanchez et al., 2021). Furthermore, fuzzy labels better reflect diagnostic uncertainties. The use of fuzzy logic systems enables the representation of partial truths and degrees of membership in categories (Hu et al., 2021), making them an ideal framework for capturing the inherent ambiguities and variabilities in EEG analysis. In addition, they can be used for uncertainty quantification, which can be incorporated into models to handle uncertainty (Ahmadieh et al., 2025). This enables higher tolerance to noisy conditions and addresses uncertainty due to the high variability of EEG patterns over time (Sorkhi et al., 2022). Recently, there has been increased interest in using uncertainty quantification in deep learning-based methods for medical applications to address diagnostic uncertainty (de Jong et al., 2025). For example, converting classification tasks to probabilistic predictions using fuzzy labels for ambiguous samples (Xu et al., 2024) can help to identify when a model is less specific, guiding clinicians on which samples might require additional manual review (Kang et al., 2021). The fact that deep learning models cannot currently represent predictive uncertainty is a recognised challenge (Prince et al., 2023) that warrants further investigation. In summary, previous studies indicate that the use of multi-rater annotations and fuzzy labels can significantly improve model performance and better reflect diagnostic uncertainty in EEG interpretation. By providing richer, more robust training data, multi-rater annotations can help to improve model performance. In addition, multi-rater annotations are essential for evaluating models against human-level performance and for understanding the inherent variability in human EEG analysis. Overall, multi-rater annotations and fuzzy labels are valuable strategies that help build more robust, expert-aligned models by capturing the full scope of human interpretations and intrinsically modelling the ambiguity and inherent uncertainty in EEG signals, leading to more nuanced predictions and potentially

enhanced accuracy, especially in clinically challenging scenarios. Together, these approaches contribute to the creation of more reliable and clinically relevant deep learning-based systems for clinical EEG analysis. A natural progression of this work is therefore to integrate consensus labels or probabilistic (fuzzy) targets, which could mitigate label noise issues, improve model performance, and better reflect diagnostic uncertainty in EEG interpretation.

More broadly, research is also needed to validate deep learning-based EEG classification systems in real-world clinical settings. While large, heterogeneous public datasets such as the TUEG are a valuable source for the initial development and evaluation of deep learning methods for general EEG pathology classification, their translation into impactful clinical (support) systems requires thorough real-world validation (El Arab et al., 2025). Pilot studies and validation in real-world clinical settings with clinician feedback are essential before these systems can be reliably applied in everyday clinical practice (El Arab et al., 2025; Hosny et al., 2022; Jacobson & Krupinski, 2021). One way to do this is through pilot studies, which assess the methods utility, safety, and effectiveness in supporting clinical decision-making and improving patient care. This step ensures practical utility (Zając et al., 2024), clinician usability (McNamara et al., 2024; Olaoye et al., 2024), effectiveness, robustness to EEG variability and other factors (Kelly et al., 2019), and fosters trust (Beger, 2025; Olaoye et al., 2024; Zajac et al., 2024). However, deploying deep learning-based methods in clinical practice requires careful consideration of potential risks and challenges. One is the risk of automation bias, where clinicians might rely on model predictions, potentially resulting in missed pathology, if models are deployed without calibrated thresholds and robust human-in-the-loop guardrails (McLaren et al., 2025; Wang et al., 2020; West et al., 2023). To mitigate these risks, the interpretability of the models is essential, as it allows for explaining predictions and thereby supports clinical judgement, enhances clinician performance, and is particularly valuable in ambiguous cases (Hasan et al., 2025; Mansilla et al., 2024). Another risk is the institutional bias for models trained on a database from a single institutional site, limiting their generalisability and potentially leading to demographic performance disparities (Bomatter & Gouk, 2025; Saab et al., 2020; Tjepkema-Cloostermans et al., 2025). Factors, such as different demographics and the use of various hardware for data collection, can contribute to these generalisation challenges (Darvishi-Bayazi et al., 2023; Khan et al., 2022). The generalisability of models across diverse multi-institutional datasets remains to be elucidated. Addressing these risks and biases requires data governance and handling protocols. This includes prioritising ethical data sharing, "findable, accessible, interoperable and reusable" (FAIR) principles, and standardised data organisation (Ahluwalia, 2021; Chiang et al., 2021; Ienca et al., 2022; Ochang et al., 2022; Reer et al., 2023). Another clinical challenge is mitigating model drift over time. For example, changes in clinical practice, data-collection equipment, or demographic changes in the patient population can progressively degrade model performance (Aguilar et al., 2024; Chen et al., 2022; Davis et al., 2022; Gonzalez-Gonzalo et al., 2022; Vela et al., 2022; Vishwanath et al., 2023). Strategies such as evaluating model robustness under realistic distribution shifts, continuous learning, and proactive detection of detrimental data shifts are vital for maintaining the reliability and validity of deep learning-based EEG analysis systems (Ceccon et al., 2024; Feng et al., 2022; Gonzalez-Gonzalo et al., 2022; Guan et al., 2025). Therefore, future clinical implementation must prioritise transparent reporting of model limitations, establish clear protocols of human oversight, and develop adaptive systems that continually learn and remain robust to inherent variability and biases in real-world clinical data (AbuAlrob et al., 2025; Mourid et al., 2025). Nevertheless, real-world application testing is pivotal for validating deep learning methods and is an essential step for translation into everyday clinical practice. Future research should focus on developing methods for seamless clinical integration (Ennab & Mcheick, 2024; Zając et al., 2024), optimising user-interface designs (McNamara et al., 2024; Olaoye et al., 2024; Zając et al., 2024), exploring adaptive learning strategies for continuous improvement against "long-tail" cases (Choudhury & Asan, 2020; Feng et al., 2022) and establishing a comprehensive framework for ongoing performance monitoring and trustworthiness evaluation across diverse real-world settings (Choudhury & Asan, 2020; Feng et al., 2022; Saenz et al., 2024).

References

Majd A AbuAlrob, Adham Itbaisha, and Boulenouar Mesraoua. Unlocking new frontiers in epilepsy through ai: From seizure prediction to personalized medicine. *Epilepsy & Behavior*, 166:110327, 2025.

- Marc Aerts, Girma Minalu, Stefan Bösner, Frank Buntinx, Bernard Burnand, Jörg Haasenritter, Lilli Herzig, J. André Knottnerus, Staffan Nilsson, Walter Renier, Carol Sox, Harold Sox, and Norbert Donner-Banzhoff. Pooled individual patient data from five countries were used to derive a clinical prediction rule for coronary artery disease in primary care. *Journal of Clinical Epidemiology*, 81:120–128, 2017. ISSN 0895-4356. doi: https://doi.org/10.1016/j.jclinepi.2016.09.011. URL https://www.sciencedirect.com/science/article/pii/S089543561630484X.
- Isabelle Aguilar, Thomas Bersani-Veroni, Luis Fernando Herbozo Contreras, Armin Nikpour, Damien Querlioz, and Omid Kavehei. Metaplastic-eeg: continuous training on brain-signals. *medRxiv*, pp. 2024–05, 2024.
- Mahika Ahluwalia. Legal governance of brain data derived from artificial intelligence. Voices in Bioethics, 7, 2021.
- Hajar Ahmadieh, Farnaz Ghassemi, and Mohammad Hassan Moradi. Eeg signals classification related to visual objects using long short-term memory network and nonlinear interval type-2 fuzzy regression. *Brain Topography*, 38(2):20, 2025.
- Takuya Akiba, Shotaro Sano, Toshihiko Yanase, Takeru Ohta, and Masanori Koyama. Optuna: A next-generation hyperparameter optimization framework. In *Proceedings of the 25th ACM SIGKDD International Conference on Knowledge Discovery & Data Mining*, KDD '19, pp. 2623–2631, New York, NY, USA, 2019. Association for Computing Machinery. ISBN 9781450362016. doi: 10.1145/3292500.3330701. URL https://doi.org/10.1145/3292500.3330701.
- Mohammad Ahmad A. Al-Ja'afreh, Geev Mokryani, and Bilal Amjad. An enhanced cnn-lstm based multi-stage framework for pv and load short-term forecasting: Dso scenarios. *Energy Reports*, 10: 1387–1408, 2023. ISSN 2352-4847. doi: https://doi.org/10.1016/j.egyr.2023.08.003. URL https://www.sciencedirect.com/science/article/pii/S2352484723011447.
- Hamdi Altaheri, Ghulam Muhammad, and Mansour Alsulaiman. Physics-informed attention temporal convolutional network for eeg-based motor imagery classification. *IEEE Transactions on Industrial Informatics*, 19(2):2249–2258, 2023a. doi: 10.1109/TII.2022.3197419.
- Hamdi Altaheri, Ghulam Muhammad, Mansour Alsulaiman, Syed Umar Amin, Ghadir Ali Altuwaijri, Wadood Abdul, Mohamed A Bencherif, and Mohammed Faisal. Deep learning techniques for classification of electroencephalogram (eeg) motor imagery (mi) signals: A review. *Neural Computing and Applications*, 35(20):14681–14722, 2023b.
- Ghadir Ali Altuwaijri, Ghulam Muhammad, Hamdi Altaheri, and Mansour Alsulaiman. A multi-branch convolutional neural network with squeeze-and-excitation attention blocks for eeg-based motor imagery signals classification. *Diagnostics*, 12(4), 2022. ISSN 2075-4418. doi: 10.3390/diagnostics12040995. URL https://www.mdpi.com/2075-4418/12/4/995.
- Juan P. Amezquita-Sanchez, Nadia Mammone, Francesco C. Morabito, and Hojjat Adeli. A new dispersion entropy and fuzzy logic system methodology for automated classification of dementia stages using electroencephalograms. *Clinical Neurology and Neurosurgery*, 201:106446, 2021. ISSN 0303-8467. doi: https://doi.org/10.1016/j.clineuro.2020.106446. URL https://www.sciencedirect.com/science/article/pii/S0303846720307897.
- Ushtar Amin, Fábio A. Nascimento, Ioannis Karakis, Donald Schomer, and Selim R. Benbadis. Normal variants and artifacts: Importance in eeg interpretation. *Epileptic Disorders*, 25(5):591–648, 2023. doi: https://doi.org/10.1002/epd2.20040. URL https://onlinelibrary.wiley.com/doi/abs/10.1002/epd2.20040.
- Ghita Amrani, Amina Adadi, Mohammed Berrada, Zouhayr Souirti, and Saïd Boujraf. Eeg signal analysis using deep learning: A systematic literature review. In 2021 Fifth International Conference On Intelligent Computing in Data Sciences (ICDS), pp. 1–8, 2021. doi: 10.1109/ICDS53782.2021.9626707.

- Marco Ancona, Enea Ceolini, Cengiz Öztireli, and Markus Gross. Towards better understanding of gradient-based attribution methods for deep neural networks, 2018. URL https://arxiv.org/abs/1711.06104.
- Marco Ancona, Enea Ceolini, Cengiz Öztireli, and Markus Gross. Gradient-based attribution methods. In Explainable AI: Interpreting, explaining and visualizing deep learning, pp. 169–191. Springer, 2019.
- Kai Keng Ang, Zheng Yang Chin, Haihong Zhang, and Cuntai Guan. Filter bank common spatial pattern (fbcsp) in brain-computer interface. In 2008 IEEE International Joint Conference on Neural Networks (IEEE World Congress on Computational Intelligence), pp. 2390–2397, 2008. doi: 10.1109/IJCNN.2008. 4634130.
- Shaojie Bai, J Zico Kolter, and Vladlen Koltun. An Empirical Evaluation of Generic Convolutional and Recurrent Networks for Sequence Modeling. arXiv preprint arXiv:1803.01271, 2018.
- Jan Beger. Not someone, but something: Rethinking trust in the age of medical ai. arXiv preprint arXiv:2504.05331, 2025.
- Kais Belwafi, Fakhreddine Ghaffari, Ridha Djemal, and Olivier Romain. A hardware/software prototype of eeg-based bci system for home device control. *Journal of Signal Processing Systems*, 89:263–279, 2017.
- James Bergstra, Rémi Bardenet, Yoshua Bengio, and Balázs Kégl. Algorithms for hyper-parameter optimization. In J. Shawe-Taylor, R. Zemel, P. Bartlett, F. Pereira, and K.Q. Weinberger (eds.), *Advances in Neural Information Processing Systems*, volume 24. Curran Associates, Inc., 2011. URL https://proceedings.neurips.cc/paper_files/paper/2011/file/86e8f7ab32cfd12577bc2619bc635690-Paper.pdf.
- James Bergstra, Daniel Yamins, and David Cox. Making a science of model search: Hyperparameter optimization in hundreds of dimensions for vision architectures. In *International conference on machine learning*, pp. 115–123. PMLR, 2013.
- Isabelle Beuchat, Senubia Alloussi, Philipp S Reif, Nora Sterlepper, Felix Rosenow, and Adam Strzelczyk. Prospective evaluation of interrater agreement between eeg technologists and neurophysiologists. *Scientific reports*, 11(1):13406, 2021. doi: https://doi.org/10.1038/s41598-021-92827-3.
- Nima Bigdely-Shamlo, Tim Mullen, Christian Kothe, Kyung-Min Su, and Kay A. Robbins. The prep pipeline: standardized preprocessing for large-scale eeg analysis. *Frontiers in Neuroinformatics*, 9, 2015. ISSN 1662-5196. doi: 10.3389/fninf.2015.00016. URL https://www.frontiersin.org/journals/neuroinformatics/articles/10.3389/fninf.2015.00016.
- Philipp Bomatter and Henry Gouk. Is limited participant diversity impeding eeg-based machine learning?, 2025. URL https://arxiv.org/abs/2503.13497.
- Carlo Bonferroni. Teoria statistica delle classi e calcolo delle probabilita. Pubblicazioni del R Istituto Superiore di Scienze Economiche e Commerciali di Firenze, 8:3–62, 1936.
- Xavier Bouthillier, Pierre Delaunay, Mirko Bronzi, Assya Trofimov, Brennan Nichyporuk, Justin Szeto, Nazanin Mohammadi Sepahvand, Edward Raff, Kanika Madan, Vikram Voleti, Samira Ebrahimi Kahou, Vincent Michalski, Tal Arbel, Chris Pal, Gael Varoquaux, and Pascal Vincent. Accounting for variance in machine learning benchmarks. In A. Smola, A. Dimakis, and I. Stoica (eds.), Proceedings of Machine Learning and Systems, volume 3, pp. 747-769, 2021. URL https://proceedings.mlsys.org/paper_files/paper/2021/file/0184b0cd3cfb185989f858a1d9f5c1eb-Paper.pdf.
- Alexander Brenner, Felix Knispel, Florian P. Fischer, Peter Rossmanith, Yvonne Weber, Henner Koch, Rainer Röhrig, Julian Varghese, and Ekaterina Kutafina. Concept-based ai interpretability in physiological time-series data: Example of abnormality detection in electroencephalography. Computer Methods and Programs in Biomedicine, 257:108448, 2024. ISSN 0169-2607. doi: https://doi.org/10.1016/j.cmpb.2024. 108448. URL https://www.sciencedirect.com/science/article/pii/S0169260724004413.

- Jeffrey W Britton, Lauren C Frey, Jennifer L Hopp, Pearce Korb, Mohamad Z Koubeissi, William E Lievens, Elia M Pestana-Knight, and Erk K St Louis. Electroencephalography (eeg): An introductory text and atlas of normal and abnormal findings in adults, children, and infants, 2016. URL http://europepmc.org/books/NBK390354.
- Jan Brogger, Tom Eichele, Eivind Aanestad, Henning Olberg, Ina Hjelland, and Harald Aurlien. Visual eeg reviewing times with score eeg. *Clinical neurophysiology practice*, 3:59–64, 2018.
- Zikun Cai, Tian jian Luo, and Xuan Cao. Multi-branch spatial-temporal-spectral convolutional neural networks for multi-task motor imagery eeg classification. *Biomedical Signal Processing and Control*, 93: 106156, 2024. ISSN 1746-8094. doi: https://doi.org/10.1016/j.bspc.2024.106156. URL https://www.sciencedirect.com/science/article/pii/S1746809424002143.
- Marina Ceccon, Davide Dalle Pezze, Alessandro Fabris, and Gian Antonio Susto. Fairness evolution in continual learning for medical imaging. arXiv preprint arXiv:2406.02480, 2024.
- Xun Chen, Chang Li, Aiping Liu, Martin J McKeown, Ruobing Qian, and Z Jane Wang. Toward openworld electroencephalogram decoding via deep learning: A comprehensive survey. *IEEE Signal Processing Magazine*, 39(2):117–134, 2022.
- Sharon Chiang, Rosalind W Picard, Winston Chiong, Robert Moss, Gregory A Worrell, Vikram R Rao, and Daniel M Goldenholz. Guidelines for conducting ethical artificial intelligence research in neurology: a systematic approach for clinicians and researchers. *Neurology*, 97(13):632–640, 2021.
- Zheng Yang Chin, Kai Keng Ang, Chuanchu Wang, Cuntai Guan, and Haihong Zhang. Multi-class filter bank common spatial pattern for four-class motor imagery bci. In 2009 Annual International Conference of the IEEE Engineering in Medicine and Biology Society, pp. 571–574, 2009. doi: 10.1109/IEMBS.2009.5332383.
- Avishek Choudhury and Onur Asan. Role of artificial intelligence in patient safety outcomes: systematic literature review. *JMIR medical informatics*, 8(7):e18599, 2020.
- P. Chrabaszcz. Neural architecture search. Master's thesis, Albert Ludwig University Freiburg, 2018.
- Djork-Arné Clevert, Thomas Unterthiner, and Sepp Hochreiter. Fast and accurate deep network learning by exponential linear units (elus), 2016. URL https://arxiv.org/abs/1511.07289.
- Mike X Cohen. Analyzing neural time series data: theory and practice. MIT press, 2014.
- Scott Cole and Bradley Voytek. Cycle-by-cycle analysis of neural oscillations. *Journal of neurophysiology*, 122(2):849–861, 2019.
- Alexander Craik, Yongtian He, and Jose L Contreras-Vidal. Deep learning for electroencephalogram (eeg) classification tasks: a review. *Journal of Neural Engineering*, 16(3):031001, apr 2019. doi: 10.1088/1741-2552/ab0ab5. URL https://dx.doi.org/10.1088/1741-2552/ab0ab5.
- Mohammad-Javad Darvishi-Bayazi, Mohammad Sajjad Ghaemi, Timothee Lesort, Md Rifat Arefin, Jocelyn Faubert, and Irina Rish. Amplifying pathological detection in eeg signaling pathways through cross-dataset transfer learning, 2023.
- Sharon E Davis, Colin G Walsh, and Michael E Matheny. Open questions and research gaps for monitoring and updating ai-enabled tools in clinical settings. Frontiers in Digital Health, 4:958284, 2022.
- Ivo Pascal de Jong, Andreea Ioana Sburlea, and Matias Valdenegro-Toro. Uncertainty quantification in machine learning for biosignal applications a review, 2025. URL https://arxiv.org/abs/2312.09454.
- Rabie Adel El Arab, Mohammad S. Abu-Mahfouz, Fuad H. Abuadas, Husam Alzghoul, Mohammed Almari, Ahmad Ghannam, and Mohamed Mahmoud Seweid. Bridging the gap: From ai success in clinical trials to real-world healthcare implementation—a narrative review. *Healthcare*, 13(7), 2025. ISSN 2227-9032. doi: 10.3390/healthcare13070701. URL https://www.mdpi.com/2227-9032/13/7/701.

- Prabhu D Emmady and Arayamparambil C Anilkumar. *EEG abnormal waveforms*. StatPearls Publishing, Treasure Island (FL), 2023. URL http://europepmc.org/books/NBK557655.
- Taweesak Emsawas, Takashi Morita, Tsukasa Kimura, Ken-ichi Fukui, and Masayuki Numao. Multi-kernel temporal and spatial convolution for eeg-based emotion classification. *Sensors*, 22(21), 2022. ISSN 1424-8220. doi: 10.3390/s22218250. URL https://www.mdpi.com/1424-8220/22/21/8250.
- Denis A Engemann, Federico Raimondo, Jean-Rémi King, Benjamin Rohaut, Gilles Louppe, Frédéric Faugeras, Jitka Annen, Helena Cassol, Olivia Gosseries, Diego Fernandez-Slezak, et al. Robust EEG-based cross-site and cross-protocol classification of states of consciousness. *Brain*, 141(11):3179–3192, 10 2018. ISSN 0006-8950. doi: 10.1093/brain/awy251. URL https://doi.org/10.1093/brain/awy251.
- Mohammad Ennab and Hamid Mcheick. Enhancing interpretability and accuracy of ai models in healthcare: a comprehensive review on challenges and future directions. *Frontiers in Robotics and AI*, 11:1444763, 2024.
- Stefan Falkner, Aaron Klein, and Frank Hutter. BOHB: Robust and efficient hyperparameter optimization at scale. In Jennifer Dy and Andreas Krause (eds.), *Proceedings of the 35th International Conference on Machine Learning*, volume 80 of *Proceedings of Machine Learning Research*, pp. 1437–1446. PMLR, 10–15 Jul 2018. URL https://proceedings.mlr.press/v80/falkner18a.html.
- Oliver Faust, Yuki Hagiwara, Tan Jen Hong, Oh Shu Lih, and U Rajendra Acharya. Deep learning for healthcare applications based on physiological signals: A review. *Computer Methods and Programs in Biomedicine*, 161:1–13, 2018. ISSN 0169-2607. doi: https://doi.org/10.1016/j.cmpb.2018.04.005. URL https://www.sciencedirect.com/science/article/pii/S0169260718301226.
- Jean Feng, Rachael V Phillips, Ivana Malenica, Andrew Bishara, Alan E Hubbard, Leo A Celi, and Romain Pirracchio. Clinical artificial intelligence quality improvement: towards continual monitoring and updating of ai algorithms in healthcare. NPJ digital medicine, 5(1):66, 2022.
- Benoît Frénay and Michel Verleysen. Classification in the presence of label noise: A survey. *IEEE Transactions on Neural Networks and Learning Systems*, 25(5):845–869, 2014. doi: 10.1109/TNNLS.2013.2292894.
- Wendong Ge, Jin Jing, Sungtae An, Aline Herlopian, Marcus Ng, Aaron F. Struck, Brian Appavu, Emily L. Johnson, Gamaleldin Osman, Hiba A. Haider, Ioannis Karakis, Jennifer A. Kim, Jonathan J. Halford, Monica B. Dhakar, Rani A. Sarkis, Christa B. Swisher, Sarah Schmitt, Jong Woo Lee, Mohammad Tabaeizadeh, Andres Rodriguez, Nicolas Gaspard, Emily Gilmore, Susan T. Herman, Peter W. Kaplan, Jay Pathmanathan, Shenda Hong, Eric S. Rosenthal, Sahar Zafar, Jimeng Sun, and M. Brandon Westover. Deep active learning for interictal ictal injury continuum eeg patterns. *Journal of Neuroscience Methods*, 351:108966, 2021. ISSN 0165-0270. doi: https://doi.org/10.1016/j.jneumeth.2020.108966. URL https://www.sciencedirect.com/science/article/pii/S0165027020303897.
- Lukas A.W. Gemein, Robin T. Schirrmeister, Patryk Chrabaszcz, Daniel Wilson, Joschka Boedecker, Andreas Schulze-Bonhage, Frank Hutter, and Tonio Ball. Machine-learning-based diagnostics of eeg pathology. NeuroImage, 220:117021, 2020. ISSN 1053-8119. doi: https://doi.org/10.1016/j.neuroimage.2020. 117021. URL https://www.sciencedirect.com/science/article/pii/S1053811920305073.
- Xavier Glorot and Yoshua Bengio. Understanding the difficulty of training deep feedforward neural networks. In Yee Whye Teh and Mike Titterington (eds.), Proceedings of the Thirteenth International Conference on Artificial Intelligence and Statistics, volume 9 of Proceedings of Machine Learning Research, pp. 249–256, Chia Laguna Resort, Sardinia, Italy, 13–15 May 2010. PMLR. URL https://proceedings.mlr.press/v9/glorot10a.html.
- Cristina Gonzalez-Gonzalo, Eric F Thee, Caroline CW Klaver, Aaron Y Lee, Reinier O Schlingemann, Adnan Tufail, Frank Verbraak, and Clara I Sánchez. Trustworthy ai: Closing the gap between development and integration of ai systems in ophthalmic practice. *Progress in retinal and eye research*, 90:101034, 2022.

- A. Gramfort, D. Strohmeier, J. Haueisen, M.S. Hämäläinen, and M. Kowalski. Time-frequency mixed-norm estimates: Sparse m/eeg imaging with non-stationary source activations. *NeuroImage*, 70:410–422, 2013. ISSN 1053-8119. doi: https://doi.org/10.1016/j.neuroimage.2012.12.051. URL https://www.sciencedirect.com/science/article/pii/S1053811912012372.
- Xiaotong Gu and Zehong Cao. A rule-based eeg classification system for discrimination of hand motor attempts in stroke patients, 2020. URL https://arxiv.org/abs/2001.11278.
- Hao Guan, David Bates, and Li Zhou. Keeping medical ai healthy: A review of detection and correction methods for system degradation. arXiv preprint arXiv:2506.17442, 2025.
- Shahram Hanifi, Andrea Cammarono, and Hossein Zare-Behtash. Advanced hyperparameter optimization of deep learning models for wind power prediction. *Renewable Energy*, 221:119700, 2024. ISSN 0960-1481. doi: https://doi.org/10.1016/j.renene.2023.119700. URL https://www.sciencedirect.com/science/article/pii/S0960148123016154.
- Mohammad Mehedi Hasan, Pedro G Lind, Hernando Ombao, Anis Yazidi, and Rabindra Khadka. Eeg-msaf: An interpretable microstate framework uncovers default-mode decoherence in early neurodegeneration. arXiv preprint arXiv:2509.02568, 2025.
- Dan Hendrycks and Kevin Gimpel. Gaussian error linear units (gelus), 2023. URL https://arxiv.org/abs/1606.08415.
- Robert Hogan, Sean R Mathieson, Aurel Luca, Soraia Ventura, Sean Griffin, Geraldine B Boylan, and John M O'Toole. Scaling convolutional neural networks achieves expert level seizure detection in neonatal eeg. npj Digital Medicine, 8(1):17, 2025.
- Matthias Hoppe. Eeg-befundung einschließlich darstellung des normalen eeg. Das Neurophysiologie-Labor, 40(1):14-43, 2018. ISSN 1439-4847. doi: https://doi.org/10.1016/j.neulab.2017.11.002. URL https://www.sciencedirect.com/science/article/pii/S1439484717300571. EEG Befunden.
- Ahmed Hosny, Danielle S Bitterman, Christian V Guthier, Jack M Qian, Hannah Roberts, Subha Perni, Anurag Saraf, Luke C Peng, Itai Pashtan, Zezhong Ye, et al. Clinical validation of deep learning algorithms for radiotherapy targeting of non-small-cell lung cancer: an observational study. *The Lancet Digital Health*, 4(9):e657–e666, 2022.
- Edward E. Houfek and Robert J. Ellingson. On the reliability of clinical EEG interpretation. *The Journal of Nervous and Mental Disease*, 128(5):425–437, 1959.
- Andrew G Howard, Menglong Zhu, Bo Chen, Dmitry Kalenichenko, Weijun Wang, Tobias Weyand, Marco Andreetto, and Hartwig Adam. Mobilenets: Efficient convolutional neural networks for mobile vision applications. arXiv preprint arXiv:1704.04861, 2017. doi: https://doi.org/10.48550/arXiv.1704.04861.
- Mandong Hu, Yi Zhong, Shuxuan Xie, Haibin Lv, and Zhihan Lv. Fuzzy system based medical image processing for brain disease prediction. *Frontiers in Neuroscience*, Volume 15 2021, 2021. ISSN 1662-453X. doi: 10.3389/fnins.2021.714318. URL https://www.frontiersin.org/journals/neuroscience/articles/10.3389/fnins.2021.714318.
- Marcello Ienca, Joseph J Fins, Ralf J Jox, Fabrice Jotterand, Silja Voeneky, Roberto Andorno, Tonio Ball, Claude Castelluccia, Ricardo Chavarriaga, Hervé Chneiweiss, et al. Towards a governance framework for brain data. *Neuroethics*, 15(2):20, 2022.
- Tomas Iešmantas and Robertas Alzbutas. Convolutional neural network for detection and classification of seizures in clinical data. *Medical & Biological Engineering & Computing*, 58(9):1919–1932, 2020.
- Thorir Mar Ingolfsson, Michael Hersche, Xiaying Wang, Nobuaki Kobayashi, Lukas Cavigelli, and Luca Benini. Eeg-tcnet: An accurate temporal convolutional network for embedded motor-imagery brain-machine interfaces. In 2020 IEEE International Conference on Systems, Man, and Cybernetics (SMC), pp. 2958–2965, 2020. doi: 10.1109/SMC42975.2020.9283028.

- Sergey Ioffe and Christian Szegedy. Batch normalization: Accelerating deep network training by reducing internal covariate shift, 2015. URL https://arxiv.org/abs/1502.03167.
- Md Kafiul Islam, Amir Rastegarnia, and Zhi Yang. Methods for artifact detection and removal from scalp eeg: A review. Neurophysiologie Clinique/Clinical Neurophysiology, 46(4-5):287–305, 2016.
- Francine L Jacobson and Elizabeth A Krupinski. Clinical validation is the key to adopting ai in clinical practice. *Radiology: Artificial Intelligence*, 3(4):e210104, 2021.
- Mainak Jas, Denis A. Engemann, Yousra Bekhti, Federico Raimondo, and Alexandre Gramfort. Autoreject: Automated artifact rejection for meg and eeg data. *NeuroImage*, 159:417-429, 2017. ISSN 1053-8119. doi: https://doi.org/10.1016/j.neuroimage.2017.06.030. URL https://www.sciencedirect.com/science/article/pii/S1053811917305013.
- Ziyu Jia, Youfang Lin, Jing Wang, Kaixin Yang, Tianhang Liu, and Xinwang Zhang. Mmcnn: A multi-branch multi-scale convolutional neural network for motor imagery classification. In Frank Hutter, Kristian Kersting, Jefrey Lijffijt, and Isabel Valera (eds.), Machine Learning and Knowledge Discovery in Databases, pp. 736–751, Cham, 2021. Springer International Publishing. ISBN 978-3-030-67664-3.
- Wei-Bang Jiang, Li-Ming Zhao, and Bao-Liang Lu. Large brain model for learning generic representations with tremendous eeg data in bci, 2024. URL https://arxiv.org/abs/2405.18765.
- Yoonji Joo, Eun Namgung, Hyeonseok Jeong, Ilhyang Kang, Jinsol Kim, Sohyun Oh, In Kyoon Lyoo, Sujung Yoon, and Jaeuk Hwang. Brain age prediction using combined deep convolutional neural network and multi-layer perceptron algorithms. *Scientific Reports*, 13(1):22388, 2023.
- Bhabesh Kalita, Nabamita Deb, and Daisy Das. Aneeg: leveraging deep learning for effective artifact removal in eeg data. *Scientific Reports*, 14(1):24234, 2024.
- Alexander Kamrud, Brett Borghetti, and Christine Schubert Kabban. The effects of individual differences, non-stationarity, and the importance of data partitioning decisions for training and testing of eeg cross-participant models. *Sensors*, 21(9):3225, 2021.
- Nick Kane, Jayant Acharya, Sandor Beniczky, Luis Caboclo, Simon Finnigan, Peter W. Kaplan, Hiroshi Shibasaki, Ronit Pressler, and Michel J.A.M. van Putten. A revised glossary of terms most commonly used by clinical electroencephalographers and updated proposal for the report format of the eeg findings. revision 2017. Clinical Neurophysiology Practice, 2:170–185, 2017. ISSN 2467-981X. doi: https://doi.org/10.1016/j.cnp.2017.07.002. URL https://www.sciencedirect.com/science/article/pii/S2467981X17300215.
- Dae Y Kang, Pamela N DeYoung, Justin Tantiongloc, Todd P Coleman, and Robert L Owens. Statistical uncertainty quantification to augment clinical decision support: a first implementation in sleep medicine. NPJ digital medicine, 4(1):142, 2021.
- Christopher J Kelly, Alan Karthikesalingam, Mustafa Suleyman, Greg Corrado, and Dominic King. Key challenges for delivering clinical impact with artificial intelligence. *BMC medicine*, 17(1):195, 2019.
- Angus Kenny, Tapabrata Ray, and Hemant Singh. A framework for design optimization across multiple concepts. *Scientific Reports*, 14(1):7858, 2024.
- Hassan Aqeel Khan, Rahat Ul Ain, Awais Mehmood Kamboh, Hammad Tanveer Butt, Saima Shafait, Wasim Alamgir, Didier Stricker, and Faisal Shafait. The nmt scalp eeg dataset: An open-source annotated dataset of healthy and pathological eeg recordings for predictive modeling. Frontiers in Neuroscience, 15, 2022. doi: 10.3389/fnins.2021.755817. URL https://www.frontiersin.org/article/10.3389/fnins.2021.755817.
- Ann-Kathrin Kiessner, Robin T. Schirrmeister, Lukas A.W. Gemein, Joschka Boedecker, and Tonio Ball. An extended clinical eeg dataset with 15,300 automatically labelled recordings for pathology decoding. NeuroImage: Clinical, 39:103482, 2023. ISSN 2213-1582. doi: https://doi.org/10.1016/j.nicl.2023.103482. URL https://www.sciencedirect.com/science/article/pii/S2213158223001730.

- Ann-Kathrin Kiessner, Robin T. Schirrmeister, Joschka Boedecker, and Tonio Ball. Reaching the ceiling? empirical scaling behaviour for deep eeg pathology classification. *Computers in Biology and Medicine*, 178: 108681, 2024. ISSN 0010-4825. doi: https://doi.org/10.1016/j.compbiomed.2024.108681. URL https://www.sciencedirect.com/science/article/pii/S0010482524007662.
- Min-jae Kim, Chul Youn Young, and Paik Joonki. Deep learning-based eeg analysis to classify normal, mild cognitive impairment, and dementia: Algorithms and dataset. *NeuroImage*, 272:120054, 2023. ISSN 1053-8119. doi: https://doi.org/10.1016/j.neuroimage.2023.120054. URL https://www.sciencedirect.com/science/article/pii/S1053811923002008.
- David King-Stephens. Ai and eeg: Should eegers rip (rest in peace)? Epilepsy Currents, 24(2):111–113, 2024.
- Diederik P. Kingma and Jimmy Ba. Adam: A method for stochastic optimization, 2017. URL https://arxiv.org/abs/1412.6980.
- Elnaz Lashgari, Dehua Liang, and Uri Maoz. Data augmentation for deep-learning-based electroencephalography. *Journal of Neuroscience Methods*, 346:108885, 2020. ISSN 0165-0270. doi: https://doi.org/10.1016/j.jneumeth.2020.108885. URL https://www.sciencedirect.com/science/article/pii/S0165027020303083.
- Imene Latreche, Sihem Slatnia, Okba Kazar, and Saad Harous. An optimized deep hybrid learning for multichannel eeg-based driver drowsiness detection. *Biomedical Signal Processing and Control*, 99:106881, 2025. ISSN 1746-8094. doi: https://doi.org/10.1016/j.bspc.2024.106881. URL https://www.sciencedirect.com/science/article/pii/S174680942400939X.
- Vernon J Lawhern, Amelia J Solon, Nicholas R Waytowich, Stephen M Gordon, Chou P Hung, and Brent J Lance. EEGNet: a compact convolutional neural network for EEG-based brain-computer interfaces. Journal of neural engineering, 15(5):056013, 2018. doi: 10.1088/1741-2552/aace8c. URL https://doi.org/10.1088/1741-2552/aace8c.
- Tiago Lemos, Luiz Felipe Campos, Afrânio Melo, Nayher Clavijo, Rafael Soares, Maurício Câmara, Thiago Feital, Thiago Anzai, and José Carlos Pinto. Echo state network based soft sensor for monitoring and fault detection of industrial processes. Computers & Chemical Engineering, 155:107512, 2021. ISSN 0098-1354. doi: https://doi.org/10.1016/j.compchemeng.2021.107512. URL https://www.sciencedirect.com/science/article/pii/S0098135421002908.
- Chusak Limotai, Nittaya Phayaph, Boonyavee Pattanasilp, Jeerawan Mokklaew, and Natlada Limotai. Effects of antiepileptic drugs on electroencephalography (eeg): Insights and applicability. *Epilepsy & Behavior*, 110:107161, 2020. ISSN 1525-5050. doi: https://doi.org/10.1016/j.yebeh.2020.107161. URL https://www.sciencedirect.com/science/article/pii/S1525505020303401.
- Shiwei Liu, Wenwen Yue, Zhiqing Guo, and Liejun Wang. Multi-branch cnn and grouping cascade attention for medical image classification. *Scientific Reports*, 14(1):15013, 2024.
- Tianjun Liu and Deling Yang. A densely connected multi-branch 3d convolutional neural network for motor imagery eeg decoding. *Brain Sciences*, 11(2), 2021. ISSN 2076-3425. doi: 10.3390/brainsci11020197. URL https://www.mdpi.com/2076-3425/11/2/197.
- Xiaoguang Liu, Shicheng Xiong, Xiaodong Wang, Tie Liang, Hongrui Wang, and Xiuling Liu. A compact multi-branch 1d convolutional neural network for eeg-based motor imagery classification. *Biomedical Signal Processing and Control*, 81:104456, 2023. ISSN 1746-8094. doi: https://doi.org/10.1016/j.bspc. 2022.104456. URL https://www.sciencedirect.com/science/article/pii/S1746809422009107.
- Sebas Lopez, G Suarez, D Jungreis, I Obeid, and Joseph Picone. Automated identification of abnormal adult eegs. In 2015 IEEE signal processing in medicine and biology symposium (SPMB), pp. 1–5. IEEE, 2015.
- S. López de Diego. Automated interpretation of abnormal adult electroencephalography. Master's thesis, Temple University, 2017. URL http://hdl.handle.net/20.500.12613/1767.

- Ilya Loshchilov and Frank Hutter. SGDR: Stochastic gradient descent with warm restarts. arXiv preprint arXiv:1608.03983, 2016. doi: 10.48550/arXiv.1608.03983.
- Ilya Loshchilov and Frank Hutter. Fixing weight decay regularization in Adam. arXiv preprint arXiv:1711.05101, 2017. doi: 10.48550/arXiv.1711.05101.
- Ilya Loshchilov and Frank Hutter. Decoupled weight decay regularization, 2019. URL https://arxiv.org/abs/1711.05101.
- H. B. Mann and D. R. Whitney. On a test of whether one of two random variables is stochastically larger than the other. *The Annals of Mathematical Statistics*, 18(1):50–60, 1947.
- Daniel Mansilla, Jesper Tveit, Harald Aurlien, Tamir Avigdor, Victoria Ros-Castello, Alyssa Ho, Chifaou Abdallah, Jean Gotman, Sándor Beniczky, and Birgit Frauscher. Generalizability of electroencephalographic interpretation using artificial intelligence: An external validation study. *Epilepsia*, 65(10):3028–3037, 2024.
- L. McInnes, J. Healy, and J. Melville. UMAP: Uniform Manifold Approximation and Projection for Dimension Reduction. *ArXiv e-prints*, February 2018.
- John R McLaren, Doyle Yuan, Sándor Beniczky, M Brandon Westover, and Fábio A Nascimento. The future of eeg education in the era of artificial intelligence. *Epilepsia*, 2025.
- Stephanie L McNamara, Paul H Yi, and William Lotter. The clinician-ai interface: intended use and explainability in fda-cleared ai devices for medical image interpretation. NPJ Digital Medicine, 7(1):80, 2024.
- John William Carey Medithe and Usha Rani Nelakuditi. Study of normal and abnormal eeg. In 2016 3rd International Conference on Advanced Computing and Communication Systems (ICACCS), volume 01, pp. 1–4, 2016. doi: 10.1109/ICACCS.2016.7586341.
- Mohamed Mohammedi, Mawloud Omar, and Abdelmadjid Bouabdallah. Methods for detecting and removing ocular artifacts from eeg signals in drowsy driving warning systems: A survey. *Multimedia Tools and Applications*, 82(12):17687–17714, 2023.
- Marina Ramzy Mourid, Hamza Irfan, and Malik Olatunde Oduoye. Artificial intelligence in pediatric epilepsy detection: balancing effectiveness with ethical considerations for welfare. *Health Science Reports*, 8(1): e70372, 2025.
- Ghulam Muhammad, M. Shamim Hossain, and Neeraj Kumar. Eeg-based pathology detection for home health monitoring. *IEEE Journal on Selected Areas in Communications*, 39(2):603–610, 2021. doi: 10. 1109/JSAC.2020.3020654.
- David O. Nahmias and Kimberly L. Kontson. Easy perturbation eeg algorithm for spectral importance (easypeasi): A simple method to identify important spectral features of eeg in deep learning models. In *Proceedings of the 26th ACM SIGKDD International Conference on Knowledge Discovery & Data Mining*, KDD '20, pp. 2398–2406, New York, NY, USA, 2020. Association for Computing Machinery. ISBN 9781450379984. doi: 10.1145/3394486.3403289. URL https://doi.org/10.1145/3394486.3403289.
- David O Nahmias, Kimberly L Kontson, David A Soltysik, and Eugene F Civillico. Consistency of quantitative electroencephalography features in a large clinical data set. *Journal of neural engineering*, 16(6): 066044, 2019.
- David O Nahmias, Eugene F Civillico, and Kimberly L Kontson. Deep learning and feature based medication classifications from eeg in a large clinical data set. *Scientific Reports*, 10(1):14206, 2020.
- Chetan S Nayak and Arayamparambil C Anilkumar. Eeg normal waveforms. statpearls. Treasure Island, FL: StatPearls Publishing. http://www.ncbi. nlm. nih. gov, 2020.

- I. Obeid and J. Picone. The Temple University Hospital EEG data corpus. Frontiers in Neuroscience, 10, 2016. doi: 10.3389/fnins.2016.00196. URL https://www.frontiersin.org/articles/10.3389/fnins.2016.00196.
- Paschal Ochang, Bernd Carsten Stahl, and Damian Eke. The ethical and legal landscape of brain data governance. *PLoS One*, 17(12):e0273473, 2022.
- Favour Olaoye, Axel Egon, and Lucas Doris. Deep learning techniques for medical image analysis and diagnosis, 2024.
- F. Pedregosa, G. Varoquaux, A. Gramfort, V. Michel, B. Thirion, O. Grisel, M. Blondel, P. Prettenhofer, R. Weiss, V. Dubourg, J. Vanderplas, A. Passos, D. Cournapeau, M. Brucher, M. Perrot, and E. Duchesnay. Scikit-learn: Machine learning in Python. *Journal of Machine Learning Research*, 12:2825–2830, 2011.
- David Picard. Torch.manual_seed (3407) is all you need: On the influence of random seeds in deep learning architectures for computer vision, 2023. URL https://arxiv.org/abs/2109.08203.
- Martyna Poziomska, Marian Dovgialo, Przemysław Olbratowski, Paweł Niedbalski, Paweł Ogniewski, Joanna Zych, Jacek Rogala, and Jarosław Żygierewicz. Quantity versus diversity: Influence of data on detecting eeg pathology with advanced ml models, 2024. URL https://arxiv.org/abs/2411.17709.
- D. Merlin Praveena, D. Angelin Sarah, and S. Thomas George and. Deep learning techniques for eeg signal applications a review. *IETE Journal of Research*, 68(4):3030–3037, 2022. doi: 10.1080/03772063.2020. 1749143. URL https://doi.org/10.1080/03772063.2020.1749143.
- Eric W. Prince, Debashis Ghosh, Carsten Görg, and Todd C. Hankinson. Uncertainty-aware deep learning classification of adamantinomatous craniopharyngioma from preoperative mri. *Diagnostics*, 13(6), 2023. ISSN 2075-4418. doi: 10.3390/diagnostics13061132. URL https://www.mdpi.com/2075-4418/13/6/1132
- Anichur Rahman, Tanoy Debnath, Dipanjali Kundu, Md Saikat Islam Khan, Airin Afroj Aishi, Sadia Sazzad, Mohammad Sayduzzaman, and Shahab S Band. Machine learning and deep learning-based approach in smart healthcare: Recent advances, applications, challenges and opportunities. *AIMS Public Health*, 11 (1):58, 2024.
- Aaron Reer, Andreas Wiebe, Xu Wang, and Jochem W Rieger. Fair human neuroscientific data sharing to advance ai driven research and applications: Legal frameworks and missing metadata standards. *Frontiers in Genetics*, 14:1086802, 2023.
- Mouad Riyad, Mohammed Khalil, and Abdellah Adib. Incep-eegnet: a convnet for motor imagery decoding. In *Image and Signal Processing: 9th International Conference, ICISP 2020, Marrakesh, Morocco, June* 4–6, 2020, Proceedings 9, pp. 103–111. Springer, 2020.
- Stephen W. Rose, J. Kiffin Penry, Billy G. White, and Susumu Sato. Reliability and Validity of Visual EEG Assessment in Third Grade Children. *Clinical Electroencephalography*, 4(4):197–205, 1973. doi: 10.1177/155005947300400405. URL https://doi.org/10.1177/155005947300400405.
- Subhrajit Roy, Isabell Kiral-Kornek, and Stefan Harrer. Deep learning enabled automatic abnormal eeg identification. In 2018 40th Annual International Conference of the IEEE Engineering in Medicine and Biology Society (EMBC), pp. 2756–2759, 2018. doi: 10.1109/EMBC.2018.8512756.
- Subhrajit Roy, Isabell Kiral-Kornek, and Stefan Harrer. Chrononet: A Deep Recurrent Neural Network for Abnormal EEG Identification. In David Riaño, Szymon Wilk, and Annette ten Teije (eds.), Artificial Intelligence in Medicine, pp. 47–56. Springer International Publishing, 2019a.

- Yannick Roy, Hubert Banville, Isabela Albuquerque, Alexandre Gramfort, Tiago H Falk, and Jocelyn Faubert. Deep learning-based electroencephalography analysis: a systematic review. *Journal of Neural Engineering*, 16(5):051001, aug 2019b. doi: 10.1088/1741-2552/ab260c. URL https://dx.doi.org/10.1088/1741-2552/ab260c.
- Khaled Saab, Jared Dunnmon, Christopher Ré, Daniel Rubin, and Christopher Lee-Messer. Weak supervision as an efficient approach for automated seizure detection in electroencephalography. *NPJ digital medicine*, 3(1):59, 2020.
- Agustina D Saenz, Amanda Centi, David Ting, Jacqueline G You, Adam Landman, and Rebecca G Mishuris. Establishing responsible use of ai guidelines: a comprehensive case study for healthcare institutions. *npj Diqital Medicine*, 7(1):348, 2024.
- Zeynel A. Samak, Philip Clatworthy, and Majid Mirmehdi. Transop: Transformer-based multimodal classification for stroke treatment outcome prediction. In 2023 IEEE 20th International Symposium on Biomedical Imaging (ISBI), pp. 1–5, 2023. doi: 10.1109/ISBI53787.2023.10230576.
- Michiel Schinkel, Frank C Bennis, Anneroos W Boerman, W Joost Wiersinga, and Prabath WB Nanayakkara. Embracing cohort heterogeneity in clinical machine learning development: a step toward generalizable models. *Scientific reports*, 13(1):8363, 2023.
- R. T. Schirrmeister, L. A. W. Gemein, K. Eggensperger, F. Hutter, and T. Ball. Deep learning with convolutional neural networks for decoding and visualization of EEG pathology. arXiv preprint arXiv:1708.08012, 2017a.
- Robin Tibor Schirrmeister, Jost Tobias Springenberg, Lukas Dominique Josef Fiederer, Martin Glasstetter, Katharina Eggensperger, Michael Tangermann, Frank Hutter, Wolfram Burgard, and Tonio Ball. Deep learning with convolutional neural networks for eeg decoding and visualization. *Human Brain Mapping*, aug 2017b. ISSN 1097-0193. doi: 10.1002/hbm.23730. URL http://dx.doi.org/10.1002/hbm.23730.
- Shashank Shekhar, Adesh Bansode, and Asif Salim. A comparative study of hyper-parameter optimization tools. In 2021 IEEE Asia-Pacific Conference on Computer Science and Data Engineering (CSDE), pp. 1–6, 2021. doi: 10.1109/CSDE53843.2021.9718485.
- Afshin Shoeibi, Navid Ghassemi, Marjane Khodatars, Parisa Moridian, Roohallah Alizadehsani, Assef Zare, Abbas Khosravi, Abdulhamit Subasi, U. Rajendra Acharya, and Juan M. Gorriz. Detection of epileptic seizures on eeg signals using anfis classifier, autoencoders and fuzzy entropies. *Biomedical Signal Processing and Control*, 73:103417, 2022. ISSN 1746-8094. doi: https://doi.org/10.1016/j.bspc.2021.103417. URL https://www.sciencedirect.com/science/article/pii/S1746809421010144.
- Unmesh Shukla, Geetika Jain Saxena, Manish Kumar, Anil Singh Bafila, Amit Pundir, and Sanjeev Singh. An improved decision support system for identification of abnormal eeg signals using a 1d convolutional neural network and savitzky-golay filtering. *IEEE Access*, 9:163492–163503, 2021. doi: 10.1109/ACCESS. 2021.3133326.
- Hafza Ayesha Siddiqa, Zhenning Tang, Yan Xu, Laishuan Wang, Muhammad Irfan, Saadullah Farooq Abbasi, Anum Nawaz, Chen Chen, and Wei Chen. Single-channel eeg data analysis using a multi-branch cnn for neonatal sleep staging. *IEEE Access*, 12:29910–29925, 2024. doi: 10.1109/ACCESS.2024.3365570.
- S J M Smith. Eeg in the diagnosis, classification, and management of patients with epilepsy. *Journal of Neurology, Neurosurgery & Psychiatry*, 76(suppl 2):ii2-ii7, 2005. ISSN 0022-3050. doi: 10.1136/jnnp.2005. 069245. URL https://jnnp.bmj.com/content/76/suppl_2/ii2.
- Maryam Sorkhi, Mohammad Reza Jahed-Motlagh, Behrouz Minaei-Bidgoli, and Mohammad Reza Daliri. Hybrid fuzzy deep neural network toward temporal-spatial-frequency features learning of motor imagery signals. *Scientific Reports*, 12(1):22334, 2022.

- Nitish Srivastava, Geoffrey Hinton, Alex Krizhevsky, Ilya Sutskever, and Ruslan Salakhutdinov. Dropout: a simple way to prevent neural networks from overfitting. *The journal of machine learning research*, 15(1): 1929–1958, 2014.
- Jens B Stephansen, Alexander N Olesen, Mads Olsen, Aditya Ambati, Eileen B Leary, Hyatt E Moore, Oscar Carrillo, Ling Lin, Fang Han, Han Yan, et al. Neural network analysis of sleep stages enables efficient diagnosis of narcolepsy. *Nature communications*, 9(1):5229, 2018.
- Eva MM Strijbis, Yannick SS Timar, Deborah N Schoonhoven, Ilse M Nauta, Shanna D Kulik, Lodewijk RJ de Ruiter, Menno M Schoonheim, Arjan Hillebrand, and Cornelis J Stam. State changes during resting-state (magneto) encephalographic studies: The effect of drowsiness on spectral, connectivity, and network analyses. Frontiers in neuroscience, 16:782474, 2022.
- Chen Sun, Abhinav Shrivastava, Saurabh Singh, and Abhinav Gupta. Revisiting unreasonable effectiveness of data in deep learning era. In *Proceedings of the IEEE international conference on computer vision*, pp. 843–852, 2017.
- Haoqi Sun, Eyal Kimchi, Oluwaseun Akeju, Sunil B Nagaraj, Lauren M McClain, David W Zhou, Emily Boyle, Wei-Long Zheng, Wendong Ge, and M Brandon Westover. Automated tracking of level of consciousness and delirium in critical illness using deep learning. NPJ Digital Medicine, 2(1):1–8, 2019.
- Christian Szegedy, Wei Liu, Yangqing Jia, Pierre Sermanet, Scott Reed, Dragomir Anguelov, Dumitru Erhan, Vincent Vanhoucke, and Andrew Rabinovich. Going deeper with convolutions. In 2015 IEEE Conference on Computer Vision and Pattern Recognition (CVPR), pp. 1–9, 2015. doi: 10.1109/CVPR.2015.7298594.
- Alon Talmor and Jonathan Berant. Multiqa: An empirical investigation of generalization and transfer in reading comprehension. arXiv preprint arXiv:1905.13453, 2019. URL https://doi.org/10.48550/arXiv.1905.13453.
- Mingxing Tan and Quoc Le. Efficientnet: Rethinking model scaling for convolutional neural networks. In Kamalika Chaudhuri and Ruslan Salakhutdinov (eds.), *Proceedings of the 36th International Conference on Machine Learning*, volume 97 of *Proceedings of Machine Learning Research*, pp. 6105–6114. PMLR, 09–15 Jun 2019. URL https://proceedings.mlr.press/v97/tan19a.html.
- IV Tatum and O William. Handbook of EEG interpretation. Springer Publishing Company, 2021.
- Juan Terven, Diana M. Cordova-Esparza, Alfonso Ramirez-Pedraza, Edgar A. Chavez-Urbiola, and Julio A. Romero-Gonzalez. Loss functions and metrics in deep learning, 2024. URL https://arxiv.org/abs/2307.02694.
- Rahul Thapa, Bryan He, Magnus Ruud Kjaer, Hyatt Moore IV, Gauri Ganjoo, Emmanuel Mignot, and James Y. Zou. SleepFM: Multi-modal representation learning for sleep across ECG, EEG and respiratory signals. In AAAI 2024 Spring Symposium on Clinical Foundation Models, 2024. URL https://openreview.net/forum?id=cDXtscWCKC.
- Marleen C Tjepkema-Cloostermans, Martijn R Tannemaat, Luuk Wieske, Anne-Fleur van Rootselaar, Bas C Stunnenberg, Hanneke M Keijzer, Johannes HTM Koelman, Selma C Tromp, Ioana Dunca, Baukje J van Der Star, et al. Expert level of detection of interictal discharges with a deep neural network. *Epilepsia*, 66(1):184–194, 2025.
- KG Van Leeuwen, H Sun, M Tabaeizadeh, AF Struck, MJAM Van Putten, and MB Westover. Detecting abnormal electroencephalograms using deep convolutional networks. *Clinical Neurophysiology*, 130(1): 77–84, 2019. doi: https://10.1016/j.clinph.2018.10.012. URL https://www.ncbi.nlm.nih.gov/pmc/articles/PMC6309707/.
- Daniel Vela, Andrew Sharp, Richard Zhang, Trang Nguyen, An Hoang, and Oleg S Pianykh. Temporal quality degradation in ai models. *Scientific reports*, 12(1):11654, 2022.

- Manoj Vishwanath, Steven Cao, Nikil Dutt, Amir M Rahmani, Miranda M Lim, and Hung Cao. Reducing intraspecies and interspecies covariate shift in traumatic brain injury eeg of humans and mice using transfer euclidean alignment. arXiv preprint arXiv:2310.02398, 2023.
- Xiaoyun Wang, Xing Wang, Chong Wang, Zhongyuan Wang, Xiangyu Liu, Xiaoling Lv, and Ying Tang. A two-stage automatic system for detection of interictal epileptiform discharges from scalp electroencephalograms. *Eneuro*, 10(11), 2023.
- Ying Wang, Ivan C Zibrandtsen, Richard HC Lazeron, Johannes P van Dijk, Xi Long, Ronald M Aarts, Lei Wang, and Johan BAM Arends. Pitfalls in eeg analysis in patients with non-convulsive status epilepticus. medRxiv, pp. 2020–10, 2020.
- Joseph West, Zahra Dasht Bozorgi, Jeffrey Herron, Howard J Chizeck, Jordan D Chambers, and Lyra Li. Machine learning seizure prediction: one problematic but accepted practice. *Journal of Neural Engineering*, 20(1):016008, 2023.
- D. Western, T. Weber, R. Kandasamy, F. May, S. Taylor, Y. Zhu, and L. Canham. Automatic report-based labelling of clinical eegs for classifier training. In 2021 IEEE Signal Processing in Medicine and Biology Symposium (SPMB), pp. 1–6, 2021. doi: 10.1109/SPMB52430.2021.9672295.
- Ross Wightman, Hugo Touvron, and Hervé Jégou. Resnet strikes back: An improved training procedure in timm, 2021. URL https://arxiv.org/abs/2110.00476.
- Tao Wu, Xiangzeng Kong, Yiwen Wang, Xue Yang, Jingxuan Liu, and Jun Qi. Automatic classification of eeg signals via deep learning. In 2021 IEEE 19th International Conference on Industrial Informatics (INDIN), pp. 1–6, 2021. doi: 10.1109/INDIN45523.2021.9557473.
- Yuxin Wu and Kaiming He. Group normalization, 2018. URL https://arxiv.org/abs/1803.08494.
- Yankun Xu, Jie Yang, Wenjie Ming, Shuang Wang, and Mohamad Sawan. Shorter latency of real-time epileptic seizure detection via probabilistic prediction. *Expert Systems with Applications*, 236:121359, 2024.
- Fei Yan, Zekai Guo, Abdullah M Iliyasu, and Kaoru Hirota. Multi-branch convolutional neural network with cross-attention mechanism for emotion recognition. *Scientific Reports*, 15(1):3976, 2025.
- Chaoqi Yang, M Westover, and Jimeng Sun. Biot: Biosignal transformer for cross-data learning in the wild. In A. Oh, T. Naumann, A. Globerson, K. Saenko, M. Hardt, and S. Levine (eds.), Advances in Neural Information Processing Systems, volume 36, pp. 78240-78260. Curran Associates, Inc., 2023. URL https://proceedings.neurips.cc/paper_files/paper/2023/file/f6b30f3e2dd9cb53bbf2024402d02295-Paper-Conference.pdf.
- Lie Yang, Yonghao Song, Xueyu Jia, Ke Ma, and Longhan Xie. Two-branch 3d convolutional neural network for motor imagery eeg decoding. *Journal of Neural Engineering*, 18(4):0460c7, aug 2021. doi: 10.1088/1741-2552/ac17d6. URL https://dx.doi.org/10.1088/1741-2552/ac17d6.
- Özal Yıldırım, Ulas Baran Baloglu, and U Rajendra Acharya. A deep convolutional neural network model for automated identification of abnormal eeg signals. *Neural Computing and Applications*, 32:15857–15868, 2020. doi: https://doi.org/10.1007/s00521-018-3889-z.
- Sergey Zagoruyko and Nikos Komodakis. Wide residual networks. arXiv preprint arXiv:1605.07146, 2016. URL https://doi.org/10.48550/arXiv.1605.07146.
- Hubert Dariusz Zając, Jorge Miguel Neves Ribeiro, Silvia Ingala, Simona Gentile, Ruth Wanjohi, Samuel Nguku Gitau, Jonathan Frederik Carlsen, Michael Bachmann Nielsen, and Tariq Osman Andersen. "it depends": Configuring ai to improve clinical usefulness across contexts. In Proceedings of the 2024 ACM Designing Interactive Systems Conference, pp. 874–889, 2024.
- Aston Zhang, Zachary C. Lipton, Mu Li, and Alexander J. Smola. *Dive into Deep Learning*. Cambridge University Press, 2023a. https://D2L.ai.

Hao Zhang, Qing-Qi Zhou, He Chen, Xiao-Qing Hu, Wei-Guang Li, Yang Bai, Jun-Xia Han, Yao Wang, Zhen-Hu Liang, Dan Chen, et al. The applied principles of eeg analysis methods in neuroscience and clinical neurology. *Military Medical Research*, 10(1):67, 2023b.

Hangyu Zhu, Laishuan Wang, Ning Shen, Yonglin Wu, Shu Feng, Yan Xu, Chen Chen, and Wei Chen. Mshnn: Multi-scale hierarchical neural network with squeeze and excitation block for neonatal sleep staging using a single-channel eeg. *IEEE Transactions on Neural Systems and Rehabilitation Engineering*, 31: 2195–2204, 2023. doi: 10.1109/TNSRE.2023.3266876.

A Appendix

A.1 Related Work

In this section, we briefly summarise the related work on deep learning methods for general EEG pathology classification that have been successfully applied to the TUH Abnormal EEG Corpus (TUAB) (López de Diego, 2017) or TUH Abnormal Expansion Balanced EEG Corpus (TUABEXB) (Kiessner et al., 2023) (see Table 3 and Table 4 in Section 3.5). In recent years, a substantial amount of research has explored various approaches to general EEG pathology classification, reporting accuracies that lie within a narrow range of 81% to 87%. However, the majority of previous work is based on the TUAB (see Table 3 in Section 3.5). In this regard, Schirrmeister et al. (2017a) introduced and applied two CNNs: Deep4Net and ShallowNet, which were originally proposed for motor imagery and then adapted for EEG pathology classification, achieving accuracies of 85.40% and 84.50%, respectively. These models⁴ have been successfully reused or reimplemented in other studies (Darvishi-Bayazi et al., 2023; Gemein et al., 2020; Khan et al., 2022; Kiessner et al., 2023; 2024; Van Leeuwen et al., 2019; Western et al., 2021; Wu et al., 2021). Since then, several different architectures have been used to classify general EEG pathology. For instance, Gemein et al. (2020) employed two additional networks: a compact CNN called EEGNet and a temporal convolutional neural network (TCN). The EEGNet has been proposed by (Lawhern et al., 2018) for EEG-based BCIs using depthwise and separable convolutions. The TCN was introduced by (Bai et al., 2018) for the sequence modelling task and has then been optimised for EEG classification with a neural architecture search (Chrabaszcz, 2018; Gemein et al., 2020). Other studies have employed different CNNs, such as 1-D CNNs (Shukla et al., 2021; Yıldırım et al., 2020), or hybrid models that combine CNN and RNN (Roy et al., 2018; 2019a), an Inception-Residual CNN (Wu et al., 2021), or an XceptionTime model (Brenner et al., 2024). Recently, a few approaches have explored the potential of a transformer-based foundation model for EEG pathology classification. The Large Brain Model (LaBraM) model (Jiang et al., 2024) (369M parameters) and the Biosignal Transformer (BIOT) model (Yang et al., 2023) (3.2M parameters) were pre-trained on a combination of different datasets using a cross-dataset training and evaluated on the TUAB dataset. Moreover, Roy et al. (2019a) proposed a deep 1D convolutional gated recurrent neural network, called ChronoNet, with exponentially varying filter sizes in the Conv1D layers. While ChronoNet achieved one of the highest accuracies (86.57%), its open-source re-implementation achieved a lower performance (81%) (Khan et al., 2022). Similarly, despite reusing the original implementation of some of these CNNs, studies reported slightly different results from the original report. The reasons for these differences include variations in the preprocessing of EEG data, such as different input lengths, different versions of the TUAB or different datasets, as well as differences in hardware and training strategies. On the TUAB, Wu et al. (2021) reported the highest accuracy of 87.10% using a model called IRCNN. Overall, the reported approaches achieved a mean specificity of above 84% and a mean sensitivity of about 75-80% on the TUAB. Most models show a lower sensitivity than specificity, indicating that they are more likely to classify pathological examples as non-pathological than vice versa. Baseline results on the TUABEXB dataset have been reported using Deep4Net, ShallowNet, TCN and EEGNet (see Table 4 in Section 3.5). These four CNNs achieved typical EEG pathology classification accuracies on TU-ABEXB, with slightly lower accuracies, ranging approximately from 82% to 86%. Consistent with previous studies on the TUAB, the models mostly achieved a lower sensitivity (72-82%) than specificity (83-96%) on the TUABEXB.

⁴are available in Braindecode, a deep learning toolbox for EEG, which is available for download at https://github.com/TNTLFreiburg/braindecode.

Although multi-branch, multi-scale, or parallel architectures (Altuwajjri et al., 2022; Belwafi et al., 2017; Ingolfsson et al., 2020; Jia et al., 2021; Riyad et al., 2020; Szegedy et al., 2015; Zhang et al., 2023a) are now beginning to gain traction in various EEG classification tasks, including motor imagery (Altuwaijri et al., 2022; Cai et al., 2024; Jia et al., 2021; Liu & Yang, 2021; Liu et al., 2023; Yang et al., 2021), emotion recognition (Emsawas et al., 2022; Yan et al., 2025), and neonatal sleep staging (Siddiqa et al., 2024; Zhu et al., 2023), only a few attempts have been made to assess the effectiveness of using CNNs with a set of three convolution scales for general EEG pathology classification. For example, Roy et al. (2019a) has considered the importance of convolutional layers with multiple filters of exponentially varying sizes (2, 4, and 8) to extract and combine features from different time scales. Inspired by the core idea of inception (Szegedy et al., 2015; Zhang et al., 2023a), Wu et al. (2021) employed stacked convolution kernels of different, yet small, scales (1, 3, and 5) in parallel. Recently, Brenner et al. (2024) employed an XceptionTime model, in which each module applies a set of three depthwise separable convolutions with different kernel sizes (11, 21 and 41). These studies have reported improvements in performance, with accuracies ranging from 85.10% to 87.10%. However, these results were based on the TUAB, and no attempts have been made to evaluate the performance of multi-scale CNNs on a larger, more heterogeneous dataset. In addition, smaller kernel sizes were preferred due to lower computational costs (Emsawas et al., 2022), which, however, tend to extract shorter temporal patterns from faster frequency bands (Cohen, 2014; Jia et al., 2021). In contrast, larger kernel sizes require higher computational costs, while they can learn long-term temporal patterns from slow frequency bands (Cohen, 2014; Jia et al., 2021). To date, research has not yet determined whether using raw EEG signals as input for a multi-branch CNN with multi-scale convolutions, which combine both long-term and short-term temporal patterns by employing kernel sizes based on clinically relevant frequency bands, is effective for classifying general EEG pathology on larger, heterogeneous datasets.

A.2 Additional Details about the Datasets

In this section, we provide additional details on the TUH Abnormal EEG Corpus (TUAB)⁵ (López de Diego, 2017) and the TUH Abnormal Expansion Balanced EEG Corpus (TUABEXB)⁶ (Kiessner et al., 2023) that we used in our experiments. The two datasets are publicly available subsets of the Temple University Hospital EEG Corpus (TUEG)⁷ (Obeid & Picone, 2016) for general EEG pathology classification, consisting of EEG recordings labelled as non-pathological or pathological. The TUEG comprises 69,582 clinical EEG recordings from 26,873 EEG sessions involving 15,001 patients over a 15-year period. Details on the number of TUAB recordings and patients are shown in Table 9, while Table 10 gives details of the number of recordings and patients in the TUABEXB dataset. For training, we used the concatenation of the TUAB training set and the TUABEXB training set, which we refer to as the TUH Abnormal Combined EEG Corpus (TUABCOMB). We evaluated our models on the predefined test set of both datasets, TUAB and TUABEXB, respectively (see Section 3.3). Details on the number of recordings and patients of the TUABCOMB are shown in Table 11. There is no overlap of patients between the training set of TUABCOMB and the evaluation sets of TUAB and TUABEXB.

A.3 Design Choices and Hyperparameter Optimisation

For our proposed Multi-BK-Net architecture described in Section 2.1, we evaluated several design choices, including architecture hyperparameters, such as total number of temporal filters, filter length of the later convolution layer, strides and types of non-linearities, as well as algorithm hyperparameters, such as learning rate, weight decay and number of training epochs. In addition, we evaluated potential performance improvements by using intermediate normalisation by batch normalisation (Ioffe & Szegedy, 2015) or group normalisation (Wu & He, 2018) as well as the use of exponential linear units (ELU, f(x) = x for x > 0 and $f(x) = e^x - 1$ for $x \le 1$) (Clevert et al., 2016) or GELU ($GELU(x) = xP(X \le x) = x\Phi(x)$) (Hendrycks & Gimpel, 2023) as activation function. The hyperparameters used and their possible values, which construct the search space, are listed in Table 12.

 $^{^5}$ v2.0.0; available for download at https://www.isip.piconepress.com/projects/tuh_eeg/html/downloads.shtml.

⁶The EEG recordings are part of the TUH EEG Corpus and are publicly available after registration on the TUH EEG Corpus website (isip.piconepress.com/projects/tuh_eeg/html/downloads.shtml. The corresponding pathology labels are available for download at github.com/AKiessner/TUHAbnormal-Expansion-dataset.

⁷v1.1.0 and v1.2.0; available for download at https://isip.piconepress.com/projects/tuh_eeg/downloads/tuh_eeg/.

Table 9: Number of recordings and patients in the TUAB dataset. For 54 patients in the training set, both non-pathological and pathological recordings are available. However, there is no overlap between patients in the training and evaluation sets. For more details on the dataset, see López de Diego (2017) and Obeid & Picone (2016).

TUH Abnormal	Training set		Evaluation set	
EEG Corpus (TUAB)	Recordings	Patients	Recordings	Patients
Non-pathological	1371	1237	150	148
Pathological	1,346	893	126	105
Total	2,717	2,130	276	253

Table 10: Number of recordings and patients in the TUABEXB dataset. There are 183 patients with both pathological and non-pathological recordings in the training set. The training and evaluation sets do not share recordings from the same patient. Details of the dataset and the labelling procedure can be found in Kiessner et al. (2023).

TUH Abnormal Expansion	Training set		Evaluation set	
Balanced EEG Corpus (TUABEXB)	Recordings	Patients	Recordings	Patients
Non-pathological	4,015	3,253	447	392
Pathological	3,975	3,166	442	378
Total	7,990	6,419	889	770

To identify the optimal set of the CNN hyperparameters (Table 12), we employed the automatic hyperparameter optimisation framework Optuna (Akiba et al., 2019), as it has been successfully used to efficiently tune the hyperparameters of CNNs (Al-Ja'afreh et al., 2023; Hanifi et al., 2024; Latreche et al., 2025; Shekhar et al., 2021). Optuna implements Sequential Model-Based Optimisation (SMBO) to efficiently search for the optimal hyperparameters by building a probabilistic model of the objective function (Akiba et al., 2019; Bergstra et al., 2011; Lemos et al., 2021). To search for the hyperparameter space and maximise the objective function, we used the Tree-structured Parzen Estimator (TPE) algorithm (Bergstra et al., 2011; 2013). We used multivariate TPE rather than independent TPE because multivariate TPE is reported to outperform independent TPE by finding better solutions faster and by better handling problems where there is an interaction between variables. The optimisation approach is described in detail in Bergstra et al. (2011; 2013); Falkner et al. (2018) and Kenny et al. (2024). In medical diagnosis, identifying all potentially pathological EEG recordings is more important than reducing false-positive results. Therefore, two objective measures validation accuracy and validation sensitivity — were considered in this study. The multi-objective function for hyperparameter optimisation is defined as maximising the mean validation accuracy and mean validation sensitivity of the 5-fold cross-validation method. For each set of hyperparameters, we performed 5-fold cross-validation on the TUABCOMB training data using StratifiedGroupKFold, available in the Scikit-learn library (Pedregosa et al., 2011), with the constraint that patients were non-overlapping between splits (80% for training and 20% for validation). The splits were made with respect to the patients to avoid using recordings from the same patient in different folds. We additionally shuffled the data before splitting to ensure that there were no chronologically ordered splits, similar to the predefined training and evaluation sets in the TUAB and TUABEXB datasets. Experiments were conducted with a time budget of 45 hours per fold for each configuration run on a single fold. Runs that exceeded the time limit were pruned after completing the first fold. Runs that crashed (e.g., network configurations that did not fit in GPU memory) were also pruned. In addition, runs with a validation accuracy or validation sensitivity of less than 75% at the first fold were pruned to speed up optimisation. We ran the optimisation process until a total of 100 trials were completed, where we jointly optimised parameters and architecture layouts. For the top 10 trials, we repeated the 5-fold cross-validation ten times and computed the mean validation accuracy and mean validation sensitivity, averaging across folds and then across runs. Finally, the best model configuration, with the highest mean accuracy and mean sensitivity, was used to train the model on the full TUABCOMB

Table 11: Number of recordings and patients in the TUABCOMB training set dataset. There are 237 patients with both pathological and non-pathological recordings. The training set of the TUABCOMB and the evaluation sets of the TUAB and TUABEXB do not share the same patients.

TUABCOMB	Training set		
	Recordings	Patients	
Non-pathological	5,386	4,490	
Pathological	5,321	4,009	
Total	10,707	8,549	

Table 12: Configuration spaces considered in the search for the Multi-BK-Net architecture. We sampled until 100 configuration trials were completed to find the best setting. Learning rate and weight decay were defined as trial.suggest_float(log=True).

Parameter	Config. Space
Total number of temporal conv filters	[20, 25, 30, 35, 40, 45, 50, 55, 60, 65, 70, 75, 80]
Normalisation	[batch, group]
Activation functions	[ELU, GELU]
Pooling mode first block	[mean, max]
Pooling mode other blocks	[mean, max]
Forth conv-pooling-block	[True, False]
Forth conv-pooling-block broader	[True, False]
Dropout	[0.4 - 0.6]
Filter length conv blocks	[10,15,20]
Input window size	6000
Weighted loss factor pathological	[1,2,3,4]
Optimiser	[AdamW]
Optimiser beta1	[0.5, 0.9]
Learning rate	$[1e^{-5} - 1e^{-1}]$
Weight decay	$[1e^{-5} - 1e^{-1}]$
Batch size	[16,32,64]
Number of epochs	[30 - 105]
Number of channels	21

training set and then evaluated on the unseen, predefined evaluation sets from the TUAB and TUABEXB (see Section 3.3 for more details). The final hyperparameters are listed in Table 1 in Section 2.1.

A.4 Additional Details on the Baseline Architectures

In this section, we provide additional details on the baseline architectures, the list of hyperparameters for training and information on the training procedure. We additionally included five architectures implemented in Braindecode as a baseline: Deep4Net (Schirrmeister et al., 2017b;a), ShallowNet (Schirrmeister et al., 2017b;a), TCN (Bai et al., 2018; Chrabąszcz, 2018; Gemein et al., 2020), EEGNet Gemein et al. (2020); Lawhern et al. (2018) and ChronoNet Roy et al. (2019a). These architectures have been utilised in several studies, demonstrating high performance on the TUAB and TUABEXB datasets across various versions and different preprocessing steps. The architectures are shown in Table 14 and Table 15. For a more detailed explanation of each architecture and its optimised hyperparameters, please refer to the corresponding studies. To ensure fairness in evaluation, we apply the same data preprocessing steps and training strategy to all architectures. While we have employed a trial-wise training strategy in this work, previous studies have mainly used a cropped training strategy (Gemein et al., 2020; Kiessner et al., 2023; 2024; Schirrmeister et al., 2017a). To adapt the architectures to our framework, we used their implemented approach for trial-wise training (Schirrmeister et al., 2017b). All models were trained on the TUABCOMB training set for 35

Table 13: Optimised hyperparameters of the four single-scale CNNs that we used as a baseline (Gemein et al., 2020; Schirrmeister et al., 2017a; Kiessner et al., 2023; Chrabąszcz, 2018). No: Number of. For Deep4Net, ShallowNet and EEGNet, the parameter final_conv_length was set to 'auto' to enable trial-wise training. In the case of TCN, an AdaptiveAvgPool1d layer was added to the final block.

Hyperparameter	Deep4Net	ShallowNet	TCN	EEGNet
No. input channels	21	21	21	21
Input time length	6000	6000	6000	6000
No. start filters	25	40	n.a.	n.a.
No. filters	n.a.	n.a.	55	n.a.
F1 (temporal filter)	n.a.	n.a.	n.a.	8
D depth multiplier	n.a.	n.a.	n.a.	2
F2 (pointwise filter)	n.a.	n.a.	n.a.	16
Final conv. length	67	394	n.a.	187
Channel factor	2	n.a.	n.a.	n.a.
Stride before pool	True	n.a.	n.a.	n.a.
Initial learning rate	0.01	0.000625	0.0011261049710243193	0.001
Weight decay	0.0005	0	5.83730537673086e-07	0
Dropout	0.5	0.5	0.05270154233150525	0.25
L2 decay	n.a.	n.a.	1.7491630095065614e-08	n.a.
Gradient clip	n.a.	n.a.	0.25	n.a.
Batch size	64	64	64	64
No. epochs	35	35	35	35
Total No. parameters	303,452	66,242	456,502	7,426

epochs using the trial-wise training strategy (Schirrmeister et al., 2017b). For all models, a batch size of 64 was used. The model parameters of Deep4Net, ShallowNet, TCN, and EEGNet were optimised using the AdamW optimiser (Loshchilov & Hutter, 2017). For more details on the hyperparameters used for training, see Table 13. For optimisation of the ChronoNet, we use the Adam optimiser (Kingma & Ba, 2017) with a learning rate of 0.001 and the binary cross-entropy loss. The learning rates for the gradient and weight decay updates were scheduled using cosine annealing (Loshchilov & Hutter, 2016), and we refrained from learning rate restarts.

A.5 Additional Details on the Evaluation Metrics

In this section, we provide additional details on the evaluation metrics and significance tests used in this study. In our experiments, we evaluated the classification performance of our proposed Multi-BK-Net and comparison models using five performance evaluation metrics: accuracy, balanced accuracy, sensitivity, specificity and F2-score. These measures were determined as shown in Table 16. As both evaluation sets are slightly imbalanced (see Table 9 and Table 10), we also reported the balanced accuracy (BACC). Since our task is to classify EEG pathology, and thus no EEG recording containing pathological EEG patterns should be classified as non-pathological, it is important to reduce the false negative rates. False positives, on the other hand, can be excluded by clinicians through a more detailed diagnostic process. As minimising false negatives is the primary concern in this task, we additionally report the F2-score, which prioritises the model's ability to identify pathological EEG recordings (recall) over the model's ability to identify positive instances while minimising false positives.

A.6 Detailed Results

A.6.1 Performance Comparison to Baseline Approaches

The classification performance of the Multi-BK-Net and all baseline models on the TUAB is shown in Figure 8. On the TUAB evaluation set, Multi-BK-Net achieved a mean balance accuracy of 87.36%, indicating

the best classification performance, which was also statistically significantly better than the baseline models (p < 0.001, Mann-Whitney U test). Compared to four of the baseline architectures, our Multi-BK-Net achieved a slightly lower specificity, which was not statistically significantly different, except for the difference with Deep4Net (p < 0.001, Mann-Whitney U test). Figure 9 compares the balanced accuracy and sensitivity of our proposed Multi-BK-Net and all baseline architectures on the TUABEXB evaluation set. Again, the Multi-BK-Net outperformed the baseline models. In particular, the Multi-BK-Net achieved a higher mean balanced accuracy of 86.99% on the dedicated test set, which was also statistically significantly different from the baseline architectures (p < 0.001, Mann-Whitney U test). Although three of the baseline models achieved a slightly higher specificity than Multi-BK-Net (89.73%), only the difference between Multi-BK-Net and Deep4Net was statistically significant (p < 0.01). Conversely, Multi-BK-Net achieved a statistically significantly higher mean specificity than ChronoNet (p < 0.05, Mann-Whitney U test).

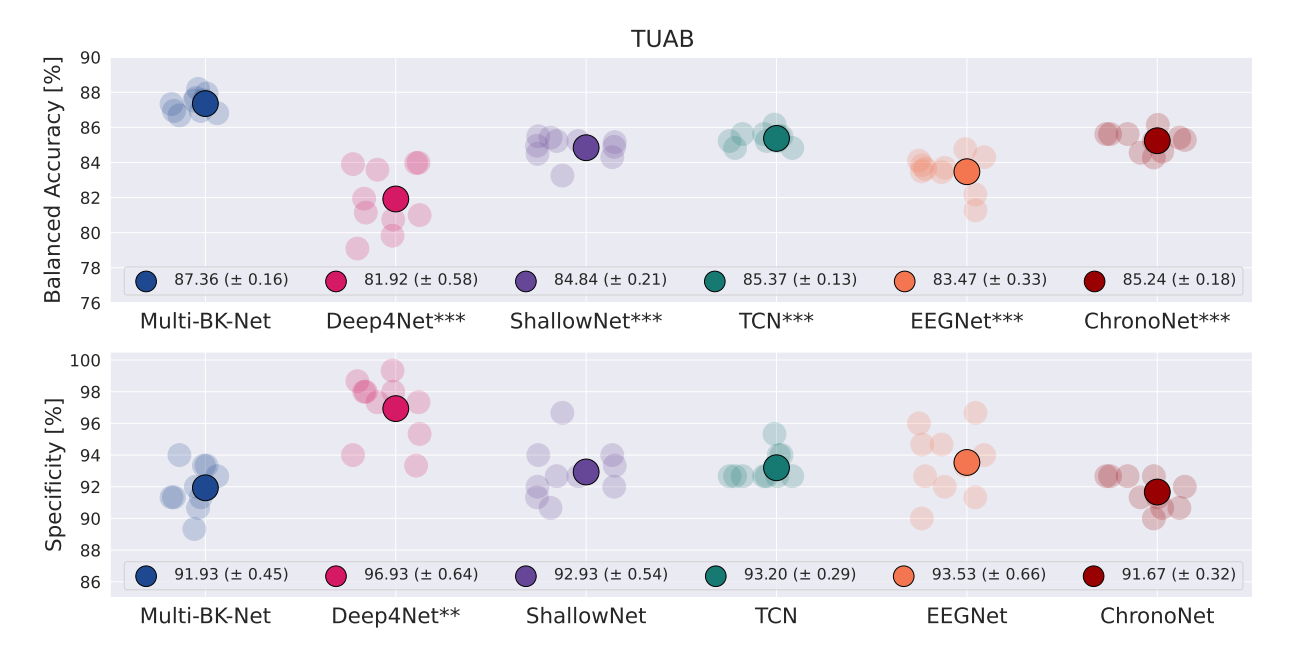


Figure 8: Performance comparison between our proposed Multi-BK-Net and five baseline architectures on the predefined TUAB evaluation set. Each transparent marker represents the performance of a single run, and each larger, bold symbol represents the mean performance score averaged across ten independent runs (n=10). The mean standard error is given in parentheses. Stars indicate statistically significant differences in performance score between the corresponding baseline architecture and the Multi-BK-Net (Bonferronicorrected two-sided Mann-Whitney U test, p < 0.05: *, p < 0.01: ***, p < 0.001: ***).

A.6.2 Performance Comparison with Previous Reported State-of-the-art Deep Learning Approaches

Several studies have employed various end-to-end deep learning methods for the task of general EEG pathology classification (see Section A.1). In this section, we provide more details on the comparison of our proposed methods to previous work. For the selection of a previously published work on end-to-end deep learning models for general EEG pathology classification, we considered different architectures that have achieved competitive classification performance and match the following criteria: To ensure a fair comparison, the selected models adopt the raw or minimally preprocessed input from the same set of multiple standard scalp EEG electrodes and are evaluated on the predefined TUAB evaluation set or on the predefined TUABEXB evaluation set. Hence, publications that reported cross-validation results (Muhammad et al., 2021; Nahmias & Kontson, 2020; Poziomska et al., 2024), used single-channel data as input (Shukla et al., 2021; Yıldırım et al., 2020), or evaluated their methods on data from a non-publicly available dataset (Kim et al., 2023; Van Leeuwen et al., 2019), were excluded from our direct comparison. Table 3 and Table 4 in Section 3.5 summarise the comparison between our Multi-BK-Net and other methods on the TUAB and TUABEXB datasets, respectively. Perhaps the most clinically relevant finding is that Multi-BK-Net, with a mean sensi-

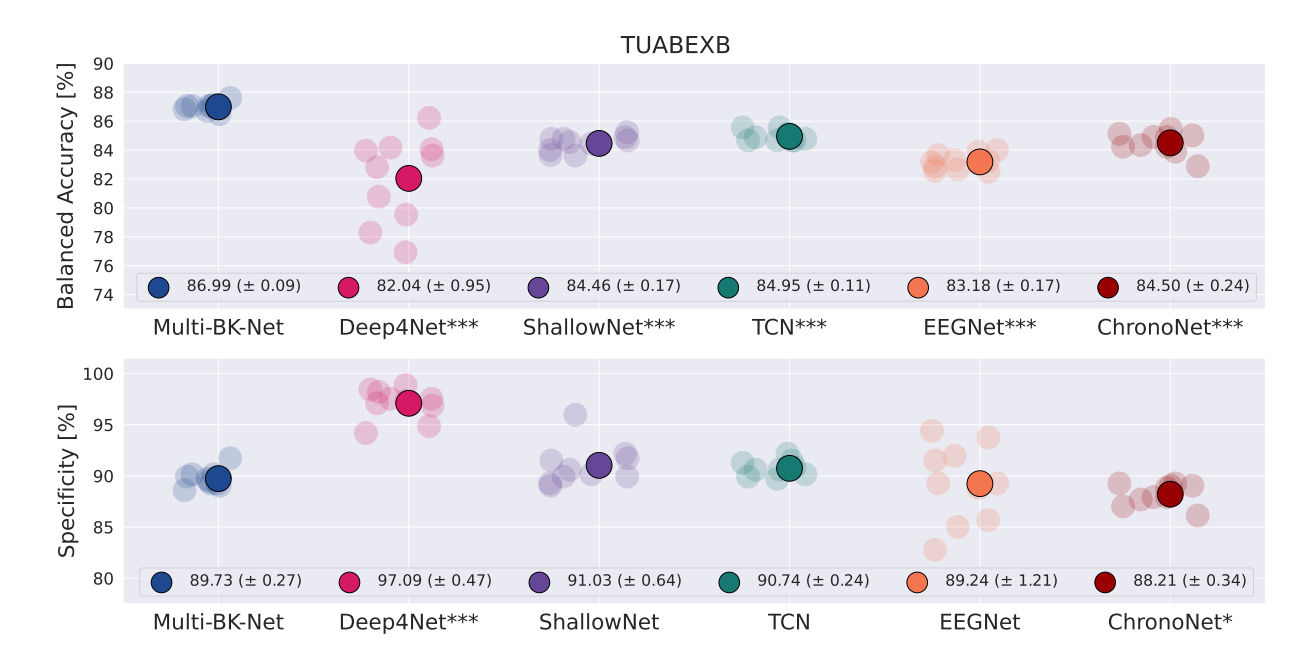


Figure 9: Performance comparison between our proposed Multi-BK-Net and all baseline architectures on the predefined TUABEXB evaluation set. Performance metrics are averaged across ten independent runs (n=10). The mean standard error is given in parentheses. Conventions as in Figure 8.

tivity of 83.10%, outperforms all other approaches, reporting a mean sensitivity averaged over multiple runs, by at least 3.26% (see Table 3). Note that Brenner et al. (2024) reported a sensitivity of 85.70% for the XceptionTime model. However, the authors used only the first window of each recording as input during evaluation and reported single-run results, which is a significant limitation of this approach. Due to the use of stochastic gradient-based algorithms with randomised weight initialisation, data ordering, and data augmentation during training, each independent training run produces a different network with better or worse performance than the average, with a variance of approximately 1% to 2% (Picard, 2023). Even if the variance between runs is not very large, there is a high probability that the performance of a single run will be an outlier, much better or much worse than the average (Picard, 2023). As a result, this variance can make it challenging to compare training configurations (Bouthillier et al., 2021; Picard, 2023). For example, comparing single runs, Multi-BK-Net achieved a sensitivity of 85.72% with accuracies of 88.41% and 87.68%, and a specificity of 90.67% and 89.33%, respectively, thus clearly outperforming the XceptionTime model. Nevertheless, to reduce stochasticity and improve comparability between training and model configurations, one should report the average of evaluation metrics over multiple runs (Wightman et al., 2021). Hence, a direct comparison of publications reporting single-run results would be unfair. Furthermore, comparing Table 3 with Table 4, it can also be seen that the mean accuracy of the Multi-BK-Net is slightly better on the TUAB than on the TUABEXB (+0.74%). At the same time, Multi-BK-Net achieved a higher mean sensitivity on TUABEXB than on TUAB (+1.15%). Interestingly, this result is consistent with previous observations (Kiessner et al., 2023), assuming that the differences are due to systematic differences in age, sex and pathological feature distribution as well as different labelling methods (see Kiessner et al., 2023, for a more detailed discussion). Furthermore, we observed that Multi-BK-Net achieved a lower sensitivity than specificity on both evaluation sets, indicating a lower ratio of false positives than false negatives. This is also consistent with the results presented in previous literature (Gemein et al., 2020; Kiessner et al., 2023; 2024; López de Diego, 2017; Schirrmeister et al., 2017a; Western et al., 2021).

Overall, one of the main findings of our study is that the proposed model achieved mean accuracies of 87–88%. However, as noted and discussed in previous work (Engemann et al., 2018; Frénay & Verleysen, 2014; Gemein et al., 2020; Kiessner et al., 2024; Poziomska et al., 2024; Sun et al., 2019), there remains the possibility that this accuracy range may be the upper limit due to imperfect inter-rater agreement and

the resulting label noise, with a model performance remaining below a perfect classification score (100%) and saturating around 88%. For the task of classifying EEG recordings as pathological or non-pathological, previous research has reported an inter-rater agreement of 86–88% between two neurologists (Housek & Ellingson, 1959; Rose et al., 1973). At the same time, Beuchat et al. (2021) have found even lower mean inter-rater agreements of 82-86% between multiple EEG technologists and neurologists. Unfortunately, the differences in classification performance cannot be compared with the inter-rater agreement on these datasets used in this study for training and evaluation, as the labels of the TUAB and TUABEXB are mainly based on the impression of a single expert, as stated in the corresponding EEG report (for more details, see Kiessner et al., 2023; López de Diego, 2017; Obeid & Picone, 2016). Also, other studies on general EEG classification suffer from the same uncertainty. However, the need to include ratings from multiple experts has been recognised in other EEG classification tasks. For instance, Stephansen et al. (2018) compared the classification performance of their model with the inter-rater agreement of six raters for the task of classifying sleep stages. The authors found that the model's accuracy increased from 76% (one rater) to 87% (consensus of six raters). Therefore, it can be assumed that the deep learning models for general EEG pathology also perform better than a single rater. It would thus be interesting to compare the classification performance of the proposed model with the inter-rater agreement of multiple raters. As the label noise remains the main limiting factor, it will be important to determine whether and to what extent label quality can be improved. For instance, using labels based on an ensemble of multiple raters would be a significant start to improving label quality. Additionally, using averaged ratings (so-called "fuzzy labels") for training could further enhance model performance, as they represent a probability of pathology, which is also helpful in identifying recordings that are ambiguous or more challenging to categorise or contain more confounding patterns. Furthermore, as shown in Beuchat et al. (2021), multiple raters tend to achieve a higher mean sensitivity (87%) than mean specificity (75%), which is the opposite of machine learning approaches, which typically achieve higher specificity than sensitivity. Thus, including multiple raters as a baseline for training could increase the sensitivity of the classification model and also might further improve model performance, as was done for sleep stage classification. Moreover, a systematic optimisation of the labelling quality might even help the models overcome the current asymptotic limits of predictive accuracy (Darvishi-Bayazi et al., 2023; Kiessner et al., 2024; Poziomska et al., 2024), and hence lead to even better-performing models for the task of general EEG pathology classification.

A.6.3 UMAP Visualisation of Learned Features

To further explain the proposed network, we visualised the learned features of the Multi-BK-Net before the classification layer using the UMAP (McInnes et al., 2018) method to map high-dimensional feature vectors into a two-dimensional UMAP space. This allowed the visual inspection of clustering and separation between pathological and non-pathological classes. For comparison, we also extracted and visualised the feature representations of the Deep4Net, as it is a single-scale CNN that is most similar in architecture to Multi-BK-Net, the TCN, which achieved the second-highest classification accuracy, and the ChronoNet, which uses a set of three convolutions. A UMAP comparison plot of the visualisation of the feature representation of the last layer before the classification layer is shown in Figure 10. In general, all models can form discernible clusters for pathological and non-pathological recordings, but with a noticeable amount of overlap. This is reflected in a reduced classification performance, which falls within a narrow range of 83% and 88%. As Multi-BK-Net shows the best classification performance, it also forms distinct and compact clusters for pathological and non-pathological recordings with minimal overlap. Smaller intra-class distances, i.e., tighter clustering, indicate a more consistent representation within each class, while larger inter-class distances, i.e., more distinct clusters, indicate that the model has learned features that effectively discriminate between the two classes. Compared to Multi-BK-Net, the three baseline models tend to form smaller and more dispersed clusters, possibly indicating greater within-class variability or a less precise representation of the pathological class. For example, Deep4Net forms less compact clusters, resulting in more dispersed clusters with larger intra-class distances. In addition, we can observe that pathological clusters are more dispersed along the component 1 axis, which may indicate greater within-class variability for pathological samples. This further suggests that these baseline models are less consistent in identifying pathological samples and are less capable of capturing the heterogeneity in pathological samples. The slightly lower effectiveness in capturing the characteristics of pathological samples may also reflect the lower sensitivity (high false negative rate) of the three baseline models compared to Multi-BK-Net. Additionally, when comparing the datasets (left vs. right column, Figure 6), we observe that all four models exhibit more distinct feature separation and better-defined clusters on the TUAB dataset than on the TUABEXB dataset. This suggests that the learned features are more discriminative for the TUAB dataset than the TUABEXB dataset. For all models, the distinction between pathological and non-pathological recordings was less pronounced on TUABEXB. Since better feature separation leads to improved classification performance, this may result in better model performance on TUAB than TUABEXB. A possible explanation for this could be that the TUABEXB is more heterogeneous compared to the TUAB (Kiessner et al., 2023), and as shown in previous work, this data heterogeneity can make EEG classification more difficult (Kiessner et al., 2023; Poziomska et al., 2024). Finally, the qualitative observations derived from the UMAP visualisations, which highlight the different degrees of feature separation achieved by various models, are consistent with quantitative performance metrics, such as accuracy and sensitivity. For instance, the distinct and compact clustering of data points, indicative of strong feature discrimination, observed for the Multi-BK-Net corresponds to higher accuracy and sensitivity scores compared to other models on both datasets. Conversely, the large intra-class distances seen in the visualisations for the pathological samples of the three baseline CNNs align with their lower sensitivity performance (67-81%). Similarly, models with poorer cluster separation in the UMAP visualisations, such as the Deep4Net, show comparable poorer quantitative performance (accuracy of 82-83%). This consistency between qualitative visualisations and quantitative results supports the validity of the UMAP analysis and provides a comprehensive understanding of model performance.

A.6.4 Ablation experiments

In this section, we provide additional details on the ablation experiments (Section 3.6) and present additional results. Compared to the five baseline architectures, our proposed Multi-BK-Net is significantly larger (1,038,683 parameters). For example, it is approximately twice the size of TCN (456,502 parameters), three times the size of Deep4Net (303,452 parameters), and eight times the size of ChronoNet (137,233 parameters). The Multi-BK-Net achieved an accuracy improvement of 2-5% over the baseline models, while sensitivity increased by more than 3.5-17.3%. Previous studies have shown that larger models perform better than smaller models (Darvishi-Bayazi et al., 2023; Howard et al., 2017; Kiessner et al., 2024; Talmor & Berant. 2019; Tan & Le, 2019; Sun et al., 2017; Zagoruyko & Komodakis, 2016). To verify that the superiority of the Multi-BK-Net over the baseline models was not due to the increased model size, we performed an ablation experiment. As the Deep4Net has the most similar architecture to our proposed Multi-BK-Net, we compared the performance of our approach with that of three larger versions of the Deep4Net (see Table 17). In particular, we increased the number of temporal filters in the Deep4Net to 35, which is the same number of filters used in the first convolution-pooling block of the Multi-BK-Net. We refer to this model as Deep4Net35, which comprises 579,182 parameters, approximately 55% of the size of Multi-BK-Net. We have also increased the number of temporal filters in the Deep4Net to 47 (Deep4Net47). This increases the number of trainable parameters to 1,026,482, which is approximately the relative size of 99% of the Multi-BK-Net. Finally, we created a variant called Deep4Net48, which contains 48 temporal filters and has 1,069,490 trainable parameters; thus, it is slightly larger than Multi-BK-Net.

To further validate the effectiveness of our multi-temporal kernel branches in the first convolution-pooling block of our proposed Multi-BK-Net, we also trained and evaluated different variants of our model, in which we removed four of the five branches while increasing the number of filters in the remaining branch from 7 to 35. Thus, the variant models consist of a single branch with 35 filters, with only one temporal kernel length in the first block. The kernel length of the variants is set to either 3, 7, 10, 13, 25 or 200. The Multi-BK-Net uses kernel lengths of 3, 7, 13, 25 and 200, while the Deep4Net uses a kernel size of 10. We refer to these variants as STKSBNet (Single-Temporal-Kernel Single-Branch Net). For example, STKSBNet3 refers to the model variant that uses a temporal kernel length of 3. Furthermore, to investigate the effect of different branches, we included an additional variant with five different temporal kernels (3, 7, 13, 25, and 200), but only one branch was used instead of five. Thus, the features of the five temporal convolutional layers are concatenated directly before the spatial convolution. We refer to this model variant as MTKSBNet (Multi-Temporal-Kernel Single-Branch Net). For more details on the size of the models used, see Table 17. We trained the STKSBNet and MTKSBNet variants as described in Section 2.1, and the Deep4Net variants as described in Section 3.2 and evaluated all variants as described in Section 3.3.

As shown in Table 5 in Section 3.6, the performance of Deep4Net increases as the number of filters increases. However, only Deep4Net47 obtained a statistically significantly higher mean F2-score and mean sensitivity on the TUABEXB set compared to Deep4Net (p < 0.05, one-sided Mann-Whitney U test). All other differences between the original Deep4Net and its larger variants were not statistically significant (p > 0.05, Mann-Whitney U test). Nevertheless, Multi-BK-Net outperforms all variants of Deep4Net statistically significantly on both datasets (p < 0.01, Mann-Whitney U test). This suggests that the performance improvement of Multi-BK-Net compared to Deep4Net is not due to increased model width or model size.

Moreover, Table 6 in Section 3.6 shows the performance of the variant models and the Multi-BK-Net on the TUAB and TUABEXB evaluation sets. It can be seen that when four branches and four of the kernel sizes are removed, there is a significant decrease in the results on both evaluation sets (p < 0.05, Mann-Whitney U test). By using a single kernel length, STKSBNets cannot extract accurate features, resulting in lower overall performance compared to Multi-BK-Net. This highlights the effectiveness of using multiple temporal kernel lengths. Furthermore, when comparing the performance of the STKSBNet variants, it is evident that the optimal kernel size for STKSBNet varies across different datasets. For TUAB, the mean accuracy is highest when the kernel size is 13, while the optimal kernel size for TUABEXB is 200. This observation is consistent with previous studies, which report that determining the optimal kernel length for EEG pathology classification is challenging due to subject and time differences (Jia et al., 2021). A possible solution is to use multiple kernels of different sizes, which also improves classification performance (Altuwaijri et al., 2022; Jia et al., 2021). Furthermore, the results show that the inclusion of multiple temporal kernels of different lengths, but with a single branch, improves performance compared to using a single kernel of a single length. This shows that multiple kernels can learn valuable features and improve classification performance. However, as shown in Table 6, incorporating multiple branches within the first block further improves performance on both datasets compared to using only a single branch (MTKSBNet). When the four branches are removed, but multiple kernel lengths are used (MTKSBNet), the mean F2-score and mean sensitivity decrease (p < 0.05, Mann-Whitney U test). This shows that the introduction of multiple input branches improves the identification of pathological samples. Overall, this ablation experiment demonstrates that incorporating both multiple temporal kernel lengths and multiple branches, as is done in Multi-BK-Net, is beneficial for classifying EEG pathology and significantly enhances the model's performance.

A.6.5 Overview of Classification Performance in Different Age and Sex Subgroups

For a more in-depth analysis of model performances, we report the classification performances on subsets created based on age and sex information in Table 18 and Table 19. The tables present a detailed performance comparison of the proposed Multi-BK-Net against five baseline architectures across various subgroups of both the TUABEXB and TUAB datasets. Subgroup analyses were conducted by stratifying the test data by age and sex and computing the corresponding metrics and confidence intervals for each subgroup. Performance metrics were computed separately for each subgroup and averaged across ten independent runs. Mean performance metrics and mean 95% confidence intervals were then calculated across ten independent runs using the normal approximation (mean $\pm 1.96 \times \text{standard error}$). With minor exceptions, e.g. on patients younger than 25 years of the TUAB, Multi-BK-Net achieved higher mean accuracies and sensitivities than the baseline models across all subsets. For instance, in Table 19, the Multi-BK-Net achieves a mean accuracy of 87.51% for the 25 years \leq age < 60 subgroup and a mean accuracy of 86.82% for the male subgroup. Similarly, in Table 18, the Multi-BK-Net obtain a mean accuracy of 88.43% for the 25 years ≤ age < 60 subgroup and a mean accuracy of 88.12% for the male subgroup. While other architectures, such as TCN and EEGNet, occasionally show very high specificity, they often achieve significantly lower sensitivity. The Multi-BK-Net, in contrast, maintains a strong performance across both sensitivity and specificity, indicating its robust capability to identify both pathological and non-pathological recordings across different subgroups correctly.

A.6.6 Training Time and Computational Requirements

We report training and inference time and memory in Table 20.

Table 14: Architecture of the four single-scale, baseline CNNs adapted for trial-wise training and as implemented in Braindecode (Gemein et al., 2020; Schirrmeister et al., 2017a; Kiessner et al., 2023; Chrabąszcz, 2018). E: Number of input electrodes. St: Stride.

Deep4Net	ShallowNet	TCN	EEGNet
$25 \times \text{Conv2D} (10 \times 1)$	$40 \times \text{Conv2D} (25 \times 1)$	55×Conv1D (16)	$8 \times \text{Conv2D} (1 \times 64)$
$25 \times \text{Conv2D} \ (1 \times E)$	$40 \times \text{Conv2D} \ (1 \times E)$	WeightNorm	BatchNorm
BatchNorm	BatchNorm	Activation (ReLU)	$16 \times \text{Conv2D} (E \times 1)$
Activation (ELU)	Activation (Square)	Dropout2d (0.25)	BatchNorm
MaxPool (3×1)	MeanPool (75×1) St (15×1)	$55 \times \text{Conv1D} (16)$	Activation (ELU)
	Activation (Log)	WeightNorm	MeanPool (1×4) St (1×4)
	Dropout (0.5)	Activation (ReLU)	Dropout (0.25)
		Dropout2d (0.25)	
		$55 \times \text{Conv1D} (1)$	
		Activation (ReLU)	
Dropout (0.5)	$2 \times \text{Conv2D } (394 \times 1)$	$55 \times \text{Conv1D} (16)$	$16 \times \text{Conv2D} \ (1 \times 16)$
$50 \times \text{Conv2D} (10 \times 1) \text{ St}(3 \times 1)$	LogSoftmax	WeightNorm	$16 \times \text{Conv2D} \ (1 \times 1)$
BatchNorm		Activation (ReLU)	BatchNorm
Activation (ELU)		Dropout2d (0.25)	Activation (ELU)
MaxPool (3×1)		$55 \times \text{Conv1D} (16)$	MeanPool (1×8) St (1×8)
		WeightNorm	Dropout (0.25)
		Activation (ReLU)	
		Dropout2d (0.25)	
Dropout (0.5)		$55 \times \text{Conv1D} (55 \times 16)$	$2 \times \text{Conv2D} (1 \times 187)$
$100 \times \text{Conv2D} (10 \times 1) \text{St}(3 \times 1)$		WeightNorm	LogSoftmax
BatchNorm		Activation (ReLU)	
Activation (ELU)		Dropout2d (0.25)	
$MaxPool (3 \times 1)$		$55 \times \text{Conv1D} (16)$	
		WeightNorm	
		Activation (ReLU)	
70.7		Dropout2d (0.25)	
Dropout (0.5)		55×Conv1D (16)	
$200 \times \text{Conv2D} $ (10×1) St(3×1)		WeightNorm	
BatchNorm		Activation (ReLU)	
Activation (ELU)		Dropout2d (0.25)	
MaxPool (3×1)		55×Conv1D (16)	
		WeightNorm	
		Activation (ReLU)	
$2 \times \text{Conv2D} (67 \times 1)$		Dropout2d (0.25) 55×Conv1D (16)	
LogSoftmax		WeightNorm	
LogSommax		Activation (ReLU)	
		Dropout2d (0.25)	
		$55 \times \text{Conv1D} (16)$	
		WeightNorm	
		Activation (ReLU)	
		Dropout2d (0.25)	
		Linear (55,2)	
		AdaptiveAvgPool1d	
		LogSoftmax	

Table 15: Architecture of the baseline architecture ChronoNet as proposed by Roy et al. (2019a). ChronoNet includes multiple filters of exponentially varying lengths in the 1D convolutional layers and dense connections within the GRU layers. Arrows represent skip connections. K: kernel_size. st: stride. p: padding. h: hidden_size

	${f ChronoNet}$	
$32 \times \text{Conv1D}(k(2,), st(2,), p(1,))$	$32 \times \text{Conv1D}(k(4,), \text{st}(2,))$	$32 \times \text{Conv1D}(k(8,), \text{st}(2,), p(3,))$
	Filter Concat	
$32 \times \text{Conv1D}(k(2,), st(2,), p(1,))$	$32 \times \text{Conv1D}(k(4,), \text{st}(2,))$	$32 \times \text{Conv1D}(k(8,), st(2,), p(3,))$
	Filter Concat	
$32 \times \text{Conv1D}(k(2,), st(2,), p(1,))$	$32 \times \text{Conv1D}(k(4,), \text{st}(2,))$	$32 \times \text{Conv1D}(k(8,), st(2,), p(3,))$
	Filter Concat	
	GRU(h(32))	
	GRU(h(32)) Filter Concat	
	GRU(h(32)) Filter Concat	
	Filter Concat	
	GRU(h(32))	
	Linear layer	
Total No. parameters	137,233	

Table 16: Performance evaluation metrics. TP is the number of examples that were correctly classified in the positive class, TN is the number of examples that were correctly classified in the negative class, FP is the number of examples that were incorrectly classified in the positive class, FN is the number of examples that were incorrectly classified in the negative class. F2-score: $\beta=2$ to emphasise the need to minimise false negatives, and $Precision=\frac{TP}{TP+FP}$ and $Recall=\frac{TP}{TP+FN}$. Higher values of the F2-score indicate better performance in terms of recall.

Performance metric	Mathematical formula
Accuracy	$\frac{(TP+TN)}{(TP+FN+TN+FP)}$
Balanced accuracy	$\frac{1}{2}(\frac{TP}{TP+FN} + \frac{TN}{TN+FP})$
Sensitivity	$\frac{\mathrm{TP}}{\mathrm{TP} + \mathrm{FN}}$
Specificity	$rac{ ext{TN}}{ ext{TN+FP}}$
F2-score	$(1+\beta^2)\left(\frac{\frac{\text{TP}}{\text{TP+FP}} * \frac{\text{TP}}{\text{TP+FN}}}{(\beta^2 * \frac{\text{TP}}{\text{TP+FP}}) + \frac{\text{TP}}{\text{TP+FN}}}\right)$

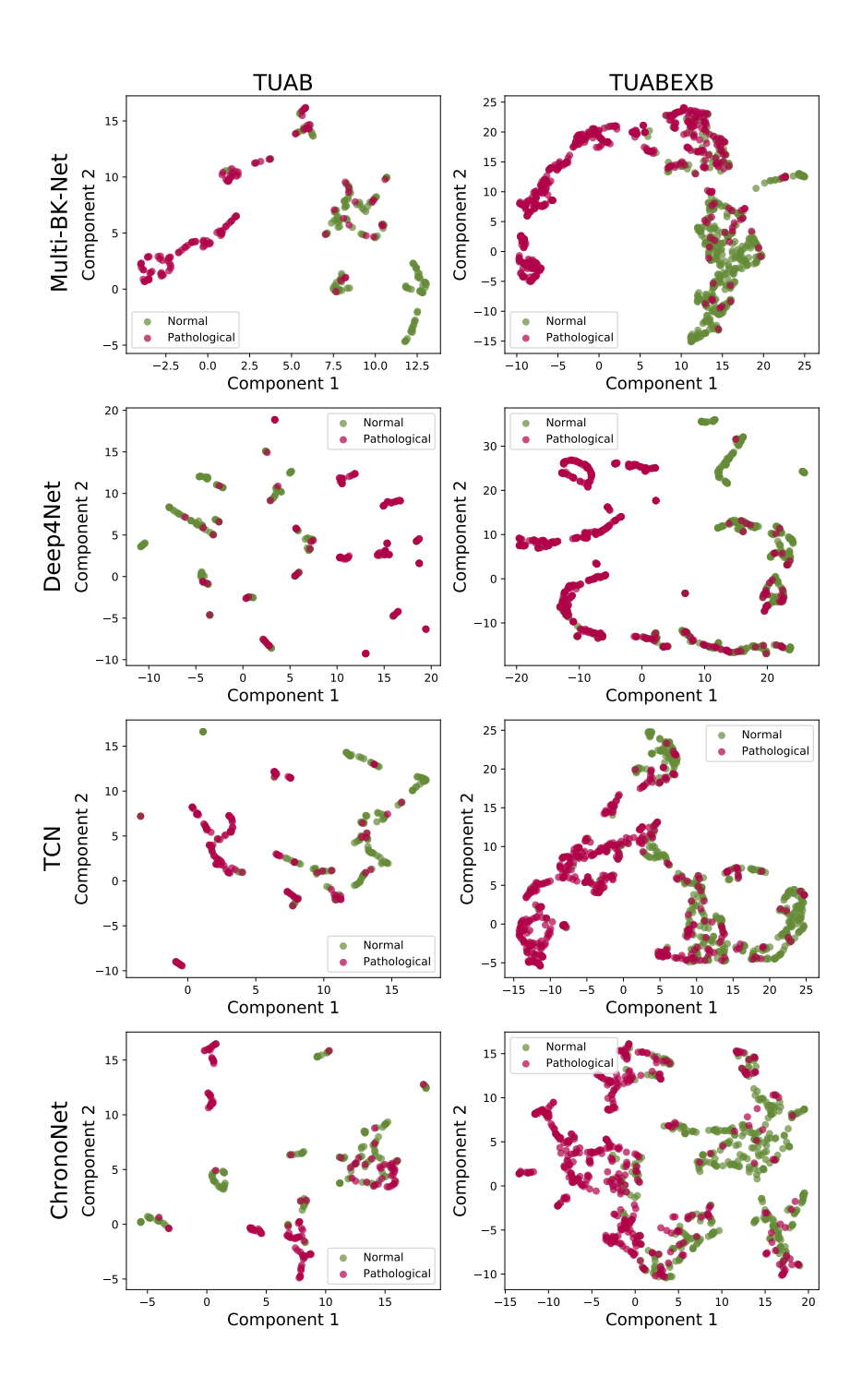


Figure 10: A comparison of UMAP visualisation of feature representations learned with Multi-BK-Net, Deep4Net, TCN and ChronoNet for pathological and non-pathological recordings on the predefined TUAB (left column) and the TUABEXB (right column) evaluation sets. Rows represent the UMAP visualisation of different models. Pink dots represent the pathological class, while green dots represent the non-pathological class.

Table 17: Size of the different architectures used in the ablation experiments. Model size is given as the number of trainable parameters.

Architecture	Model size
Deep4Net	303,452
Deep4Net35	579,182
Deep4Net47	1,026,482
Deep4Net48	1,069,490
STKSBNet3	1,057,632
STKSBNet7	1,057,772
STKSBNet10	1,057,877
STKSBNet13	1,057,982
STKSBNet25	1,058,402
STKSBNet200	1,064,527
MTKSBNet	1,038,683
Multi-BK-Net	1,038,683

Table 18: Performance comparison between our proposed Multi-BK-Net and five baseline architectures on different subgroups of the predefined TUAB evaluation set. Performance metrics were computed separately for each subgroup and averaged across 10 independent runs (n=10). Confidence intervals (95% CI) represent the mean based on the normal approximation (n=10). ACC: Accuracy [%], SENS: Sensitivity [%], SPEC.: Specificity [%]. Bonferroni-corrected, two-sided Mann-Whitney U test, p < 0.05: *, p < 0.01: ***, p < 0.001: ***; n=10).

Group	Architecture	ACC. [95%CI]	SENS. [95%CI]	SPEC. [95%CI]
age < 25 y.	Deep4Net	90.56 [88.23-92.88]	74.00 [65.63-82.37]	96.92 [94.46-99.39]
(n=18)	ShallowNet	94.44 [92.15 - 96.74]	90.00 [83.47-96.53]	96.15 [92.78-99.53]
	TCN	93.33 [91.16-95.51]	94.00 [88.01-99.99]	93.08 [91.57-94.58]
	EEGNet	92.31 [90.72-93.90]	76.00 [70.77-81.23]	96.19 [93.86-98.52]
	ChronoNet	93.89 [91.35-96.43]	88.00 [79.33-96.67]	96.15 [93.64-98.67]
	Multi-BK-Net	92.78 [89.51-96.04]	86.00 [77.63-94.37]	95.38 [92.05-98.72]
$25 \text{ y.} \leq \text{age} < 60 \text{ y.}$	Deep4Net	83.39***[82.20-84.58]	69.12** [64.71-73.52]	92.55 [88.71-96.38]
(n=174)	ShallowNet	85.86***[85.15-86.58]	75.44 [73.42-77.46]	92.55*[90.35-94.74]
	TCN	86.32***[85.88-86.76]	71.76***[71.05-72.48]	95.66 [95.17-96.15]
	EEGNet	85.00***[84.48-85.52]	65.29***[63.73-66.86]	97.64 [96.95-98.33]
	ChronoNet	88.10 [87.63-88.58]	73.82** [72.79-74.86]	97.26 [96.83-97.70]
	Multi-BK-Net	89.08 [88.43-89.73]	77.65 [76.30-78.99]	96.42 [95.51-97.32]
$60 \text{ y.} \leq \text{age}$	Deep4Net	78.69***[77.24-80.14]	79.43 [73.16-85.71]	77.42 [68.38-86.46]
(n=84)	ShallowNet	79.64** [78.42-80.87]	88.30 [86.67-89.94]	64.84* [59.64-70.04]
	TCN	81.19** [80.43-81.95]	84.34**[83.55-85.13]	75.81 [74.11-77.51]
	EEGNet	80.95** [80.10-81.80]	76.60***[74.19-79.02]	88.39***[85.53-91.25]
	ChronoNet	79.64** [78.52-80.77]	84.53** [83.32-85.74]	71.29 [68.55-74.03]
	Multi-BK-Net	83.93 [83.06-84.80]	89.06 [87.73-90.38]	75.16 [72.84-77.48]
female	Deep4Net	80.74***[79.64-81.85]	72.86* [66.42-79.29]	86.59 [81.43-91.75]
(n=148)	ShallowNet	82.03***[81.12-82.94]	80.48 [78.06-82.89]	83.18**[80.26-86.09]
	TCN	84.53***[84.07-84.99]	76.83***[76.00-77.66]	90.24 [89.54-90.93]
	EEGNet	84.05***[83.34-84.77]	69.52***[67.46-71.59]	94.82**[93.78-95.87]
	ChronoNet	84.66***[84.07-85.26]	76.83***[75.87-77.78]	90.47 [89.60-91.34]
	Multi-BK-Net	87.43 [86.94-87.92]	82.86 [81.33-84.38]	90.82 [89.50-92.15]
male	Deep4Net	84.38***[82.81-85.94]	74.44** [70.13-78.76]	94.00 [89.61-98.39]
(n=128)	ShallowNet	87.42 [86.58-88.26]	82.38 [80.96-83.81]	92.31 [89.57 - 95.04]
	TCN	86.02** [85.35-86.68]	79.05** [78.14-79.95]	92.77 [91.76 - 93.78]
	EEGNet	84.61***[83.85-85.37]	71.43***[69.41-73.45]	97.38 [96.19-98.58]
	ChronoNet	87.34 [86.59-88.09]	80.95 [79.82-82.09]	93.54**[92.46-94.62]
	Multi-BK-Net	88.12 [87.58-88.67]	82.70 [81.06-84.33]	93.38 [92.60-94.17]

Table 19: Performance comparison between our proposed Multi-BK-Net and five baseline architectures on different subgroups of the predefined TUABEXB evaluation set. Performance metrics were computed separately for each subgroup and averaged across 10 independent runs (n=10). Confidence intervals (95% CI) represent the mean based on the normal approximation (n=10). ACC: Accuracy [%], SENS: Sensitivity [%], SPEC.: Specificity [%]. Bonferroni-corrected, two-sided Mann-Whitney U test, p < 0.05: *, p < 0.01: ***, p < 0.001: ***; n=10).

Group	Architecture	ACC. [95%CI]	SENS. [95%CI]	SPEC. [95%CI]
age < 25 y.	Deep4Net	81.94** [80.60-83.29]	49.58***[44.76-54.41]	98.13** [96.92-99.33]
(n=144)	ShallowNet	81.11** [80.12-82.10]	66.67** [64.39-68.94]	88.33 [86.08-90.59]
	TCN	82.78* [81.71-83.85]	68.12** [66.63-69.62]	90.10 [88.40-91.81]
	EEGNet	77.88***[76.71-79.06]	65.56** [62.73-68.38]	84.41** [81.58-87.24]
	ChronoNet	76.67***[75.50-77.84]	67.50** [65.65-69.35]	81.25***[79.10-83.40]
	Multi-BK-Net	85.62 [84.44-86.81]	72.29 [70.92-73.66]	92.29 [90.54-94.05]
$25 \text{ y.} \le \text{age} < 60 \text{ y.}$	Deep4Net	82.10***[80.37-83.83]	59.64***[54.93- 64.35]	98.65***[98.06-99.23]
(n=462)	ShallowNet	84.78***[84.24-85.32]	69.64***[67.68-71.61]	95.94***[95.24-96.64]
	TCN	85.45** [84.93-85.98]	72.55***[71.59-73.51]	94.96***[94.65-95.28]
	EEGNet	84.22***[83.65-84.79]	69.74***[66.01-73.48]	94.89 [92.92 - 96.86]
	ChronoNet	86.45** [86.12-86.78]	75.46***[74.34-76.58]	94.55** [93.92-95.18]
	Multi-BK-Net	87.51 [87.20-87.82]	80.00 [79.24-80.76]	93.05 [92.55-93.54]
$60 \text{ y.} \leq \text{age}$	Deep4Net	82.20***[79.68-84.71]	78.48***[74.15-82.82]	90.95***[88.51-93.39]
(n=282)	ShallowNet	85.71 [85.35-86.07]	88.79** [87.57-90.00]	78.45 [76.13-80.77]
	TCN	85.28** [84.92-85.65]	88.38***[87.89-88.87]	77.98 [76.62-79.33]
	EEGNet	84.26** [83.51-85.00]	86.97***[85.64-88.30]	77.86 [73.89-81.83]
	ChronoNet	85.32* [84.56-86.08]	89.29** [88.64-89.95]	75.95 [74.09-77.82]
	Multi-BK-Net	86.84 [86.19-87.49]	91.36 [90.99-91.74]	76.19 [74.19-78.19]
female	Deep4Net	81.11***[79.01-83.21]	65.96***[61.21-70.70]	97.14***[96.21-98.07]
(n=467)	ShallowNet	83.79***[83.37-84.21]	76.21***[74.51-77.91]	91.81* [90.55-93.06]
	TCN	84.58** [84.17-84.99]	77.54***[76.96-78.12]	92.03** [91.35-92.70]
	EEGNet	82.33***[81.98-82.69]	75.62***[73.31-77.94]	89.43 [87.00-91.86]
	ChronoNet	84.35** [83.83-84.86]	79.75** [79.02-80.48]	89.21 [88.56-89.85]
	Multi-BK-Net	85.95 [85.62-86.29]	81.96 [81.39-82.53]	90.18 [89.83-90.52]
male	Deep4Net	83.25***[81.58-84.92]	68.22***[63.93-72.51]	97.05***[96.05-98.04]
(n=422)	ShallowNet	85.28***[84.90-85.67]	79.90***[78.50-81.30]	90.23 [88.92 - 91.54]
	TCN	85.43***[84.88-85.98]	81.09***[80.41-81.76]	89.41 [88.53-90.29]
	EEGNet	84.19***[83.76-84.63]	78.91***[76.38-81.44]	89.05 [86.67-91.42]
	ChronoNet	84.72***[84.03-85.40]	82.03***[81.11-82.95]	87.18* [86.29-88.07]
	Multi-BK-Net	88.18 [87.78-88.57]	86.98 [86.44-87.52]	89.27 [88.34-90.20]

Table 20: Mean training and inference times across runs (n=10) in hours: minutes and mean CUDA memory across runs in GB. Training times are for training only, i.e. excluding loading and pre-processing of data. These times are only intended to give a rough estimate of training and inference times. Inference time is based on 276 recordings of the TUAB evaluation set.

Architecture	Training Time	Training Memory (GB)	Inference Time	Inference Memory (GB)
Deep4Net	1:05	7.8	0:03	0.60
ShallowNet	1:06	4.01	0:05	10.30
TCN	2:08	2.88	0:02	0.51
EEGNet	1:06	2.61	0:02	0.82
ChronoNet	1:04	2.61	0:04	0.14
Multi-BK-Net	12:26	1.59	0:02	1.70